Use of Chemically Synthesised Atomically Precise Gold Nanoclusters in Catalytic Hydrogenation

A thesis submitted in partial fulfilment of the requirements for the degree of Master of Science in Chemistry

Sam Nesbitt

University of Canterbury

Department of Chemistry

May 2018

Abstract

Heterogeneous catalysis is of extreme importance to chemical and energy industries due to its versatility and advantages over homogeneous catalysis. One of the main focuses in heterogeneous catalysis research is on developing an understanding of the catalytically active sites at the atomic/molecular level. Such research is carried out with the aim of developing improved conventional industrial catalysts. Discovery of catalytic activity of Au revolutionized heterogeneous catalysis in the past two decades. New catalysts benefit from Au's improved catalytic activity and selectivity in certain reactions as well as demonstrated activity under ambient conditions with a relatively low cost and environmental impact. Atomically precise ultra-small clusters offer an opportunity to define active sites of heterogeneous catalysts with unprecedented precision. The work in this thesis focused on the hydrogenation of substituted nitro-aromatics, a group of industrially important building blocks for a wide range of chemical processes, using supported, atomically precise, Au nanoclusters.

The first part of this thesis is focused on the role the support has in stabilising Au nanoclusters deposited on the surface, against sintering during activation treatments, and catalytic reactions. Protection against sintering was of extreme importance in this work, as the nanoclusters needed to maintain their original sizes, so as to elucidate the true nature of their catalytic properties. Two characterisation methods, UV-Vis DRS and powder XRD were used to determine if sintering had occurred in the case of Au nanoclusters deposited and activated on the surface of the support, and if so, to what degree had it affected the size of the nanoclusters.

The second part of this thesis focused on supported, atomically precise, Au nanoclusters for use as nanocatalysts for the hydrogenation of substituted nitro-aromatics under mild reaction conditions. The aim was to determine if a size effect existed between atomically precise Au nanoclusters with a difference of only 1 or 2 Au atoms. The reactions conducted using such nanocatalysts were assessed in terms of the products yield, and the activity of each reaction, so as elucidate the effect of Au nanocluster size on these parameters. Effect of the nature of support, Au metal loading (in selected cases) and even how catalytic activity varied depending on substrate (*e.g.* with the presence of different functional groups on the nitro-aromatic ring) was also investigated.

Table of Contents

Acknowledgements

I would first and foremost like to thank (now Associate Professor) Vladimir Golovko for all his, wisdom, advice, constructive criticism and any other way he helped me over the two years of my Master's degree. I would also like to thank Associate Professor Matt Watson for all his help and advice. I would like to thank Danny Leonard, Nick Oliver and Wayne Mackay for all their technical and electrical expertise. Without them a lot of this work would not be possible. I would like to thank the members of the Golovko group, Ryan and especially Mai for all her help and support. Thank you to Joel from the Downard group. Your chat was always of a high quality. I'd also like to thank Iman Hashemi of the Yip group for his great discussions on photocatalysis. I'd like to thank the members of the Kruger group, Ben, Shane, Dave and Rob and Will from the Fitchett group for their quality yarns and an enjoyable two years of postgraduate life. I'd also like to thank all the members of the University of Canterbury Chemistry Department and anyone else who helped me.

Also thank you to my parents and family for all their help and support.

"*God made the bulk; the surface was invented by the Devil*"

- Nobel Laureate Wolfgang Pauli

Declaration

I declare that the work presented in this thesis is based on my own research except where specifically acknowledged in the text.

List of Abbreviations

-	AAS	Atomic Absorption Spectroscopy
-	℃	Degrees celsius
-	$CHCl_3$	Chloroform
-	DCM	Dichloromethane
-	DOS	Density of States
-	Dppee	[Bis(2-Diphenylphosphino)ethyl]Ether
-	EtOH	Ethanol
-	EXAFS	Extended X-ray Absorption Fine Structure
-	FCC	Face Centred Cubic
-	g	Gram(s)
-	GC	Gas Chromatography
-	GC-FID	Gas Chromatography Flame Ionisation Detector
-	HAADF	High-Angle Annular Dark-Field
-	HAP	Hydroxyapatite
-	Hdppa	N,N-Bis(diphenylphosphino)amine
-	HOMO	Highest Occupied Molecular Orbital
-	HPLC	High Performance Liquid Chromatography
-	HRTEM	High-Resolution Transmission Electron Microscopy
-	ICP-MS	Inductively Coupled Plasma Mass Spectrometry
-	IR	Infrared spectroscopy
-	L	Litre(s)
-	LUMO	Lowest Unoccupied Molecular Orbital
-	MAS-NMR	Magic Angle Spinning Nuclear Magnetic Resonance
-	MeOH	Methanol
-	mg	Milligrams
-	mL	Millilitre(s)
-	mmol	Millimole(s)
-	mol	Mole(s)
-	nm	Nanometre(s)
-	NMR	Nuclear Magnetic Resonance spectroscopy
-	PMPS	Polymethylphenylsilane

-	PP_3	[Tris(2-(Diphenylphosphino)ethyl)]Phosphine
-	ppm	Parts per million
-	PTFE	Polytetrafluoroethylene
-	rpm	Revolutions per minute
-	SCXRD	Single Crystal X-ray Diffraction
-	SMe_2	Dimethyl Sulfide
-	SMSI	Strong Metal-Support Interaction
-	STEM	Scanning Transmission Electron Microscopy
-	TEM	Transmission Electron Microscopy
-	TGA	Thermogravimetric analysis
-	THF	Tetrahydrofuran
-	UV-Vis	Ultraviolet-Visible spectroscopy
-	UV-Vis-DRS	Diffuse reflectance Ultraviolet-Visible spectroscopy
-	XAS	X-ray Absorption Spectroscopy
-	XES	X-ray Emission Spectroscopy
-	XRD	X-ray Diffraction

Chapter 1 - Introduction

1.1 Catalysis

The role of catalysis is of extreme importance in the production of bulk chemicals, fine chemicals, fuels and in the bioprocesses in the modern industrialised world. Catalysis can be considered the greatest contributor to the chemistry industry's synthesis of chemicals, materials and pharmaceuticals, where, by volume 95% of all products rely on catalysis as a means of synthesis and 70% of all processes involved in the manufacture of these products rely are catalytically based.[1] The purpose of a catalyst in the chemical industry is simple; catalysts enhance the rates of reaction and allow for selective synthesis of desired products while reducing the use of environmentally damaging or harsh chemicals, lowering required high pressure or temperature reaction conditions required otherwise, and minimising formation of harmful or undesired by-products. A catalyst is defined as "a substance that increases a rate of reaction without modifying the overall standard Gibbs energy change in the reaction"[2]. The catalysts involvement in a reaction is cyclic, with reactants binding in some way to the catalyst then leaving as products, regenerating the catalyst to its original state. Ideally catalysts should not be consumed or should remain unchanged by a reaction. However, the reality is that due to the processes occurring during reactions a catalysts' chemical state or composition could change, often negatively affecting its activity or selectivity. Such catalyst deactivation processes lead to the need for replacement or treatment of the catalyst to regenerate its original state.

1.2 How a Catalyst Works

A catalyst is a functional material that contains active sites which adsorb reactants and affect their reaction rates without changing the thermodynamic equilibrium of the reaction itself. A catalyst is able to increase the reaction rate or activity by lowering the activation

energy involved in the transformation of reactants to products by offering a less energetic pathway for the reaction to follow compared to an uncatalysed reaction. This is important, as often, the means to increasing uncatalysed reaction rates involves higher temperature processes which can lead to the thermal decomposition of products and reactants or drive the reaction towards pathways which result in the formation of unwanted products.

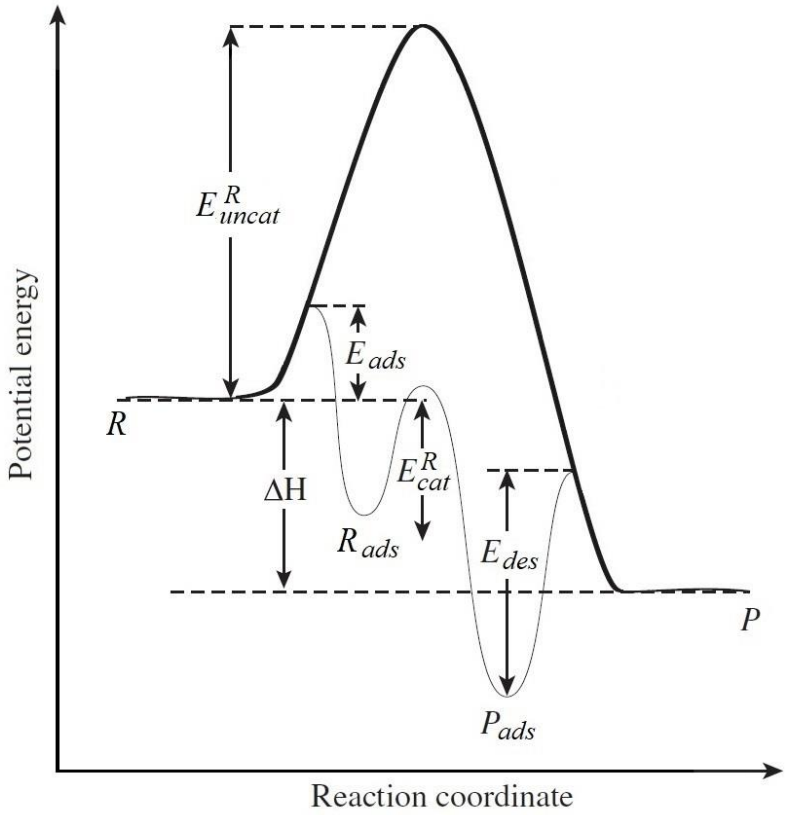

Figure 1.1 Potential energy diagram of a gas-phase reaction R → P, uncatalysed (bold line) or catalysed using a heterogeneous catalyst (fine line).

The concept of changing the reaction rate without changing the thermodynamic equilibrium of the reaction itself is illustrated with a gas-phase model reaction over a heterogeneous catalyst in Figure 1.1. Due to the reaction taking place at the catalyst surface rather than in the gas phase, this model can also be applied to liquid phase reactions. The uncatalysed reaction is shown as proceeding forward through an activated state with the

activation energy given as $E_{R,\,uncat}$. The enthalpy of this reaction is given as ΔH which remains unchanged through both the uncatalysed and catalysed reaction paths. If a catalyst is introduced to the system, the reaction can then proceed through a multi-step reaction, with the reactant ideally adsorbing to the surface to give a new reactant state R_{ads}. For this step there can be an activation energy, given as E_{ads}, for adsorption to the surface, however this is dependent on the system. After the reactant is adsorbed to the catalyst surface it can then undergo reaction (process is dependent on the surface as to how this proceeds) to produce P_{ads} with the activation energy given as $E_{R,\,cat}$. With the completion of the transformation from reactant to product, the product state P_{ads} is desorbed from the catalyst surface with an activation energy E_{des}. This illustrated example demonstrates how introducing a catalyst into a reaction system will affect the overall activation energies without changing the initial reactant and final product states by providing a favourable pathway for the reaction.

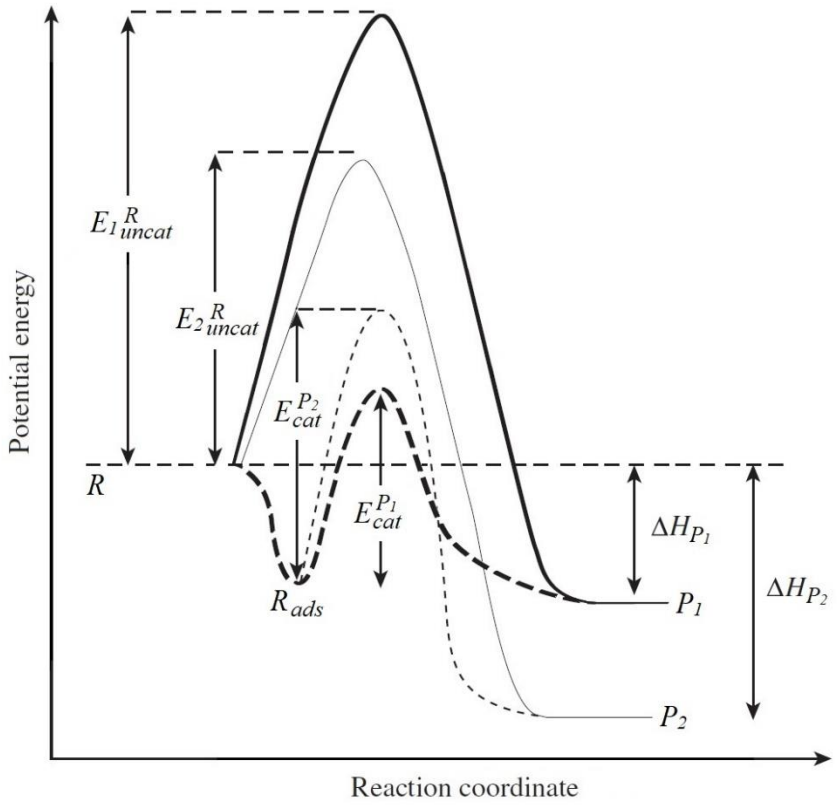

Figure 1.2. Simplified potential energy diagram of the selectivity changing in a reaction with the introduction of a catalyst (Reactant adsorption and product desorption energies omitted).

Introducing a catalyst to a reaction system can also have a favourable effect on the outcome of the reaction by affecting selectivity of the process. This is an important practical application of catalysts, as products that would not normally be obtained from an uncatalysed reaction can be synthesised by selecting an appropriate catalyst. This concept is illustrated in Figure 1.2 where the reactant has the possibility to give two products. In the uncatalysed reaction the activation energies $E_{1R,uncat}$ and $E_{2\ R,uncat}$ are determinant in the formation of the products P_1 and P_2 respectively. This is under the assumption that there is no significant difference in the Arrhenius constants between each reaction and thus P_2 is selectively formed in the uncatalysed reaction as it is formed more rapidly as it possesses the lower activation energy. In the catalysed reaction the reactant R_{ads}, adsorbed on the catalyst surface, if alternate products are possible, can now give either P_1 or P_2, provided that there is the possibility in

reversal of activation energies for either pathway. Unlike the catalysed reaction, if there is no significant difference in the pre-exponential constants (derived from the empirical relationship between the activation energy and average kinetic energy) of the possible products, then P_1 is selectively formed given the lower activation energy of $E_{P1,cat}$ compared to $E_{P2,cat}$ even if P_2's formation is thermodynamically more favourable. This ability to alter selectivity is crucial in catalysis especially when a reactant has two or more groups that can provide reaction centres but only one product is desired from the outcome of the reaction.

1.3 Heterogeneous Catalysis

1.3.1 Heterogeneous versus Homogeneous Catalysis

Heterogeneous catalysis is of extreme importance to chemical and energy industries due to its versatility and advantages over homogeneous catalysis; as such, it is more widely applied in industrial processes. For the purposes of this thesis a heterogeneous catalyst will be considered as a solid (generally with a high surface area) with a varied polymorphic form or structural phase, which contains metal nanoparticles (1 – 100 nm in size) that are deposited on a support. The term support is thus used as most catalytically active materials used in heterogeneous catalysis require the aid of an additional material to facilitate their use, though some heterogeneous catalysts are found in bulk or unsupported forms. Heterogeneous catalysts constitute a separate phase to that of the reaction medium. This makes catalyst separation from obtained products and purification relatively easy and enables use of batch, continuous flow, and plug flow reactors with reagents present in gas or liquid phases under a variety of reaction conditions which is of great importance for industrial manufacturing purposes.

A homogeneous catalyst is, by definition soluble, within the reaction medium as there is no distinct separate catalyst phase; so, products obtained require costly separation and purification techniques which limits utilisation of homogeneous catalysts. Possessing this property limits homogeneous catalysts to use in liquid-phase reactions where there are many

examples of industrial applications (often benefiting from stereoselectivity of organometallic catalysts); in the gas-phase reactions the reaction conditions are unfavourable due to the poor volatility and thermal stability of homogeneous catalysts.

Thermal stability generally restricts the use of homogeneous catalysts to lower temperatures, often dependent on the solvent used to solubilise the catalyst and its stability as a function of temperature, limiting use; however these issues can be partially overcome with the use of higher pressures.[3] A heterogeneous catalyst is limited under thermal conditions only by the stability of the catalyst. The unsupported nature of homogeneous catalysts can negatively affect their recyclability, as recovery is more difficult with conventional techniques often leading to deactivation of the catalyst, again due to the inherent solubility of the system. Heterogeneous catalysts can also be deactivated under certain reaction conditions, but simple reactivation processes, such as thermal treatments under a specific atmosphere can be employed to restore activity.

Homogeneous catalysts possess a number of ideal qualities that heterogeneous catalysts lack, necessitating further research into the development and improvement of current heterogeneous catalyst systems. The active sites in homogeneous catalysts are usually well-defined due to the fact the catalysts are generally transition metal complexes containing a single central metal atom protected by ligands. Active sites on heterogeneous catalysts are often poorly-defined. This is due to the nature of a heterogeneous support and metal particle, where different areas of a nanoparticle can possess different catalytic properties. This has driven research into finding heterogeneous catalysts with well-defined, catalytically active sites prompting the development of single-atom heterogeneous catalysts.[4-5]

Catalyst modification is also relatively easy for homogeneous catalysts, where the steric and electronic properties of the metal centre can be tuned by varying coordinating ligands. For

example, electronic properties of the system could be tuned by choice of the donor atoms of ligands or changing the donating abilities of ligands by selecting electron withdrawing or donating substituents. Basic concepts developed in organometallic and organic chemistry have allowed numerous synthetic methods to be employed in the modification of homogeneous catalysts.[6]

Modification of the support and catalyst is also an important area of heterogeneous catalysis as it allows a degree of tunability in catalytic properties and expands the range of available catalyst systems for a variety of catalytic processes. Catalysts can be pre-modified, where a modifier is applied to the support before deposition of metal particles or post-modified, where a modifier is applied to the system after the deposition of metal particles. Co-modification, where the support is modified during the metal particle deposition process is also used but much less commonly than the previous two methods.[7] Doping with metal or non-metal ions is one form of pre-modification that can be carried out on various supports, resulting in changes in their surface, electronic, optical and photo/electro-chemical properties allowing application in a wider range of catalytic reactions than un-doped supports. Calcination or reduction are post-modification thermal treatments where the nanocatalyst is heated under O_2 or H_2 atmospheres respectively to give active catalysts due the removal of ligands or formation of metal particles possessing certain oxidation states.[8] The control over particle size, or tunability of the active site at the molecular level, offered by these conventional synthetic methods is still extremely difficult when compared to the degree of control homogeneous catalyst modifications offer.

Homogeneous catalysts often possess high chemo-, regio- and stereo-selectivity for the synthesis of desired products. This property is a consequence of the ease of modification, which is offered in the case of homogeneous catalysts *via* the choice of metal centre, ligands, and reaction conditions, contributing to high selectivity. Much like the lock and key model system

given for enzymatic catalysis,[9] the site at which a substrate binds during reaction can be constrained by fine-tuning of the shape, size and electronic properties of protecting ligands, allowing the synthesis of a desired product whereas the possibility of multiple products exists without appropriate control of the active site.

Heterogeneous catalysts have much lower chemo-, regio- and stereoselectivity in the synthesis of products, which is a result of the difficulty in modification, where the tuning of steric and electronic properties in such catalysts proves to be a challenging endeavour in obtaining a precise degree of control. Many industrial processes rely on changing the metal particle component of a supported heterogeneous catalyst, rather than tuning the electronic and steric properties of the particles themselves to provide selectivity in the reaction of certain reagents to obtain desired products, as shown in Figure 1.3.

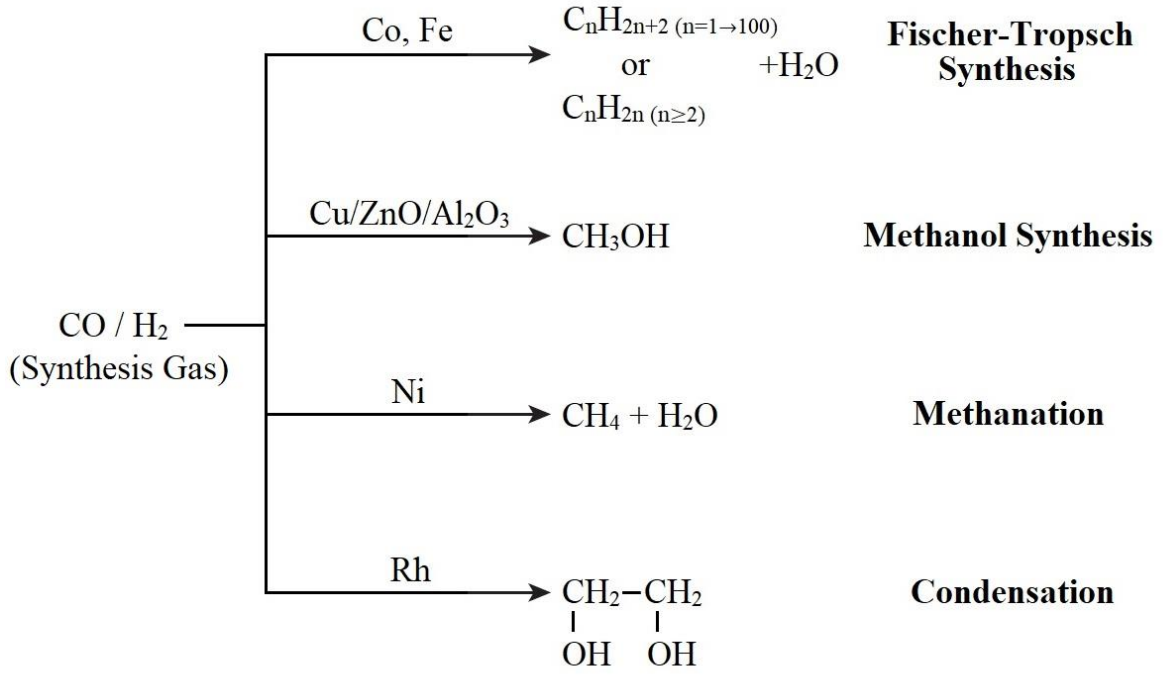

Figure 1.3. Changing selectivity in industrial processes for various reactions utilising Syngas (Synthesis Gas)

Research has shown that the size of metal particles can affect selectivity.[10-11] Using Au as an example, as the size of a metal particle decreases, the partial molecular behaviour emerges, which results in an increase of d-electron density, altering selectivity in reactions.[12] The shape of the metal particles has been shown to contribute to altering selectivity in reactions, with differing polyhedral arrangements consisting of varied crystalline lattice phases, demonstrating changes in selectivity in catalytic reactions.[13] This is attributed to the active metal-structure dependent altering of activation energies where even small changes in the difference between multiple activation barriers for competing reactions of only a few kcal/mol, a small percentage of the absolute value for each barrier, can lead to a change in product selectivity.[14] Supports also have an influence in changing selectivity in catalytic reactions. This has been demonstrated experimentally with the same active metal on different supports catalysing different reaction pathways to obtain different products in a catalytic reaction utilising the same substrates and reaction conditions.[15-16] There is a wide variety in the unique properties that various supports possess in terms of surface area, pore texture, chemically inert, acidic or basic properties, geometric and electronic properties. More importantly, is the dispersal of deposited metal particles to smaller size-regimes, which provides a higher specific metal surface area when compared to a larger particle or the bulk form. These properties are all contributing factors towards the varying selectivity's different supports display, and drive research to help develop understanding of surface processes and their effects in heterogeneous catalysts on the molecular level.

The understanding of catalytic reaction mechanisms is of paramount importance to developing highly stable, active and selective catalyst systems. To achieve breakthroughs in catalyst design, the reaction mechanisms and pathways of catalytic processes must be clearly and unequivocally understood, to allow control at the molecular level, at which a catalysts active site operates at. This is because reaction kinetics and surface intermediates are excellent

ways to validate reaction mechanisms and are explicitly related to the nature and properties of a catalytically active reaction site. Given that the pathways and mechanisms for a given reaction can be deduced by the analysis of these parameters, a high level of precision and accuracy from spectroscopic and chemical characterisation methods is needed to allow their elucidation. The availability of such data can inform rational catalyst design and lead to well-tuned active sites that can be formed in reproducible and well-defined ways that allow for the implementation of more efficient and selective industrial catalytic processes.

One of the greatest advantages homogeneous catalysis possesses is the greater understanding of the molecular species and reaction mechanisms involved in catalytic chemistry. This is due to the use of transition metal organometallic complexes with well-defined active sites, well understood fundamental steps in catalytic reactions, and a wide range of techniques used for *ex*- and *in-situ* characterisation. A fundamental example for specifying the preferred reaction pathway a homogeneously catalysed reaction can take, has come from the 16/18 electron rules postulated by Tolman. The two rules state that "diamagnetic organometallic complexes of transition metals may exist in a significant concentration only if the metal's valence shell contains 16 or 18 electrons" and that "organometallic reactions, including catalytic ones proceed by elementary steps involving only intermediates with 16 or 18 metal valence electrons."[17] These rules have been successfully employed in the elucidation of individual steps of a catalytic cycle to give reaction mechanisms when used in conjunction with established rules in relation to the coordination number and oxidation state of a metal centre that dictate the distinct steps seen in transition metal catalysed reactions.

Complementing the rules of organometallic chemistry are direct chemical and spectroscopic techniques that allow in-depth characterisation of catalysts, catalyst-bound intermediates, resting states of a catalyst and the determination of rate expressions given the relative ease of monitoring substrate concentrations during reactions. Given that homogeneous

catalysed reactions are carried out under ambient conditions *in-situ* spectroscopic studies can be carried out with relative ease; where they are carried out under relatively harsh conditions, in relation to heat and pressure, special systems can be employed to allow *in-situ* studies with the caveat of some degradation in qualitative analysis.[18] IR spectroscopy is the main technique used to identify reaction products, intermediates and a catalysts resting state; the latter being important in determining catalytic kinetics given that pre-equilibrium and steady state approximations used to describe the kinetic behaviour of a catalytic system and are closely related to the resting state. Catalytic species can also be interpreted and characterised allowing for close monitoring of reaction conditions where variables such as concentrations of substrates, temperature, and pressure can be controlled allowing the optimization of reactions and preventing undesirable outcomes such as catalyst deactivation. NMR spectroscopy is used to give more detailed structural information, than that obtained from IR spectroscopy, in the characterisation of catalyst precursors and active intermediates as well substrate/product distribution information. Higher catalyst concentrations are required for NMR spectroscopic experiments to improve the signal-to-noise ratio and may not correspond with actual catalytic reaction concentrations and true *in-situ* conditions.[19] Single crystal XRD, mass spectrometry, and elemental analysis are used *ex-situ* to characterise organometallic complexes and reaction products. The electronic properties of organometallic complexes and their corresponding ligands are used *ex-situ* characterised using IR, NMR, UV-Vis, and EXAFS spectroscopic techniques. With technological and analysis method advances, EXAFS has been used for *in-situ* identification where it can provide information on the average coordination numbers (number of nearest neighbour atoms and to some degree next-nearest neighbour atoms) and interatomic distances.[20]

In homogeneous catalysis characterisation and modelling, coupled with advances in coordination chemistry, have allowed a greater understanding of reaction kinetics and

pathways, and facilitated the fundamental understanding of mechanisms in of these reactions at the molecular level allowing design of generations of much improved catalysts. Heterogeneous catalysis has existed almost at the opposite end of this spectrum with respect to molecular level understanding and fine-tuning for some time due to catalytic active sites being poorly defined, and difficultly in employing *in-situ* characterisation techniques. The methods used for the characterisation of heterogeneous catalysts are often *ex-situ* indirect methods, which look at the catalyst before and after a catalytic reaction and the products obtained. Often the mechanism are inferred, from these parameters, rather than the direct study of the reactions occurring at the surface and surface parameters of the catalyst during the reaction process.[21] A typical method for catalyst characterisation is to use techniques such as BET (Brunauer-Emmett-Teller isotherm) surface analysis, powder X-ray diffraction, electron microscopy or AAS (Atomic Absorption Spectroscopy) to analyse an as-prepared or 'activated' catalyst sample. The data obtained from these analytical methods is then correlated to the catalysts activity derived from experimentation, with concepts such as particle size effects or metal support interactions, attributed to these observations alone. This methodology can be regarded as sub-optimal, with solid state and surface dynamics of active catalyst systems as well as other contributing, structural and kinetic aspects, not being taken into consideration when attempting to elucidate reaction mechanisms for heterogeneous catalytic reaction cycles (Figure 1.4). This demonstrates that *ex-situ* analysis alone is not sufficient to provide a critical assessment in the characterisation of heterogeneous catalysts and determination of related reaction mechanisms. Due to these factors there has been much speculation and guesswork into the actual processes and mechanisms occurring during heterogeneously catalysed reactions with models such as the Mars and Van Krevelen,[22] Langmuir-Hinshelwood or Rideal-Eley mechanisms being postulated.[23]

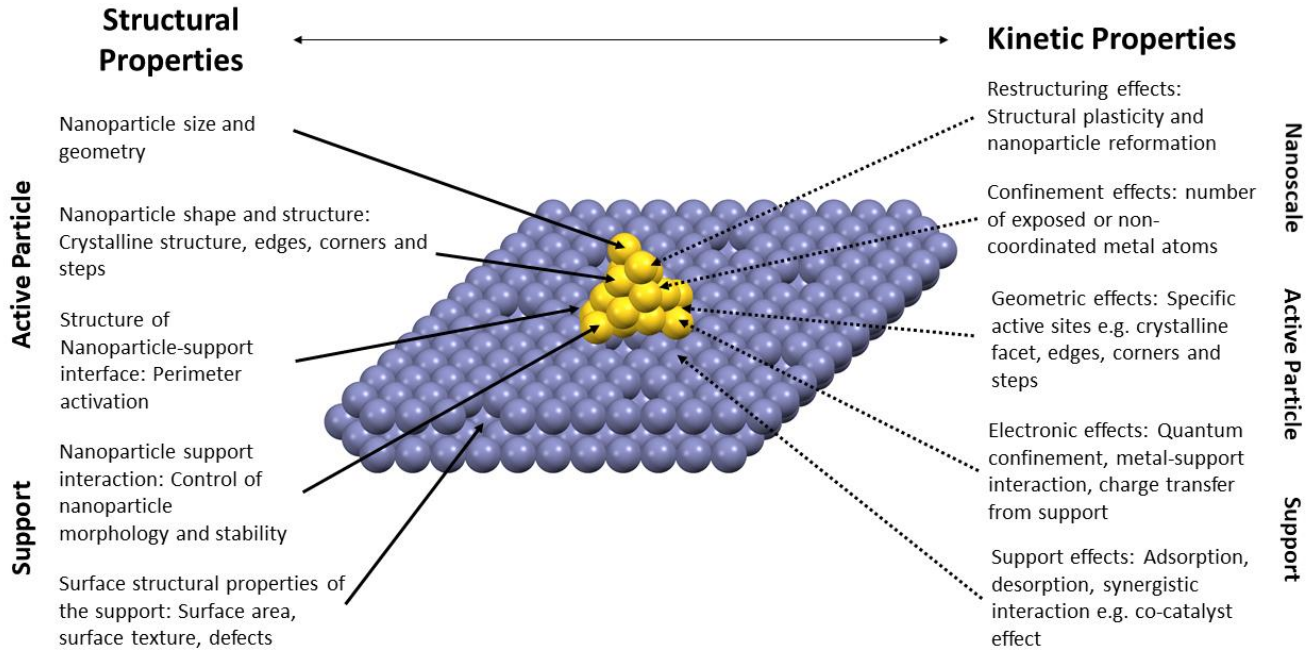

Figure 1.4. Aspects at the molecular level found in supported heterogeneous catalytic systems that require *in-situ* characterisation to enable the elucidation of reaction mechanisms (Adapted from [24])

Given the reasons outlined above, there is an emphasis placed on the use of *in-situ* characterisation techniques in heterogeneously catalysed processes given the nature of the surface processes occurring on these catalysts during reactions and the limitations of indirect characterisation methods. As a functional material, the geometric and electronic structural properties of a heterogeneous catalyst must exhibit some degree of plasticity during the catalytic cycle, with changes to the atomic structure having to possess, at the least, some small magnitude of reversibility. Without this reversibility, irreversible structural change, whether it occurs to the support or to deposited metal particles, can negatively affect the performance of the catalyst, with deactivation or reduced substrate selectivity being the main outcomes.[25] The use of *in-situ* investigations of catalysts however, is a highly involved process and thus seldom performed under working catalytic conditions. *In-situ* investigations should serve to give real-

time analysis of the geometric and electronic structures of a heterogeneous catalyst in parallel with reagent interaction during the catalytic cycle and resulting catalytic activity. Observation of the bulk or surface structures found in materials employed in heterogeneous catalytic processes at high temperatures or reactant pressures, however, is commonly at the apex of the physical limits for analytical methods used for characterisation.[26] In heterogeneous catalysis there is an added dimension resulting from the experimental limitations between *in-situ* vs. *operando* studies with the latter requiring that analysis must be performed under the exact reaction conditions used in industrially catalysed processes.[27] Often with *in-situ* characterisation, a theoretical deduction is made that the geometric and electronic properties of a catalyst, under conventional experimental conditions will exist in the same active state as under high-performance working (*operando*) conditions. It has been determined though, that catalysts that demonstrate high catalytic activity are able to respond dynamically to the reaction environment and will occur in certain and highly specific states, as a consequence of the chemo-physical conditions of the system during the catalytic process.[28] The demand for such intensive characterisation of catalysts in order to delineate the nature of the catalytic mechanism for certain reactions, and under a variety of different operating conditions, has necessitated the development of characterisation tools and methods in order to address the limitations found in current heterogeneous catalysis research.[29]

Technological advancements have allowed the steady evolution of spectroscopic techniques for the *in-situ* and *operando* characterisation at the molecular level of heterogeneous catalysts in order to elucidate reaction mechanisms. The techniques covered in this section are not an exhaustive list but are representative of the most suitable techniques at this time used for *in-situ* and *operando* characterisation. Raman spectroscopy increasingly emerges as a method for the *in-situ* characterisation of the molecular structure and surface chemistry of catalytic active sites in supported metal-oxide heterogeneous catalysts to provide information

on direct structure-activity/selectivity relationships in these systems. While it is has been mostly used for *in-situ* studies, there are an increasing number of *operando* studies that utilise this technique.[30] Raman spectroscopy is able to provide detailed structural information at the molecular level on the nature of catalytic active sites with the added advantage of use in all reaction mediums (gas, solid and liquid), operation over at the high temperatures and pressures found in industrially catalysed processes, time-resolved spectroscopy and the ability to be operated in tandem with other popular techniques (IR, UV-Vis, GC and MS).[31]

MAS (Magic Angle Spinning) NMR is another technique that has benefitted from technological and experimental advancements and been used for *in-situ* characterisation studies given the subsequent expansion of its capabilities for elucidation of heterogeneous catalytic mechanisms.[32] MAS NMR allows investigation at the molecular level and can give information on the interaction of adsorbed products and reactants with the catalytic active site, with specific characterisation on a substrates state and mobility during reaction and the nature of the catalytic active site. Given appropriate experimental methodology, time-resolved observation, direct and indirect identification of reaction intermediates and primary products can also be achieved using this technique. This is performed using isotopic labelling experiments that allow not only the following of the reactions progress by tracking the nuclei (^{1}H, ^{13}C, ^{15}N, ^{31}P) possessed by certain reactants and subsequent catalytic reaction products, but also the investigation of the catalytic active site using nuclei (^{1}H, ^{23}Na, ^{27}Al, ^{29}Si, ^{31}P) found at a supported catalysts' surface. The direct testing of reaction mechanisms can also be carried through label tracing experiments where the crucial placement of ^{2}H or ^{13}C isotopes on a reactant allows specific information to be gathered in these studies.[33]

XAS (X-Ray Absorption Spectroscopy) and XES (X-Ray Emission Spectroscopy) are two powerful techniques where technological advancements have (especially for XES) have enabled their use for the *in-situ* characterisation of dynamic structural changes occurring in

heterogeneous catalysts under specific working conditions in order to determine the catalysts' structure-performance relationship during the catalytic reaction process. XAS and XES techniques are able to characterise the electronic and geometric structures of specific elements, and more importantly, the short-range geometry such as that found at a catalytic active site, with typical data extracted being coordination numbers, interatomic distance to the nearest neighbouring atom, and localised electron density.[34] When used for *in-situ* characterisation, these techniques can identify the elemental composition and structure of the active site as well as information on the electronic and geometric structure of an absorbing atom and the structures of a supported catalysts surface adsorption sites responsible for the interaction with reactants. Characterisation of structural changes at a catalysts active site under *in-situ* conditions is vital to further the understanding of a catalysts function and elucidation of reaction mechanisms.[35]

While these techniques offer new opportunities to advance the foundations of heterogeneous catalysis, the acquisition of a detailed molecular insight into the mechanisms responsible for the catalytic activity of these systems remains a challenge. This highlights the need for model systems comprised of single metal atoms or atomically precise metal-nanoclusters, to conduct *in-situ* and *operando* studies on, for the purpose of reaction mechanism elucidation needed for the fundamental understanding of the behaviour of active sites to allow the rational design of more efficient and selective catalysts.[36]

1.3.1.1 Reaction Mechanisms in Heterogeneous Catalysis

In heterogeneous catalysis it is the surface of the solid catalyst that allows the catalytic process to occur, where the presence of active sites provide adsorption centres for reactant molecules. The interaction of the reactant with the catalyst surface will ideally lead to the activation of a substrate and its transformation through interaction with other substrates, to provide an adsorbed product. This adsorbed product will then desorb, whereby the active site

will revert to an initial state and allow the adsorption of another reactant thus enabling the catalytic reaction cycle.[37] It is the properties of a catalyst that will dictate the form and chemistry of a reactants' interaction on a surface. The energetics have already been discussed in terms of the activation energies and how they affect selectivity, so this section will give three well-documented mechanisms for surface reactions in heterogeneously catalysed processes.[38] Given that the reaction occurs at the catalyst surface it will be assumed that the adsorption process will be the same in the liquid phase as it is in the gas phase.

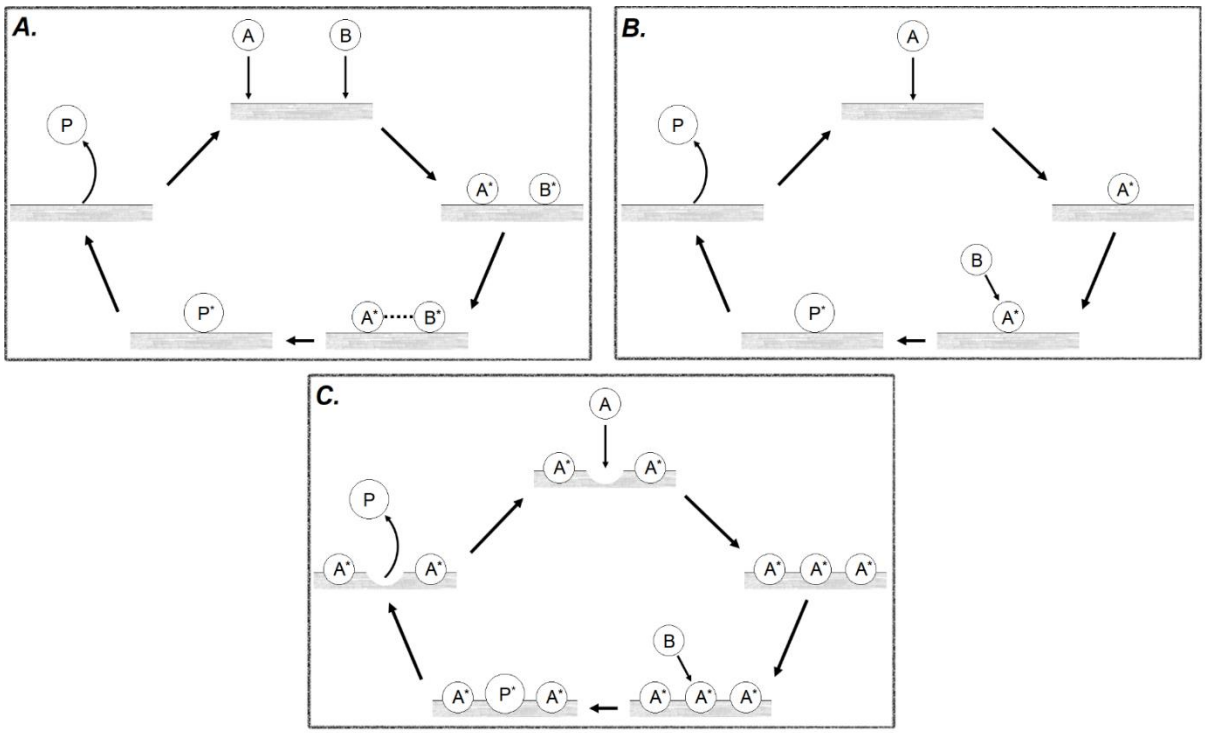

Figure 1.5. (A) Langmuir-Hinshelwood Mechanism, (B) Eley-Rideal Mechanism, (C) Mars-Van Krevelen Mechanism

1.3.1.2 Langmuir-Hinshelwood Mechanism

The Langmuir-Hinshelwood mechanism was proposed by Langmuir in 1921 and further developed by Hinshelwood in 1926.[39] For the Langmuir-Hinshelwood mechanism (A in Figure 1.5) both reactants *A* and *B* are adsorbed onto active sites (as indicated by A^* and $B^{*)}$

on the catalyst surface before any reaction takes place. Surface diffusion allows interaction between the adsorbed reactants which react to form the adsorbed product P^*, which is subsequently desorbed from the surface as the product *P*.

1.3.1.3 Eley-Rideal Mechanism

The Eley-Rideal mechanism was proposed in 1938 by Eley and Rideal.[40] For the Eley-Rideal mechanism (B in Figure 1.5) the reactant *A* is first adsorbed onto an active site on the catalyst surface. The reactant B from the reaction medium then collides with A^*, facilitating the chemical reaction to form the adsorbed product P^* which is subsequently desorbed from the surface as the product *P*.

1.3.1.4 Mars-Van Krevelen Mechanism

The Mars-Van Krevelen Mechanism differs from the previous two mechanisms as the surface itself is actively involved in the reaction: Reactant *A* is chemically bonded to the catalyst lattice at surface vacancies, forming a thin reactant film over the catalyst surface and acting as an active site. Reactant *B* then collides with *A* forming the adsorbed product (*P**), which is then desorbed as *P*. A vacancy is left behind with the desorption of the product from the catalyst surface which is then reoccupied with the reactant *A*. Although it has been depicted in Figure 1.5 *C.* that the vacancy has been occupied by the reactant from the reaction medium, the original mechanism proposed by Mars and Van Krevelen in 1954,[41] detailed this process as occurring from the bulk rather than the gas or liquid phase. The issue concerning the origin of the atoms that fill these vacancies seems to be trivial, whether the atoms are

supplied from the reaction medium or bulk phase, as this variance has no actual bearing on the active processes operating in this reaction mechanism.

1.3.2 Adsorption

Adsorption of reactants on a heterogeneous catalysts surface is regarded as the most important step in the catalytic reaction cycle. The catalyst is responsible for providing a surface where adsorption will often preferentially take place at the active sites, since the active sites are generally partially uncoordinated and chemically suited for adsorbing reactants. There are two types of adsorption in heterogeneous catalysis, physisorption (physical adsorption) and chemisorption (chemical adsorption). Physisorption is considered in almost all catalytic reactions to be a precursor to chemisorption with the physisorbed adsorbate existing in a 'precursor' or intermediate state before it is, chemisorbed to the vacant active site, desorbed before it has a chance to adsorb, or diffuses to an unoccupied active site in the event it chemisorbs over occupied active sites.[42] Physisorption is a relatively weak surface interaction which results from van der Waals forces between the adsorbate (reactant) and adsorbent (surface). The heat for adsorption for this interaction is relatively low, ~10-30 kJ mol^{-1} and comparable to heats of fusion, with the absence of electron transfer, although there is a small chance of structural distortion to the adsorbate. Physisorption is always exothermic and has a low activation energy with the adsorption process proceeding rapidly at low temperatures where an equilibrium can be quickly established, however with increasing temperature there is a sharp decrease in the adsorbates' equilibrium quantity. The rate in physisorption is also pressure dependent with multiple layers formed at the surface in a non-specific way at high pressure coverage, constrained only by the magnitude of the surface area.[43]

Chemisorption in contrast is a relatively strong surface interaction which is governed by the formation of chemical bonds (electrostatic or covalent forces) between the adsorbate and

adsorbent. The heat for adsorption for this interaction is relatively high, ~100-400 kJ mol^{-1} (for reference the heat of combustion for graphite is 393.5 kJ mol^{-1})[44] and comparable to heats of reaction, with electron transfer to the adsorbate resulting in increased reactivity when compared with free adsorbates. Chemisorption is usually exothermic and generally requires high activation energies with the rate of adsorption being strongly temperature dependent with low temperatures resulting in low rates but often increasing rapidly at higher temperatures. The rate is strongly pressure dependent like in physisorption, but unlike physisorption the surface coverage is only limited to the formation of a monolayer with highly selective adsorption occurring at specific sites on the surface.[45]

Table 1.1 Chemisorption abilities of bulk metals[46]

		Gases						
Group	**Metals**	**O_2**	**C_2H_2**	**C_2H_4**	**CO**	**H_2**	**CO_2**	**N_2**
A	Ti, Zr, Hf, V, Nb, Ta, Cr, Mo, W, Fe, Ru, Os	+	+	+	+	+	+	+
B_1	Ni, Co	+	+	+	+	+	+	−
B_2	Rh, Pd, Pt, Ir	+	+	+	+	+	−	−
B_3	Mn, Cu	+	+	+	+	±	−	−
C	Al, Au	+	+	+	+	−	−	−
D	Li, Na, K	+	+	−	−	−	−	−
E	Mg, Ag, Zn, Cd, In, Si, Ge, Sn, Pb, As, Sb, Bi	+	−	−	−	−	−	−

+ strong chemisorption ± weak chemisorption − chemisorption unobservable

Examples of this selectivity can be seen in Table 1.1, of note is Au, which has been highlighted as it is generally considered inert but can chemisorb O_2, acetylene, ethylene and CO but not H_2 or CO_2. Au however is active in catalytic hydrogenation reactions and this issue will be addressed in a later section.

1.3.3 The Support

The choice of material that is used as the support in heterogeneous catalysis is often an important one as supports often dictate the stability and sometimes even enable activity of the catalyst system.[47] Metal-oxides, such as titanium dioxide (TiO_2), are commonly used as heterogeneous catalyst supports. Titania has a wide range of properties, displaying a variety of structures and polymorphic forms, with nanostructured titania supports possessing differing physiochemical properties compared with the bulk. TiO_2 nanotubes are an example of the latter case. They are considered a 1D nanostructure compared to 0D TiO_2 nanoparticles; possessing a high surface area, activity in photocatalytic reactions and improved ion-exchange ability. TiO_2 also has four distinct crystalline bulk phases - anatase, rutile, brookite and akaogiite, where the chemical composition is the same but the crystal structure changes in terms of unit cell size and space groups, and each phase has different electronic, optical, structural and thermodynamic properties making titania suited for various catalytic processes.[48]

The support is a very important part of heterogeneous catalysis due to the unique surface chemistry, surface dynamics, such as charge transfer to and stabilisation of metal nanoparticles. Generally, supports used in heterogeneous catalysis are categorised as being inert or active. The active supports can allow the adsorption/desorption of reactants and products on their surface during the catalytic process or can activate metal nanoparticles *via* co-catalyst effects. The inert supports do not participate in the catalytic process, serving as just a material on which metal nanoparticles are immobilised. An important determinant for catalytic activity on an active support comes from the metal-support interface due to synergetic catalytic effects. Tuning the chemical and structural properties at this junction through small alterations in either the support or nanoparticle could result in enhanced catalytic activity or changes in selectivity. On inert supports, only the metal nanoparticle serves as an active site and generally the support

has a weak interaction with nanoparticles deposited on the surface which can result in a low resistance to sintering over the surface due to low thermal stability.

Sintering is problematic in heterogeneous catalysis and has been shown to result in catalyst deactivation or decreased activity as metal particles irreversibly agglomerate into larger nanoparticles. This is especially true in the case of nanometre-sized clusters which have lower thermal and structural stabilities compared to larger nanoparticle forms. The participation of the support in the catalytic process is also theorised to alter the mechanism by which reactions occur as mentioned earlier, with the Langmuir-Hinshelwood and Mars-Van Krevelen mechanisms being attributed to active supports and the Eley-Rideal mechanism attributed to inert supports as only the supported nanoparticle is the adsorption/desorption site for reactants and products. To reiterate, most often these mechanisms are only theorised, with many more variations postulated due to the large number of determining factors and conditions being attributed to the origin of catalytic activity.[49-50]

1.3.5 Support Effects

Beyond the properties mentioned in the previous section there are a number of support-induced changes that can affect the metal particles deposited on the surface, especially when they exist in the nanoparticle size regime. Structural changes enacted by a support on deposited nanoparticles can be an important determining factor in the size, shape, and structural stability of nanoparticles under treatment and working conditions. An example is the phenomenon of sintering in heterogeneous catalysts where nanoparticle-support interactions can affect the Ostwald ripening or Smoluchowski ripening (diffusion coalescence processes) with the alteration of these pathways being dependent on the support material.[51] The energy of a metal nanoparticles binding to a surface is determined not only by the number of metal-surface bonds, but, also by additional metal-oxide interfacial bonding interaction in the case of metal-oxide

supports. The latter also serves to diminish sintering rates on catalysts provided high enough bond-strengths are present. It has been determined experimentally that the strength of a nanoparticles' binding with the support generally increases with increasing nanoparticle size, with few exceptions, due to size-dependent metal particle adsorption energies.[52] Metal-oxide supports have dominant point defects in the form of oxygen vacancies which can be neutral (F centre), single (F^+ centre) or doubly (F^{2+} centre) ionised. Hence, these are strong adhesion sites for deposited metal nanoparticles. These are often referred to as F centres (originating from Farben, the German word for colour) the tendency of their existence in a material to change the appearance through excitations in the visible region of the spectrum due to electrons trapped at these sites. The coordination number of these sites is also varied depending on the position on the lattice surface, be it an edge, step, corner or terrace. The properties and characteristics of oxygen vacancies will vary depending on the nature of the metal element of the oxide electronic structure, polymorphic structure, reducibility and bonding change with the material.[53] The density of oxygen vacancies on a surface is often increased through targeted preparation, treatment or doping of the support. Studies conducted with Au and Ag nanoparticles, two metals prone to sintering,[54-55] have shown that these sites can offer some resistance to sintering through strong metal-support binding resulting from higher adhesion energies alongside the increased likelihood of a metal nanoparticle being anchored at these sites.[56-57]

1.3.5.1 Strain Effects

The structures of metal nanoparticles can also be influenced by strain effects resulting from the failure of the supports lattice parameters to match those of the deposited nanoparticles; this is especially common at the nanoparticle-support interface where the metal adatoms tend to preferentially adopt the structure of support, straining the lattice of the nanoparticle as bond lengths are distorted. Strain effects are further compounded as the polytopal arrangements of

nanoparticles tend to change with a decrease in size,[58] with the nanoparticle morphology also possibly being changed as the geometry adopts a more stable conformation to minimise the total energy.[59] Strain is also able to induce chemical changes in nanoparticles through the alteration of electronic properties.[60-61] It is generally accepted that as metal-metal bond lengths increase, the width of the metal nanoparticles *d* band narrows, leading to the *d* band centre shifting toward the Fermi level. This is due to the fact that *d* filling will not change for the metal, so the *d* states are shifted to compensate for this. Shifts to higher energy generally will result in the stronger binding of adsorbates to the nanoparticle often resulting in lowered catalytic activity.[62] The opposite is observed with the contraction of metal-metal bond lengths, as the energy of the antibonding states is lowered, resulting in a lowering of the energy of the *d* states are in relation to the Fermi level which weakens bonding. This reduction of metal-adsorbate bond strength has been experimentally determined *via* CO adsorption on Pd nanoparticles,[63] and theorised as one of the factors (along with quantum size effects and surface morphology) why gold nanoparticles are more reactive for the chemisorption of O_2 and CO.[64]

1.3.5.2 Charge Transfer

Along with structural changes to metal nanoparticles the support can induce changes in nanoparticles' electronic structures which affect the nanoparticles performance in catalytic reactions (selectivity and activity), as well as stability and morphology. Charge transfer is the movement of electrons from the support to nanoparticles on the surface, or from the nanoparticles to the support in a heterogeneous catalyst. The nature of this interaction is dependent on the composition of the nanoparticle and support, nanoparticle (shape, size and exposed facets), support structure and morphology, the reducibility of the support, and defects present on the surface. On metal-oxide supports the density of oxygen vacancies can be an important factor.[65-66] Charge transfer has been shown to occur from the support to the nanoparticle in the Au-based catalysts with the negative charging of the nanoparticle deposited

on the surface resulting in the strengthening of the metal-support interaction.[67] In contrast, charge transfer has been shown to occur from the nanoparticle to the support in Cu and Ag based catalysts with the nanoparticles reducing the surface of the metal-oxides they were deposited on *via* direct electron transfer.[68]

Heterogeneous catalysts consisting of Au nanoparticles supported on metal-oxides have been widely investigated in terms of charge transfer effects on the catalytic performance. Several relevant examples will be provided in this section. Charge transfer was found to affect the chemical reactivity of Au adatoms due to charge redistribution at the Au/CeO_x interface on a mixed CeO_2/TiO_2 support. On this support Au nanoparticles were found to preferentially nucleate at Ce nanoclusters which were proposed to all be in the reduced Ce^{3+} state on the TiO_2 (110) surface. The charge redistribution at these sites allowed the strong adsorption of CO_2 and facilitated its activation for hydrogenation to methanol.[69] Charge transfer has been confirmed as a determining factor in catalytic activity, where Au_5 deposited on a MgO ultrathin film, was shown to be able to activate O_2 with direct electron tunnelling being attributed to the formation of an electron-rich surface and charge transfer from the support to the nanocluster.[70] Au_8 deposited on a defect poor MgO surface was found to be catalytically inactive for CO combustion, with the same cluster being catalytically active for the same reaction on a defect rich MgO surface where oxygen vacancies were responsible for enabling charge transfer from the support to the nanoclusters.[71] Charge transfer from oxygen vacancies can be a "double edged sword" and could lead to the catalyst deactivation as a result of agglomeration of deposited Au species during catalyst preparation using the deposition-precipitation technique. An excess of oxygen vacancies on CeO_2 was found to reduce catalytically active Au^{3+} species to less active Au^{+} species with strong charge transfer leading to the agglomeration of formed Au nanoparticles on the supports surface and subsequent catalyst deactivation.[72] Another example of the complex nature of charge transfer is that it can be dependent on the size and

shape of the nanoparticle with electron transfer either increasing or decreasing in relation to these properties;[73-74] the morphology of the nanoparticle can be altered as a result of charge transfer resulting in higher bond strengths between the deposited nanoparticle and support.[75]

1.3.5.3 Strong Metal-Support Interactions (SMSI)

Strong metal-support interactions are a physiochemical phenomenon displayed in metal-oxide (and some nonoxide) supports and can be a key determinate in the catalytic performance of heterogeneous systems. Tauster *et al.* conceived this term after conducting high temperature H_2 reduction of Group VIII noble metals supported on TiO_2 that resulted in good dispersion of the metal without evidence of sintering but also resulted in the dramatic suppression of H_2 and CO adsorption .[76] This has been ascribed to the encapsulation of deposited nanoparticles with a thin partially-reduced layer of the substrate; this layer forms due to the structural rearrangement of the support as metal-support interactions are maximised during high temperature reduction treatments with the formation of oxygen vacancies allowing a stronger support interaction over the metal nanoparticle surface.[77] For a time SMSI was avoided in heterogeneous catalysts given the perceived negative effects on catalytic activity as encapsulation meant the blocking of active sites on deposited metal nanoparticles. Encapsulation can also result in the suppression of electron transfer between the metal and support, and adsorption of small molecules such as those commonly used in catalytic hydrogenation reactions (e.g. H_2 and CO). Researchers have recently made the discovery that the encapsulation of metal nanoparticles is reversible under oxidative treatment conditions resulting in improved catalytic activity, an alteration in the electronic interaction between the support and metal due to electron transfer, and suppression of significant agglomeration in metal nanoparticles; this reversibility under oxidative treatment is commonly referred to as classical SMSI.

In addition to encapsulation there are geometric and electronic effects that are induced on metal nanoparticles subject to SMSI. Nanoparticle morphology can be changed with nanoparticles subject to SMSI, wetting the surface of the partially-reduced support after being treated under strongly reducing conditions. This was thought to account for an observed increase in nanoparticle stability as the number of uncoordinated sites on the nanoparticle is reduced.[78] The interaction has shown a size-dependence and can strongly affect the morphology, and subsequently the electronic properties of smaller nanoparticles given that the catalytically active surface is in a relatively close proximity to the nanoparticle support interface. The opposite is true for larger metal nanoparticles, so only minor effects are observed with little to no change in a catalysts behaviour.[79] The electronic effect results as the electronic structure of a metal nanoparticle is perturbed from its original state by the interaction of the nanoparticle with the metal-oxide surface. Charge redistribution at the metal nanoparticle/metal-oxide interface is a consequence of this reactive interfacial contact. It is governed by the degree of electron transfer from the support to the nanoparticle that occurs, which is often dictated by the size of metal nanoparticles and the electronic structure of the metal-oxide. The charge distribution that is one to a few atomic layers thick and is localised around the interface can possess electron density different to that of the individual metal nanoparticle and oxide support, thus creating new, unique catalytically active sites with improved activity and selectivity.[80]

Au is an interesting case as due to the lower work function (ø) and surface energy possessed by Au nanoparticles (that has been found to decrease as the size of the nanoparticles decrease)[81] and the fact encapsulation had not been observed, it was believed that SMSI could not exist in supported Au nanoparticle catalysts. Metal nanoparticles such as Pt, Pd, Rh, Ni, and Ir possess relatively high surface energies and high work functions, where ø metal > ø substrate (often given in terms of a high ø metal where E_F substrate > E_F metal) is a requirement

for the encapsulation of metal nanoparticles on the surface at the equilibration. Due to equilibration resulting from the interfacial charge transfer process between the substrate and metal nanoparticle, positive space charges are formed where the substrate terminates allowing the diffusion of substrate cations over the negatively charged nanoparticle surface resulting in encapsulation.[82] It was found however that in contrast to the classical SMSI, studies conducted with Au nanoparticles deposited on ZnO nanorods[83] and HAP supports[84-85] demonstrated that oxidative pre-treatments resulted in encapsulation of nanoparticles with the thin substrate layer, which proved to be reversible occurring under reductive treatments.[86] This reversibility occurred at lower temperatures *cf.* easily reducible transition metal-oxides (TiO_2, Ta_2O_5, Nb_2O_5) that display classical SMSI.[87]

1.4 Nanocatalysis

With the advancements since the end of the 1990s that have been made in nanoscience, the concept of nanocatalysis by design has emerged as a bridge between heterogeneous and homogeneous catalysts. Research into the field nanocatalysis seeks to overcome the limitations of these systems and offer the advantages that each of these catalysts possess and provide unique properties to allow further advancement in the field of catalysis.[88] Nanocatalysis can be defined as the use of nanomaterials as a means for carrying out hetero- or homogeneously catalysed reactions. A distinction will be made between nanocatalysts and nanostructured catalysts with nanocatalysts referring to the size of the active component existing in the nanometre scale (< 10 nm) whether it be supported or unsupported. An example is ligand-protected, atomically precise Au nanoclusters where they are either deposited on a support or employed as homogeneous solutions (unsupported) in the liquid phase reactions. A nanostructured catalyst is a material in which the surface structure and composition or internal structure and composition has been organised at the nanoscale to provide a significant increase to the surface area so as to increase activity.[89-90]

While technically all catalysis can be considered nanocatalysis as the active site exists at the nanoscale, a more correct statement would be that catalytic interactions occur at the nanoscale. There is a clear distinction between the use of nanomaterials and bulk materials (conventional catalysis) in terms of the catalytic interactions occurring in these systems. Nanocatalysts have a very high degree of structural sensitivity with selectivity, chemisorption and catalytic activity depending on the size, morphology, and composition of nanoparticles as well as the choice of material they are supported on. There is no more ubiquitous example of this than the high activity of Au nanoparticles smaller than ~5 nm in catalytic reactions even at sub-zero temperatures where larger-sized nanoparticles and bulk Au are inactive.[91] The explanation for this activity can be found in the intrinsic properties that emerge in Au and other metal nanoparticles as their sizes reach the nanometre range. At these sizes shape, size, support, oxidation state, and quantum confinement effects are the determining factors in the stability, activity, selectivity, and surface-to-volume ratio of nanoparticle catalysts and allow for tailoring of the physical and chemical properties of the catalyst.[92]

With careful and precise design, nanocatalysts can offer safer catalysts with minimal waste from ambient reaction conditions, unnecessary reactant use and synthesis of unwanted by-products, with improved selectivity and activity through informed selection of composition and size of nanoparticle. Improved atom economy, energy efficiency, and optimal feedstock utilization can also be improved by nanocatalysis over conventional catalysis with a reduction in the overall use of precious metals where the same activity can be generated with a nanocatalyst that contains only a fraction of a percentage of the total metal content of a bulk conventional catalyst.[93]

1.5 Gold Nanoclusters and Their Unique Properties

Gold nanoparticles were used in the process of glass staining in a colloidal form for centuries without any scientific evaluation into the causation of such interesting interactions with light that had facilitated their use. Michael Faraday began what can be considered as the first scientific study on gold nanoparticles where he theorised the existence of small gold particles, and noted that the variations in colour observed in colloidal gold solutions were due to differences in particle sizes.[94] Following Faraday's discovery there was limited research on gold nanoparticles until breakthroughs in synthesis methods coming from Turkevich[95] and Frens.[96] Applications for gold nanoparticles in catalysis were almost non-existent until separate studies by Haruta[97] and Hutchings[98] showed that supported gold nanoparticles were catalytically active in the oxidation of carbon monoxide and the hydrochlorination of acetylene respectively. What was remarkable about Haruta's research was that it showed that, not only were supported gold nanoparticles active for carbon monoxide oxidation at temperatures as low as -70 °C, but these catalyst systems were also more active and stable during sustained reaction than conventional catalysts.

Following the separate discoveries of the catalytic activity of supported gold nanoparticles, there was little initial interest on further research on such catalytic systems, apart from continuing efforts by Haruta[99], even with breakthroughs in synthesis of ligand-protected gold nanoparticles.[100] It has only been in the last twenty years that the versatility of gold nanoparticles in heterogeneous and homogeneous catalyst systems, have been revealed, demonstrating activity in a wide range of oxidative and reductive processes.[101-103] Most of the heterogeneous catalysts prepared for these processes relied on simple synthesis techniques such as deposition precipitation, co-precipitation or impregnation. Fabrication of the homogeneous catalysts relied on gold nanoparticle formation using wet chemical synthesis methods that did not inhibit the growth of the Au core during reduction steps. These methods of synthesis would

typically lead to catalyst systems with large (> 5 nm), polydisperse gold nanoparticle species. The studies conducted with these catalyst systems showed activity in oxidative and reductive processes, but also showed that there was a correlation between decrease of gold nanoparticle size and increase of catalytic activity.[8, 104-105]

Within the last ten years there has been a new breakthrough in gold nanoparticle research with the development of wet chemical synthesis methods that give ligand-protected, atomically-precise, sub-nanometre (< 2 nm), gold nanoclusters. The Brust-Schiffrin method (Scheme 1) is one of the most widely used and modified methods used in the field of Au nanocluster synthesis.[106] Researchers have devised many variations of this reaction utilising careful, and precise control of reaction conditions, reductants, and choice of protecting ligands which has allowed the library of available atomically-precise Au nanoclusters accessible to researchers to grow at a rapid rate.[107]

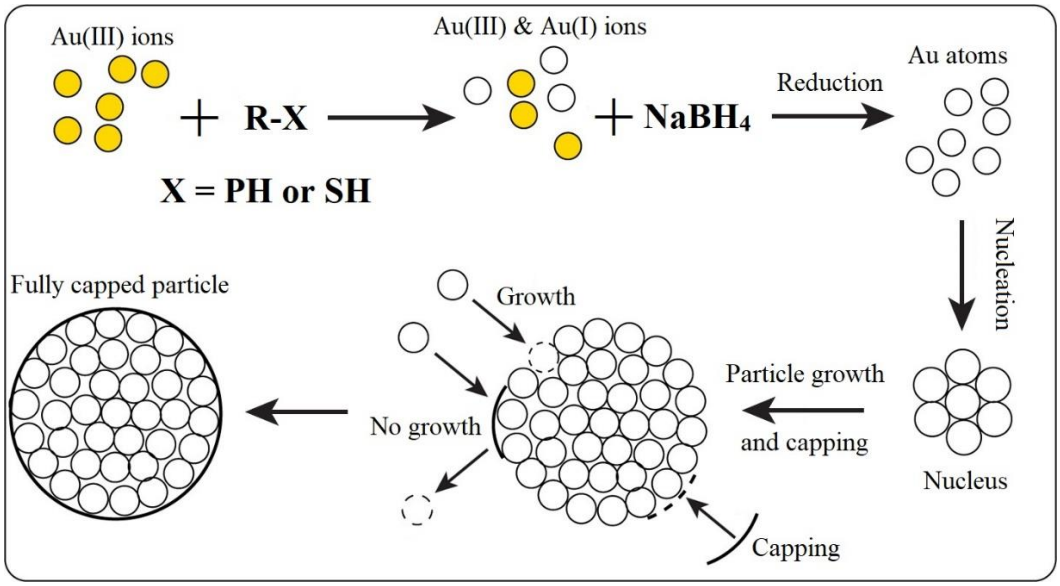

Scheme 1. General reaction scheme for the Brust-Schiffrin method (Adapted from [108])

This advance has opened a whole new avenue for the future development of nanocatalyst systems due to the unique electronic and structural properties that sub-nanometre gold nanoclusters possess that differentiate them from their bulk monometallic form and larger gold

nanoparticles. The atomic packing geometries of sub-nanometre gold nanoclusters change with the number of gold atoms; such clusters can have structures that display polytopal arrangements with truly unique arrangements of atoms not seen in bulk lattices. This is in contrast to larger crystalline nanoclusters and colloids which adopt face centred cubic structures. Due to the unique arrangements of gold atoms in the metal cores, the nanoclusters have a higher percentage of low-coordinate gold atoms compared to larger nanoparticles which is considered to be a contributing factor to the higher catalytic activity of clusters. It has been shown that some sub-nanometre gold nanoclusters can take fcc-like structures if they are protected by bulky thiolate ligands but still possess the unique electronic properties of sub-nanometre gold nanoclusters.[109] The changes in the packing geometries of gold nanocluster cores have been shown experimentally and theoretically using X-ray crystallography and DFT methods. A number of studies demonstrated that even one gold atom difference in the structure of a nanocluster can completely change the polyhedral arrangement of the core.[110-115] Ligand protected, atomically precise, sub-nanometre, gold nanoclusters can even show polymorphism in their core structure depending on the nature of the ligand used in synthesis.[116]

Gold nanoparticles larger than 2 nm display metallic and plasmonic properties, where the collective excitation of electrons within a conduction band leads to strong surface plasmon resonances (SPR) that dominate their optical properties.[117] Below this size range sub-nanometre, gold nanoclusters behave as semi-conductors or molecular species due to strong electron energy quantisation (Figure 1.6). These changes in the electronic structure correspond to transitions from metallic to semi-conductor and eventually to molecular electronic structures, which can display one electron HOMO-LUMO electronic transitions[118]. It has been noted that "due to the strong quantum confinement effect adding or removing one gold atom significantly changes the structure and the electronic and optical properties of the nanocluster."[119]

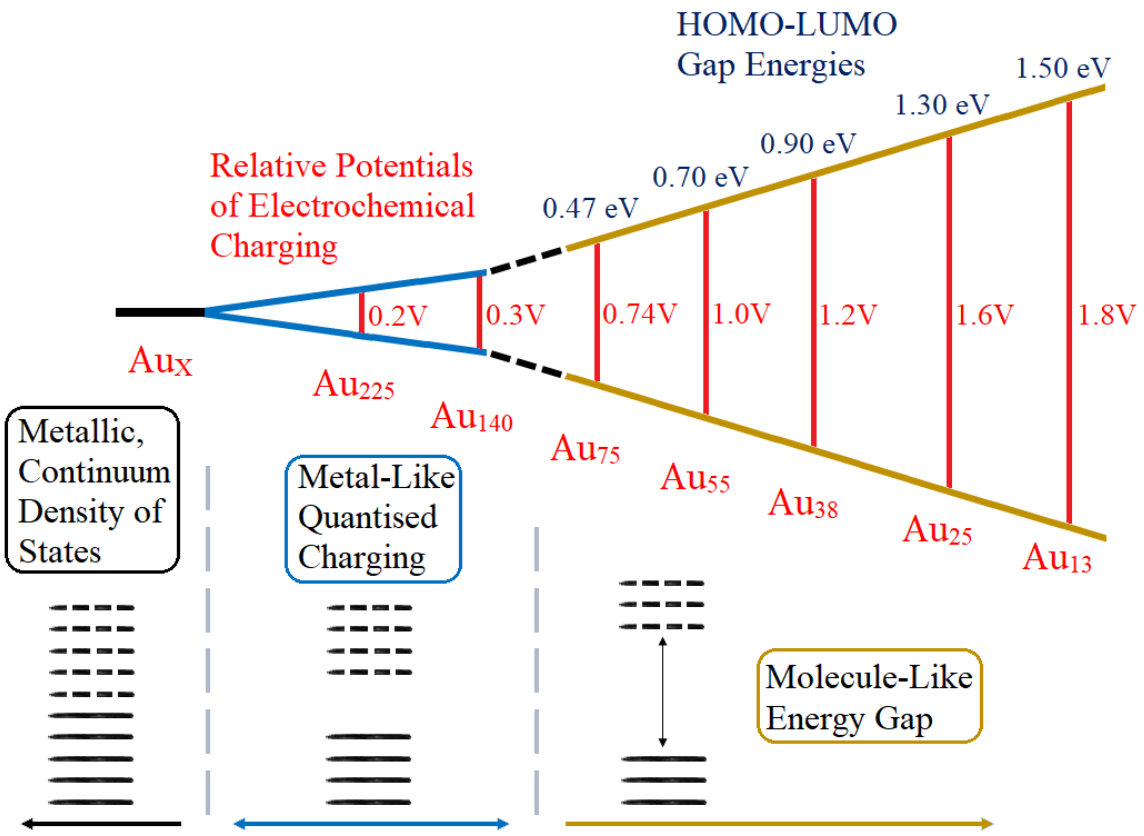

Figure 1.6. How band gap energies change as a function of Au_x nanocluster size (Adapted from [120])

The catalysis by Au nanoclusters in the presence of reactants in the liquid phase has not been investigated as intensely as that in the presence of gas phase reactants and even less so when conducted as hydrogenation reactions; a simple literature search will show that there are around ten times more studies focused on the oxidation reactions utilising Au nanoclusters than on the hydrogenation reactions. While Au in its bulk-form shows no activity for hydrogen chemisorption and dissociation (Table 1.1), supported Au nanoclusters and -particles are capable of catalysing a growing number of selective hydrogenation reactions. Fujitani *et al.* found that by using the H_2-D_2 exchange reaction, Au nanoclusters deposited on TiO_2 (110) were able catalyse the formation of HD with an exponential increase in activity occurring as the mean average of particle size decreased from ~10 nm to ~1.3 nm.[121] The active site for this

exchange reaction is not known as of this time but three sites have been proposed, the perimeter interface between gold nanoclusters and the support, low-coordination sites such as edges and corners on the cluster itself, and free Au cations.[122]

1.6 Scope of this Work

Supported Au catalysts have begun to attract interest for use in catalytic hydrogenation reactions due to their unique selectivity for desired compounds, compared to the Pd, Pt and Cu based catalysts traditionally used in industrially catalysed processes. This selectivity is often achieved with just supported Au nanoparticles without the use of modifiers. The only limitation for Au supported catalysts is their relatively low activity compared to the traditional catalysts. Research has shown that lower size ranges of Au nanoparticles result in improved catalytic activity, but the catalytic activity is averaged over the entire size range. The aim of this work is to determine if catalytic activity and selectivity over supported, atomically precise Au nanoclusters changes with the difference of only one or two Au atoms in the catalytic hydrogenation of substituted nitroaromatics. To the best of my knowledge no previous study exists on the size effects of atomically precise Au nanoclusters in the catalytic hydrogenation of substituted nitro-aromatics.

Because maintaining the size of atomically precise nanoclusters is key to elucidating their catalytic activity, a study was conducted on how effective the support used in achieving the suppression of sintering in the atomically precise Au nanoclusters used in this work.

The role of the support in affecting the activity and selectivity of the atomically precise nanoclusters was investigated using three metal-oxide supports, TiO_2 (anatase and degussa P25), and CeO_2, that are commonly used in research on Au nanoparticles for catalytic reactions. The fourth support, HAP, a nonoxide, has been used to a lesser extent in research, but displays interesting properties such as sintering resistance and a SMSI at lower temperatures than found on supports displaying classical SMSI.

The effect that higher metal weight loadings have on catalytic activity was investigated as the 0.2% Au weight loading used predominantly in this work, is relatively lower than the 1.0% to 2.5% Au weight loadings commonly used in previous studies.

Chapter 2 Characterisation Methods

This chapter describes the basic principles and instrumentation systems of three of the main characterisation methods used in this thesis.

2.1 Gas Chromatography (GC)

Gas Chromatography was the most commonly used method in this thesis as all reactions in this work were conducted in the liquid phase. Gas Chromatography was used for the qualitative and quantitative analysis of product mixtures obtained from the heterogeneously catalysed hydrogenation of substituted nitroaromatics.

Gas Chromatography is a method used to separate individual compounds in a mixture and allow their identification and quantification through the partitioning of individual species between two phases. The first phase is a stationary phase with the second being a mobile phase (carrier gas). A sample is introduced into the system and subsequently vaporised through an injection port to allow its elution through the column as it is carried through by the mobile phase (Figure 2.1). Inert gases such as He or N_2 are commonly used as the mobile phase so as to avoid chemical interaction with compounds during analysis. The separation of the components occurs from the differing strengths of intermolecular interactions a species can have with the stationary phase. These interactions alter the times that species are retained on the stationary phase before their elution and are calculated as retention times which are a sum of the time spent in the mobile and on the stationary phase from the time of injection until the time the species reaches the detector.[123]

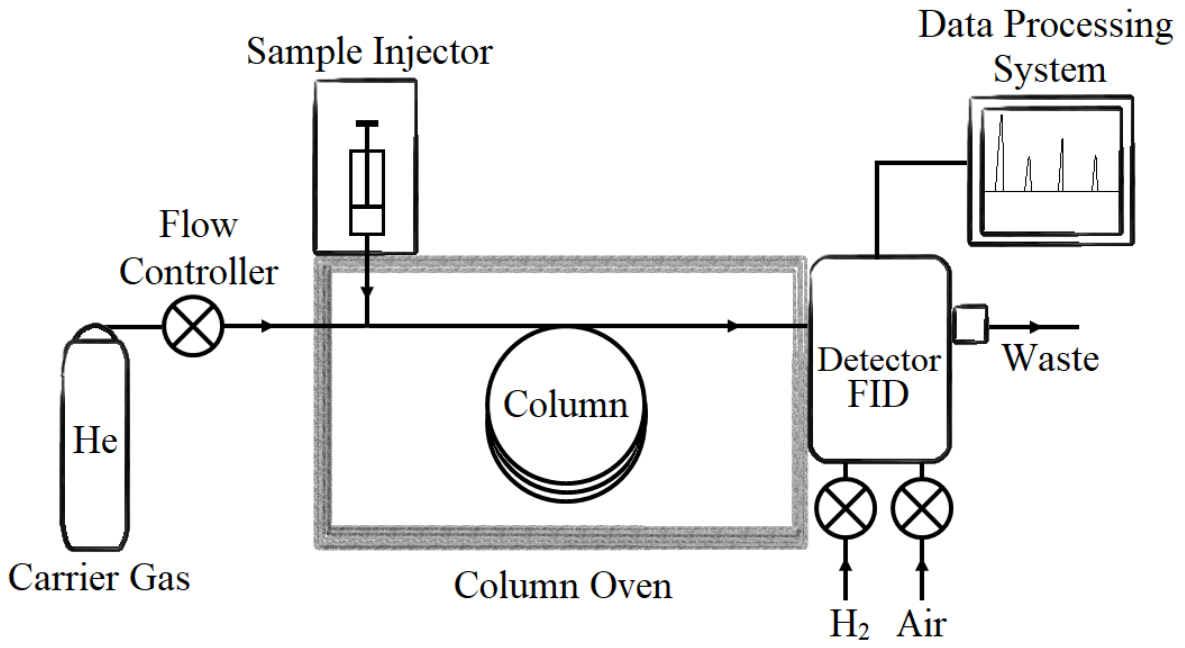

Figure 2.1. Diagram of a Gas Chromatograph instrument equipped with a FID detector.

The stationary phase can be either a liquid phase (Gas-Liquid Chromatography) that can allow partial absorption or a solid phase (Gas-Solid Chromatography) that allows adsorption of compounds from the solute under analysis. Gas-Liquid Chromatography is widely used in research and this work while Gas-Solid Chromatography is seldom used given its limitations. The liquid in the stationary phase is immobilised inside the column in two ways resulting in two types of columns that can be used, packed or capillary columns. Packed columns use an inert, high surface area solid support (e.g. diatomaceous earth) on which the stationary liquid phase is coated and then dry-packed into a column of an appropriate material (typically stainless steel). Capillary columns unlike packed columns do not contain a packing material. Capillary columns have a thin liquid-like polymer film coating the inside of the tube wall of the column. This thin film is chemically bonded often via cross-linking which allows for the formation of thicker more stable films.[124]

The oven which the contains the column is an important part of the GC process as it provides an easy and efficient way to control temperature. Temperature is an important part of

the GC analysis procedure as it influences compounds retention times on the column and thus the resulting separation of single compounds.

There are around 60 types of detectors that can be used in Gas Chromatography with most based around the formation of ions through combustion or ionisation of eluted compounds, that then interact with the detector to produce an electronic signal that is interpreted by a data processing program and converted into a readable chromatograph. The most widely available and commonly used detector is a FID (Flame Ionisation Detector) and has also been used in this work. In a FID the eluted compounds are burned in a hydrogen-air flame where the production of ions and free electrons is measured by the detector. The ions and free electrons are collected, with attraction originating from a polarising voltage, at an electrode and create a measurable current which is proportional to the rate of ionisation and amount of sample that is burned. In this way FID when coupled with an internal standard method can be used for the qualitative and quantitative analysis of compounds, especially hydrocarbons and volatile organic compounds.[125] By using calibration mixtures with known sample concentrations that are prepared from pure samples of compounds, results obtained from the GC-FID process can referenced to these to allow the determination of compound concentrations in reaction mixtures.

2.2 Powder X-Ray Diffraction

Powder X-Ray Diffraction (XRD) is a technique used to provide information about the phase and crystallinity of a solid material such as a Au supported catalyst. In this work Powder XRD was used to characterise supported Au nanocatalysts to determine if aggregation had occurred in the Au nanoclusters deposited on the surface after calcination or reduction treatments and catalysts recovered after catalytic reactions.

Powder XRD is a method used for characterising polycrystalline materials and considered a bulk characterisation method that provides information on the phase (polymorph), preferred crystal orientation and crystallinity of a material as well as other structural parameters such as particle size, internal strain, and defects. This differs from single-crystal XRD which is used for absolute structure determination of a single crystal from the bulk of a material, given that it can provide exact atomic positions in a sample and thus interatomic distances and angles.

In XRD generally a Cu or Mo source located in an X-Ray tube (Figure 2.2) is used to produce monochromatic (single-wavelength) X-Ray beam which is electromagnetic radiation of a short-wavelength. At ~0.1 – 100 Å, these short-wavelengths are around the same order of magnitude as the spacing between the atomic planes in a sample which will allow the generation of a diffraction pattern. A collimator is used to focus the X-Ray beam directed at the sample. Diffraction in XRD occurs from the elastic scattering of X-Ray photons which is primarily caused by the interaction with an atoms electrons, with the atoms themselves forming a periodic lattice. Using Braggs Relationship (*Equation 2.1*) the derivation of lattice spacing is possible in from the coherent and incoherent scattering (which give constructive and destructive interference respectively) of X-Rays as the interact with the lattice planes in a sample.

$$n\lambda = 2d \sin\theta$$

(*Eq 2.1*)

Scattering provides a three-dimensional electron density map which provides a diffraction pattern from the in-phase reflected X-Rays captured by a detector, where the position and orientation of atoms in the crystal can be determined allowing for the structural elucidation of the sample.[126]

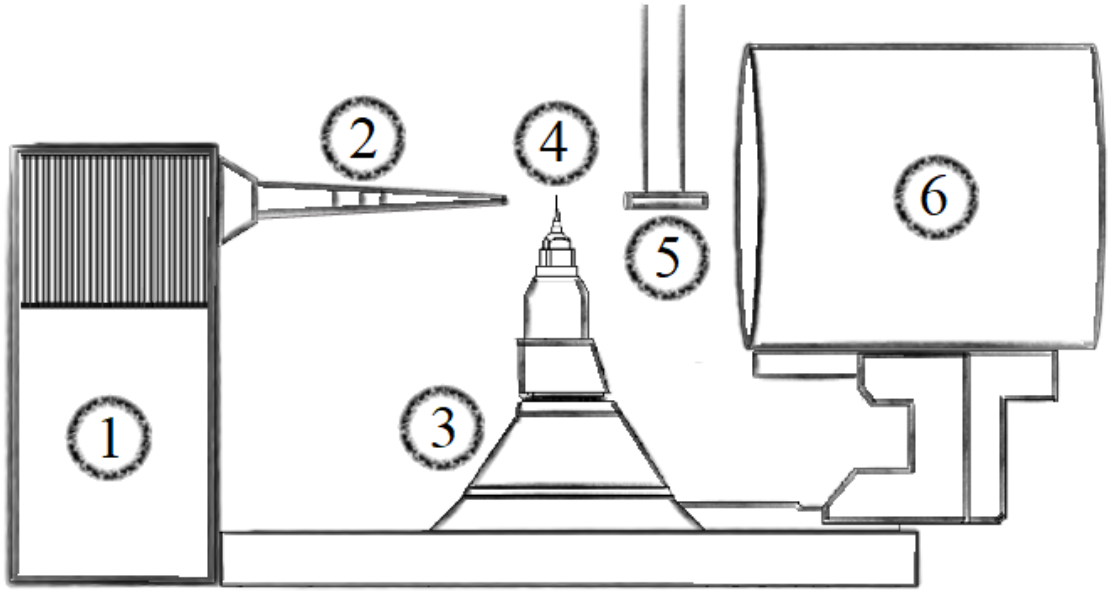

Figure 2.2. Main components of an X-Ray Diffractometer [1] X-Ray Tube, [2] Collimator, [3] Goniometer, [4] Sample Holder, [5] Beam Stop, [6] CCD Detector.

In single-crystal XRD the diffracted, constructively interfering X-Rays give the angle of maximum intensity, 2θ, when the incident X-Rays interact with an atoms electron density in a crystal. This allows Braggs Relationship to be used to calculate the spacings between the atomic planes which are unique to the compound and result in phase identification. In Powder XRD this process is much the same however the diffracted X-Rays maximum intensities are measured as a function of the angle 2θ, which exists between the beam axis and the diffracted X-Ray (Figure 2.3). In a polycrystalline powder sample the X-Rays interact with a small fraction of the powder particles which are orientated in random directions. Because of this random orientation of powder particles there is a requirement that an atomic plane must be at a certain θ in relation to the beam axis for constructive interference to be observed. Rotation of the sample during data collection increases the likelihood of this condition being met, meaning a higher percentage of particles can contribute to diffraction. This diffraction leads to

the forming of a circular diffraction pattern which is processed to give a 2-dimensional powder plot.[127]

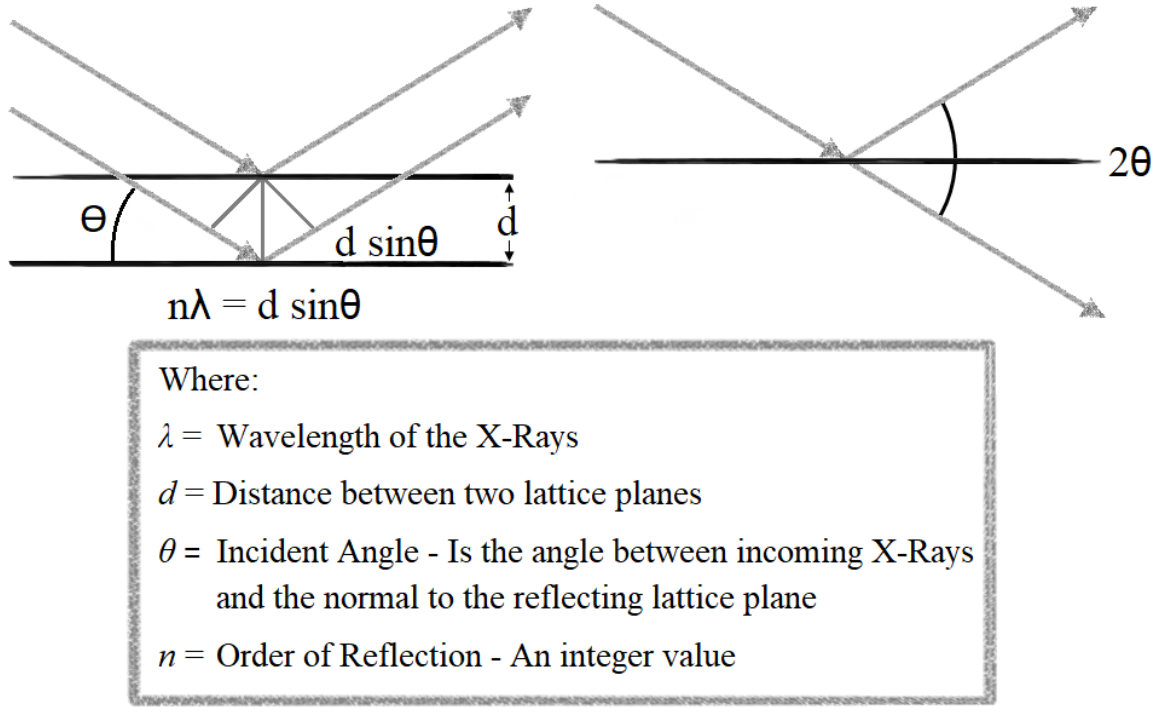

Figure 2.3 Diffraction in Single-crystal XRD (Left) and Powder XRD (Right).

2.3 Ultra Violet and Visible Spectroscopy (UV-Vis)

Ultra Violet-Visible (UV-Vis) Spectroscopy is a technique used for chemical analysis and structural determination where information is obtained from characteristic wavelengths that occur in materials due to electronic transitions as they are irradiated with photons from the ultra-violet and/or visible regions of the electromagnetic spectrum.[128] In this work UV-Vis Spectroscopy was to characterise synthesised Au nanoclusters and as-made, treated and recovered catalysts to determine if aggregation of deposited nanoclusters had occurred.

In UV-Vis analyses, the absorption of a photon as a function of wavelength is measured. Given that the photons frequency is related to the magnitude of electron excitation, the wavelength of maximum absorbance (λ_{max}) can be found as it corresponds to the energy gap

(ΔE) in the transition from the ground to excited states in a material. The Beer-Lambert Law (*Equation 2.3*) is used to describe the change in ratios of intensities, or transmittance as monochromatic light passes through an absorbing medium.

$$log_{10}\frac{I_0}{I} = \varepsilon lc$$

(*Eq 2.3*)

This states that when monochromatic incident beam of light with a certain intensity (I_0) passes through a sample then due to absorption (scattering losses can also result in diminished intensity) the intensity of the transmitted light will be reduced. The relationship between the incident intensity and the transmitted intensity is dependent on the path length (l) of the absorbing sample and the concentration (c) with the intensity of the transmitted light decreasing exponentially as either of these factors increase. The molar absorption coefficient (ε) is a measurement of the fraction of incident light absorbed per unit mass of a material that absorbs some energy of an incident photon (an absorber).

UV-Vis Spectroscopy is carried out in either a transmission mode (for liquid samples) or a diffuse-reflectance mode (for solid samples). In transmission mode the liquid sample is placed in a curvette and placed in the path of a monochromatic beam of photons emitted over a certain range of wavelengths, where a fraction of the photons are absorbed by the sample and a fraction are transmitted. The transmitted photons are captured by a detector UV-Vis spectrometer where λ_{max} is related to ΔE, which is characteristic for a given sample. From this the instrument is able to provide a plot the absorbance (A) versus wavelength (λ) where absorbance is derived from the Beer-Lambert Law in the form of $A = -log(I/I_0)$.[129]

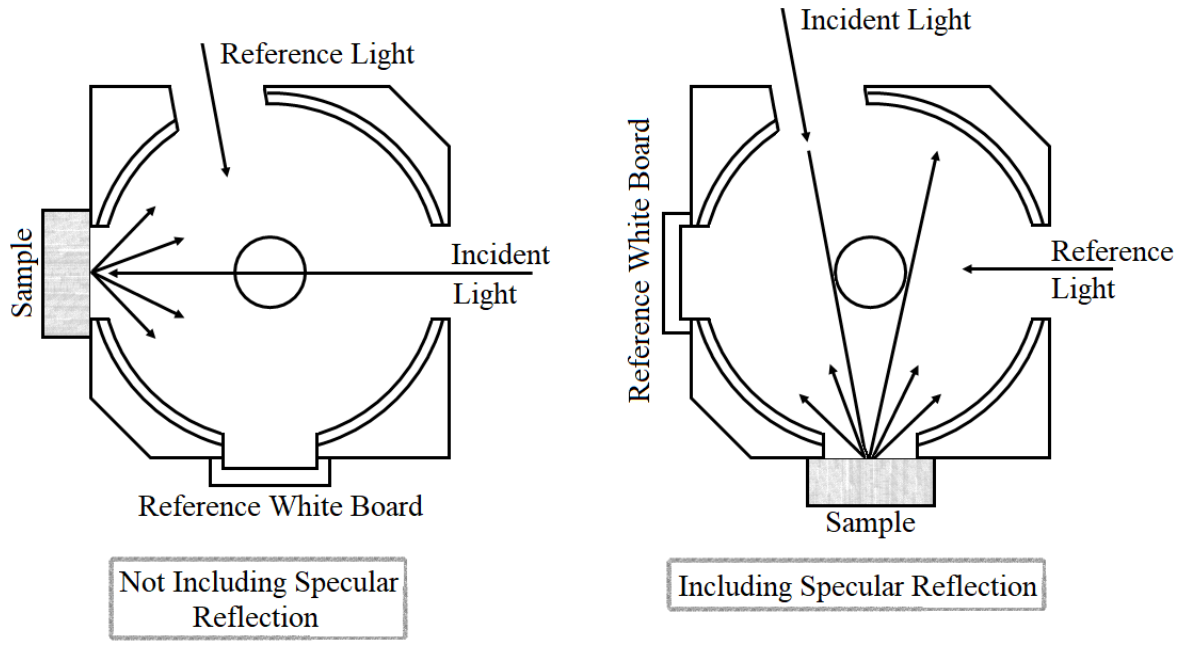

Figure 2.4. Measurement of diffuse reflection using an integrating sphere, not including (left) and including (right) specular reflection.

UV-Vis Diffuse Reflectance Spectroscopy (UV-Vis DRS) is the measurement of incident light scattered in different directions (diffuse reflectance) after interaction with a solid (opaque) material, since light is unable to penetrate the sample. The measurement of diffuse reflected light is most often performed with the use of an integrating sphere (Figure 2.4) which allows the detection of photons scattered in all directions after reflection.

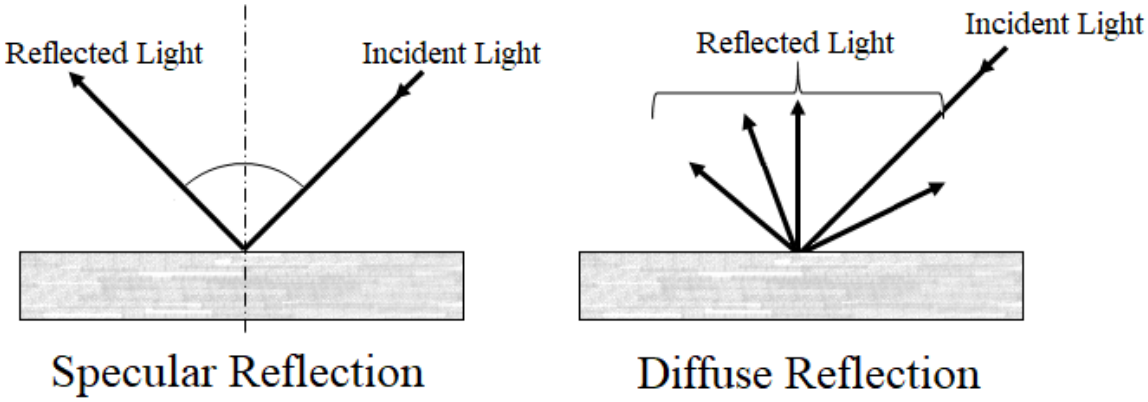

Figure 2.5. Diagram of Specular and Diffuse reflection.

The interaction of light with a solid can result in two types of reflections depending on how a sample is positioned in relation to the angle of incident light; diffuse and specular (Figure 2.5). With specular reflection, the sample is placed at an angle (often 8°) which reflects light at a singular outgoing direction of equal value to the incoming incident light. In DRS spectroscopy, specular reflection contains little information about HOMO-LUMO transitions due to the absence of absorption with the sample and has the possibility of adding to spectral noise. With diffuse reflection the incident beam is directed at 0° so only diffuse reflected light is measured; any specular reflected light exiting the integrating sphere in this way will not be detected. The incident beam is able to slightly penetrate the surface where it interacts and is re-emitted at varying non-incident angles by scattering centres in the sample.[130]

In a typical UV-Vis DRS analysis using an integrated sphere, the spectrophotometer will measure the amount of diffuse light reflected from the sample with the obtained value given as comparative reflectance. The comparative reflectance is in relation to the reflectance of a reference standard white board (often $BaSO_4$ or PTFE), where the absolute reflectance is taken to be 100%. From the obtained comparative reflectance value (R), the Kubelka-Munk function $F(R)$ can be derived from the following equation:

$$F(R) = \frac{(1-R)^2}{2R}$$

(*Eq 2.4*)

Spectra obtained from UV-Vis DRS measurements are generally plotted as $F(R)$ against wavelength λ so they compared with transmission spectra or qualitative analyses.[131]

Chapter 3 Experimental Procedures

All materials obtained from commercially available sources and used without further purification.

3.1 Synthesis of Au Nanoclusters and Their Precursors

$HAuCl_4 \cdot nH_2O$ The protocol for the preparation was adapted from a previous procedure detailed by Brauer.[132] Pure gold metal was dissolved in a solution of *aqua regia*, HNO_3:HCl (1:3 = v/v) in a round bottomed flask covered with filter to paper to allow evolved NO_x to escape. After a few days under rapid stirring a yellow-orange solution was obtained. The solution was rotovaped to dryness to obtain $HAuCl_4 \cdot nH_2O$. Product was stored in the freezer to prevent degradation.

$AuCl(SMe_2)$ The protocol for the preparation was adapted from a previous procedure detailed by Hooper *et al.*[133] Reaction was performed under a N_2 atmosphere using standard Schlenk techniques. HAuCl4·nH_2O (2.5 g, 6.35 mmol) was dissolved in dry MeOH (60ml) and had SMe_2 (2.80 g, 19.05 mmol) in dry MeOH (50ml) added under rapid stirring where a white precipitate began to form. The solution was stirred (800 rpm) for 2 hrs until no colour remained in the solution. The solution was cooled to 0℃ and the product isolated by filtration using a filter stick *in vacuo*. The product was washed with cold EtOH (1 × 10ml) and diethyl ether (3 × 10ml). The product was dried *in vacuo* to yield a white solid.

PhC≡CAu PhC≡CAu was synthesised according to the previous procedure detailed by Wan *et al*.[134] Reaction performed in the absence of light. $AuCl(SMe_2)$ (100.0 mg, 0.34 mmol) and phenylacetylene 47.8 µl (44.5 mg, 0.44 mmol) had 60.3 µl of NEt_3 (44.0 mg, 0.44 mmol) added under stirring (800 rpm). The mixture was stirred for 2 hrs. The solution was evaporated to dryness using reduced pressure evaporation to give a pale yellow solid, which was washed with milliq H_2O (2 × 5 ml), EtOH (2 × 5ml) and diethyl ether (5 ml).

$HdppaAu_2(SbF_6)$ (Hdppa = N,N-Bis(Diphenylphosphino) Amine) $HdppaAu_2(SbF_6)$ was synthesised according to the previous procedure detailed by Wan *et al*.[134] Reaction performed in the absence of light. $AuCl(SMe_2)$ (14.8 mg, 0.05 mmol) and Hdppa (9.7 mg, 0.025 mmol) in DCM (3.0 ml) were stirred for 5 mins. A MeOH (0.1 ml) solution of $AgSbF_6$ (17.1 mg, 0.05 mmol) was added under stirring (800 rpm) and the solution turned into a suspension immediately. The reaction was allowed to continue for 15 min. The resulting solution was then centrifuged for 4 min at 10000 rpm, and the AgCl precipitate was filtered off. The filtrate was evaporated to dryness using reduced pressure evaporation and washed with diethyl ether (2 × 5 ml) to give $HdppaAu_2(SbF_6)$.

$[Au_4(PP_3)]Cl_4$ (PP_3 = [Tris(2-(Diphenylphosphino)ethyl)] Phosphine) $[Au_4(PP_3)]Cl_4$ was synthesised according to the previous procedure detailed by Chen *et al*.[135] Reaction performed in the absence of light. A solution of PP_3 (0.201 g, 0.3 mmol) in acetone (45 ml) was added to a suspension of $AuCl(SMe_2)$ (0.353 g, 1.2 mmol) in acetone (75 ml). The mixture was stirred for 2 hrs to give a white precipitate, which was collected by filtration using a filter stick *in vacuo*. Washed with acetone (2 × 5ml), diethyl ether (2 × 5ml) and n-pentane (2 × 5ml) and dried *in vacuo* to give a white powder.

Dppee Ligand (Dppee = [Bis(2-Diphenylphosphino)ethyl Ether) The Dppee ligand was synthesised according to the previous procedure detailed by Zhang *et al*.[136] Reaction was performed under a N_2 atmosphere using standard Schlenk techniques. 2-Chloro-ethyl ether (0.29 ml, 2.5 mmol) was added to a dry Schlenk flask. Dry THF (20 ml) was then added to the Schlenk flask. After 15 mins stirring (900 rpm), potassium diphenylphosphide solution (10.5 ml, 0.5 M in dry THF) was slowly added to the system. The reaction was allowed to proceed for 24 hrs at 30°C. The solvent was then removed on a rotovap and the product extracted twice with DCM (10 ml). The DCM extractions were combined and filtered. The filtrate was evaporated to give a pale-yellow oil.

$[Au_2(Dppee)](Cl)_2$ $[Au_2(Dppee)](Cl)_2$ was synthesised according to the previous procedure detailed by Zhang *et al*.[136] Reaction was performed under a N_2 atmosphere using standard Schlenk techniques in the absence of light. Dppee (0.4423 g, 1 mmol) was added to a dry Schlenk flask. Dry DCM (5 ml) was added to the flask. After 20 mins stirring (900 rpm), a $AuCl(SMe_2)$ solution (20 ml, 0.1 mmol ml^{-1} in dry DCM) was quickly added to the system. The reaction was allowed to proceed for 36 hrs. The solvents were removed on a rotovap and the product was dried under vacuum for 12 hrs and stored in a vacuum desiccator.

$[Au_{19}(PhC{\equiv}C)_9(Hdppa)_3](SbF_6)$ $[Au_{19}(PhC{\equiv}C)_9(Hdppa)_3](SbF_6)$ was synthesised according to the previous procedure detailed by Wan *et al*.[134] Reaction performed in the absence of light. To a DCM (4.0 ml) suspension containing $PhC{\equiv}CAu$ (44.7 mg, 0.15 mmol) and $HdppaAu_2(SbF_6)$ (28.4 mg, 0.025 mmol), a freshly prepared solution of $NaBH_4$ (0.95 mg in 1.0 ml EtOH) was added dropwise under stirring (800 rpm). The reaction was allowed to continue for 18 hrs. The mixture was evaporated to dryness using reduced pressure evaporation to give a dark solid which was dissolved in DCM (2.2 ml) and centrifuged for 4 min at 10000 rpm. The supernatant was filtered and a dark solid precipitated with the addition of excess diethyl ether:n-hexane (1:1 = v/v). The mixture was then centrifuged for 10 min at 10000 rpm and the supernatant poured off leaving a dark solid. This dissolution-precipitation procedure was repeated until the supernatant became colourless which yielded $[Au_{19}(PhC{\equiv}C)_9(Hdppa)_3](SbF_6)$.

$[Au_{20}(PP_3)_4](Cl)_4$ $[Au_{20}(PP_3)_4](Cl)_4$ was synthesised according to the previous procedure detailed by Wan *et al*.[137] Reaction was performed in the absence of light. A solution of $[Au_4(PP_3)](Cl)_4$ (93.4 mg) in DCM (80 ml) had a solution of $NaBH_4$ (22.1 mg in 3.0 ml EtOH) added dropwise under stirring (900 rpm). The mixture was then stirred for 10 hrs. The solution was then evaporated to dryness using reduced pressure evaporation to give a black solid. The solid was dissolved in DCM (3.0 ml) and MeOH (0.1 ml), and the solution centrifuged for 4 min at 10000 rpm. The brown supernatant was poured off and filtered and a dark solid precipitated with the addition of excess n-pentane. The mixture was then centrifuged for 10 min at 10000 rpm and the supernatant poured off leaving a dark solid. This dissolution-precipitation procedure was repeated until the supernatant became colourless which yielded $[Au_{20}(PP_3)_4](Cl)_4$.

$[Au_{22}(Dppee)_7](Cl)_2$ $[Au_{22}(Dppee)_7](Cl)_2$ was synthesised according to the previous procedure detailed by Zhang *et al*.[136] Reaction was performed under a N_2 atmosphere using standard Schlenk techniques in the absence of light. $[Au_2(Dppee)](Cl)_2$ (102 mg) was dissolved in dry DCM (85 ml). After stirring (900 rpm) for 10 mins a solution of $NaBH_4$ (14.35 mg in 3.5 ml EtOH) was quickly added to the system. The reaction continued for 20 hrs before the solution was evaporated using reduced pressure evaporation leaving a black solid. The product was then extracted twice with DCM (10 ml). The extractions were combined, filtered and evaporated to dryness using reduced pressure evaporation to give a black solid. The black solid was then dissolved in a minimum amount of DCM and centrifuged for 4 min at 10000 rpm. The supernatant was then purified using silica gel chromatography. A column was packed with Silica Gel 60 (230-400 mesh size) and a DCM/ethyl acetate/methanol (8/2/3 ratio respectively) solvent mixture was used as the elutant to obtain a pure fraction of $[Au_{22}(Dppee)_7](Cl)_2$. The fraction was then evaporated using reduced pressure evaporation to yield $[Au_{22}(Dppee)_7](Cl)_2$.

Nitrosobenzene Nitrosobenzene was freshly prepared, given its propensity to decompose over a short period of time, to be used to prepare the standard solution for identifying its retention time in GC analysis and calculating its calibration coefficient. Nitrosobenzene was synthesised according to the previous procedure detailed by Coleman *et al.*[138] with some modification. A mixture of nitrobenzene (2.5 mL, 24.4 mmol) and ammonium chloride solution (1.5 g, 28.0 mmol in 500 mL miliq H_2O) was stirred vigorously (800 rpm). Zinc powder (3.72g, 55.75 mmol) was added in small portions over a period of 30 mins. One hour after the addition of zinc powder the solution was filtered through a Büchner funnel and the zinc oxide residues were washed with boiling miliq H_2O. The filtrate and washings were combined and immediately cooled to 0℃ with the addition of ice. To the cold solution of β-phenylhydroxylamine, an ice-cold solution of concentrated sulfuric acid (7.5 mL) and enough ice to cool the solution to -3℃ was added under vigorous stirring (800 rpm). To this mixture an ice-cold solution of sodium dichromate dihydrate (1.7g, 5.7 mmol in 60 mL miliq H_2O) was added rapidly under stirring. After 10 mins the Nitrosobenzene was collected on a Büchner funnel, washed with 100 mL miliq H_2O and dried under suction. The powder was then recrystallised from a small amount of EtOH to give Nitrosobenzene.

The Au nanoclusters and their precursors were characterised with NMR, IR and UV-Vis spectroscopic techniques and Thermogravimetric Analysis (TGA). Nitrosobenzene was characterised with NMR spectroscopy.

3.2 Synthesis of Hydroxyapatite (HAP) Support

HAP was synthesised according to the previous procedure detailed by Liu *et al.*[139] Solution A was prepared by dissolving 11.80 g of $Ca(NO_3)_2 \cdot 4H_2O$ in an EtOH-water mixture (100 ml; 1:1 = v/v) maintained at 0 ℃. The pH of the solution was adjusted to 11 with the addition of ammonia solution followed by stirring (900 rpm) for 1 hr. Solution B was prepared by placing 4.03 g $(NH_4)_2HPO_4$ into milli-Q H_2O (50 ml) and ammonia solution until the pH became 11. Solution B was injected into Solution A over a period of 30 mins and the mixture stirred (1000 rpm). The mixture was continuously mixed in an ice-bath at 0 ℃ for another 3 hrs and the resulting slurry was aged for a further 24 hrs with no stirring. The precipitate was obtained by centrifugation (10000 rpm for 10 mins) and the supernatant poured off. The precipitate was washed this way3 times with milli-Q H_2O and recentrifugation to separate the precipitate. The precipitate was dried for 24 hrs using a freeze drier and calcined at 500 ℃ for 4 hrs in static air in a tube furnace.

HAP was characterised using Powder XRD, IR and N_2 adsorption/desorption isotherms for surface area analysis.

3.3 Characterisation of Materials

The NMR spectra of the Au nanoclusters and their precursors were obtained using an Oxford/Varian AS500 500 MHz spectrometer. The NMR of all synthesised compounds, precursors and nanoclusters closely matched the previously reported literature spectrums. $AuCl(SMe_2)$'s spectrum was recorded in $CDCl_3$. The ^{13}C-NMR gave ~ δ 76.99 ppm (3C). The ^{1}H-NMR gave two singlets at δ 2.75 and 1.54 ppm with the peak at 1.54 ppm indicating the presence of H_2O in the sample. $HdppaAu_2(SbF_6)$'s spectrum was recorded in $CDCl_3$. The ^{13}C-NMR gave a triplet at ~ δ 76.99 ppm. The ^{1}H-NMR gave a triplet ~ δ 7.60 ppm, a doublet ~ δ 7.51 ppm, and a singlet ~ δ 1.53 ppm. $[Au_2(Dppee)](Cl)_2$'s spectrum was recorded in CD_2Cl_2.

The ^{31}P-NMR gave a singlet at δ 89.42 ppm, a doublet ~ δ 31.64 ppm, a triplet ~ δ 24.82 ppm and a singlet at δ -1.24 ppm. The peak at δ 89.42 ppm is most likely unreacted diphenylphosphine that has coordinated with Cl ions, the doublet at ~ δ 31.64 ppm is most likely a decomposition product in the form of phosphine oxides and the singlet at δ -1.24 ppm is most likely a diphenylphosphine decomposition product. $[Au_{19}(PhC{\equiv}C)_9(Hdppa)_3](SbF_6)$'s spectrum was recorded in CD_2Cl_2. The ^{31}P-NMR gave a singlet at δ 75.86 ppm. $[Au_{20}(PP_3)_4](Cl)_4$'s spectrum was recorded in $CDCl_3$. The ^{31}P-NMR gave a singlet at δ 64.01 ppm, singlet at δ 54.62 ppm, a quadruplet at δ 47.63 ppm, a singlet at δ 40.50 ppm, a singlet at δ 37.94 ppm, a singlet at δ 32.00 ppm, and a a singlet at δ 18.40 ppm. $[Au_{22}(Dppee)_7](Cl)_2$'s spectrum was recorded in CD_2Cl_2. The ^{31}P-NMR gave a singlet at δ 49.71 ppm, a singlet at δ 29.27 ppm and a doublet at δ 24.70 ppm. The singlet at δ 29.27 ppm was likely due to the formation of dppee oxides. Nitrosobenzene's spectrum was recorded in $CDCl_3$. The The ^{13}C-NMR gave ~ δ 166.2 ppm (1C), ~ δ 129.5 ppm (2C), ~ δ 124.7 ppm (1C) ~ δ 121 ppm (2C). The ^{1}H-NMR gave a quadruplet ~ δ 7.84 ppm, a doublet ~ δ 7.70 ppm, and a quadruplet ~ δ 7.40 ppm.

The IR spectrum of PhC≡CAu was recorded using a Bruker Alpha Platinum ATR spectometer. Peaks were recorded at *v* 3052, 1955, 1592, 1481, 1440, 760, 686, 534, 529.

The UV-Vis absorption spectra for $[Au_{19}(PhC{\equiv}C)_9(Hdppa)_3](SbF_6)$, $[Au_{20}(PP_3)_4](Cl)_4$, and $[Au_{22}(Dppee)_7](Cl)_2$ was recorded using a Cintra 4040 UV-Vis spectrometer. The spectrums were all recorded in CH_2Cl_2. The spectrums (Figure 3.1) all closely matched the reported spectrums. $[Au_{19}(PhC{\equiv}C)_9(Hdppa)_3](SbF_6)$ had a peak at λ 540 nm and a slight peak around λ 380 nm. $[Au_{20}(PP_3)_4](Cl)_4$ had a peak at λ 480 nm and a peak around λ 350 nm. $[Au_{22}(Dppee)_7](Cl)_2$ was rather featureless apart from the increasing absorbance being at ~ λ 800 nm. This however closely matches the literature UV-Vis spectrum for this nanocluster

when it was recorded 3 days after purification following its synthesis which is the same amount of time that this spectrum was recorded after purification following its synthesis.

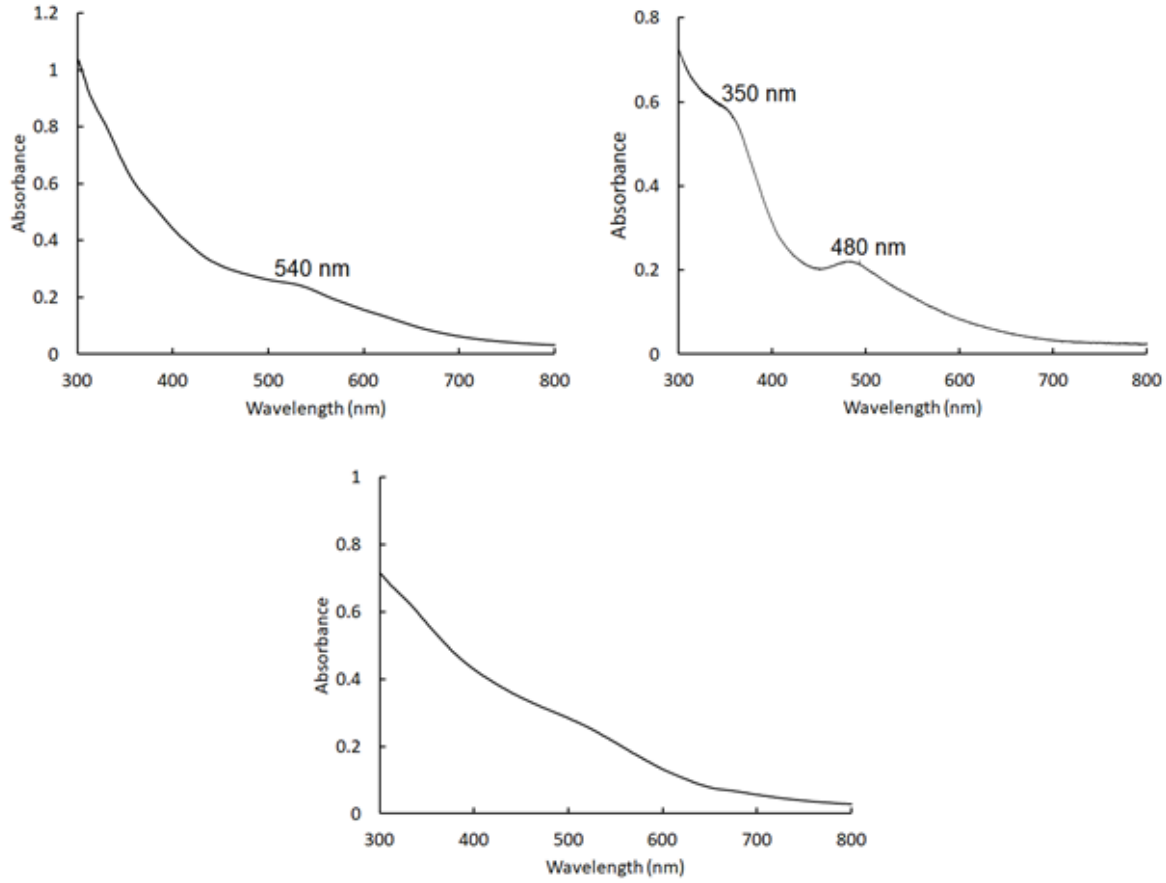

Figure 3.1. UV-Vis Spectrums of $[Au_{19}(PhC{\equiv}C)_9(Hdppa)_3](SbF_6)$ (top left), $[Au_{20}(PP_3)_4](Cl)_4$ (top right) and $[Au_{22}(Dppee)_7](Cl)_2$ (bottom).

Thermogravimetric analysis was performed using an Alphatech SDT Q500 under a N_2 atmosphere. The nanoclusters were heated at a rate of 10℃/min from room temperature to 800℃. The TGA showed 27.03% for $[Au_{19}(PhC{\equiv}C)_9(Hdppa)_3](SbF_6)$, 43.51% for $[Au_{20}(PP_3)_4](Cl)_4$, and 25.19% for $[Au_{22}(Dppee)_7](Cl)_2$ weight loss from the initial weight (Figure 3.2). The expected values of weight loss were calculated at 40.41%, 42.55% and 41.69% respectively based on the expected loss from their phosphine-based ligands. The analysis for $[Au_{20}(PP_3)_4](Cl)_4$ matched closely with the literature data, however no literature data existed for $[Au_{20}(PP_3)_4](Cl)_4$ and $[Au_{22}(Dppee)_7](Cl)_2$. Given that the analyses were conducted on different days the errors could be attributed to instrumental error.

As detailed in Chapter 6 a small amount of 4,4'-Dinitroazobenzene crystallised out of all the reaction mixtures after they were cooled in the freezer. It was characterised with NMR and IR spectroscopic techniques. The NMR spectra was obtained using an Oxford/Varian AS500 500 MHz spectrometer. 4,4'-Dinitroazobenzene's spectra was recorded in $(CD_3)_2SO$. The ^{13}C-NMR gave ~ δ 150.6 ppm (2C), ~ δ 147.6 ppm (2C), ~ δ 125.8 ppm (4C), ~ δ 124.75 ppm (4C). The ^{1}H-NMR gave a double doublet at δ 8.19 ppm, and a double doublet at δ 8.44 ppm. The IR spectrum of 4,4'-Dinitroazobenzene was recorded using a Bruker Alpha Platinum ATR spectrometer. Peaks were recorded at *v* 1600, 1510, 1479, 1338, 1317, 1172, 1093, 1006, 857, 813, 751, 683, 506. This data closely matched the literature data for 4,4'-Dinitroazobenzene.

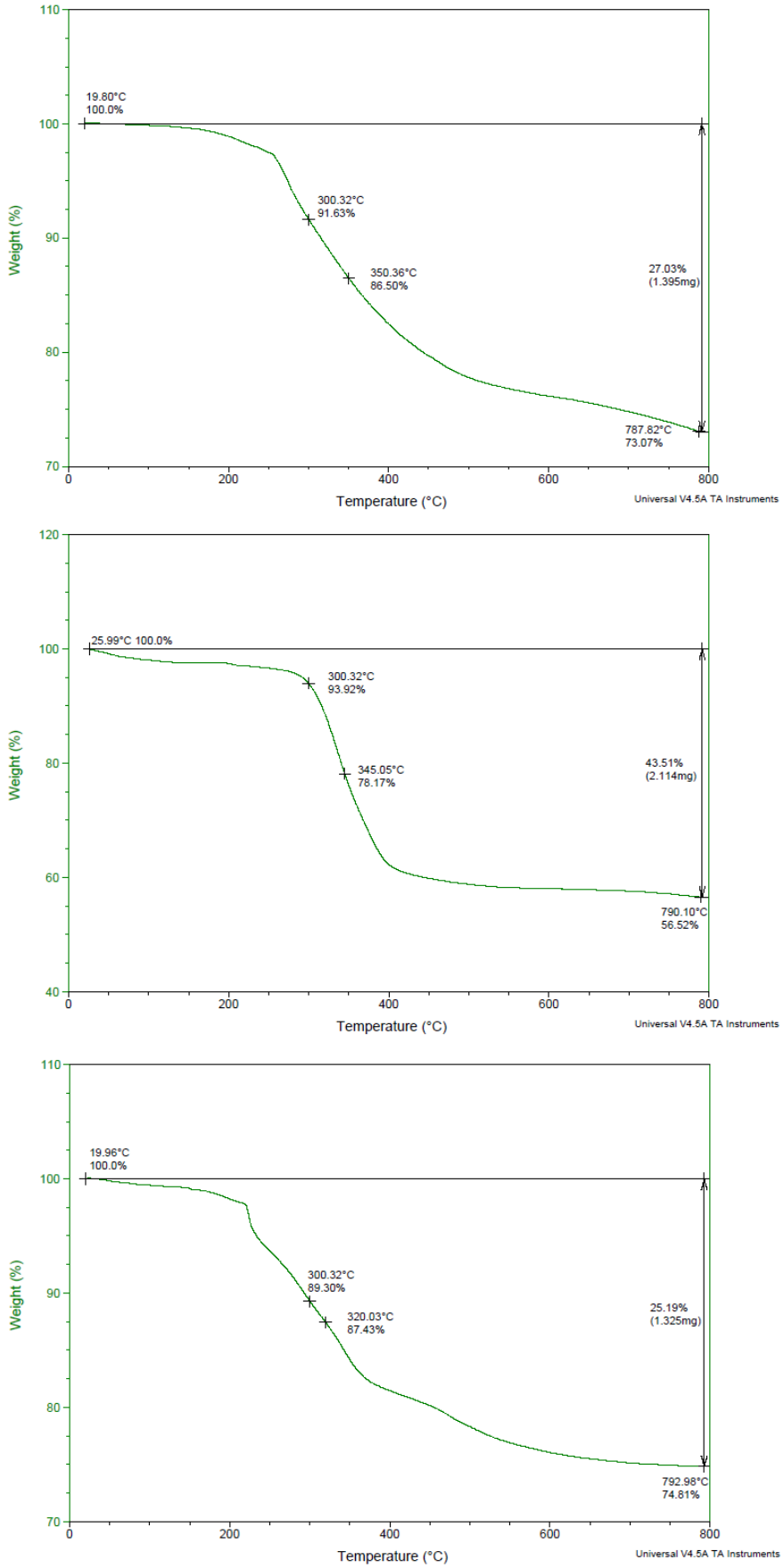

Figure 3.2. TGA curves for $[Au_{19}(PhC{\equiv}C)_9(Hdppa)_3](SbF_6)$ (Top), $[Au_{20}(PP_3)_4](Cl)_4$ (Middle), and $[Au_{22}(Dppee)_7](Cl)_2$ (Bottom).

Analysis of HAP was performed using Powder XRD and IR spectroscopy. Powder XRD was performed using an Agilent Supernova SCXRD diffractometer with CuKα radiation. The sample was packed into a ~ 80 mm long piece of Rtx-50 GC column tubing and mounted on a sample needle and analysed using powder experiment mode.

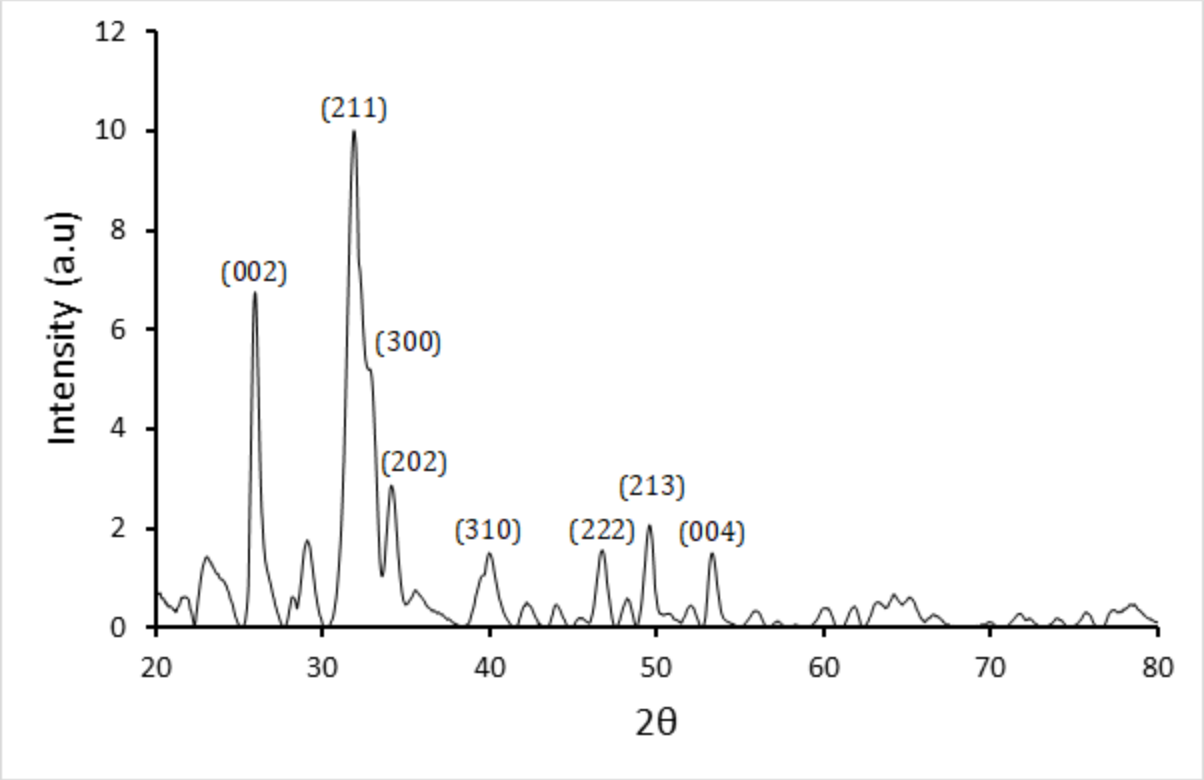

Figure 3.3. Powder XRD diffractogram of synthesised HAP.

The Powder XRD diffractogram (Figure 3.3) closely matches that of HAP found in the literature.

The IR spectrum of HAP was recorded using a Bruker Alpha Platinum ATR spectometer. Peaks were recorded at *v* 3570, 1431, 1092, 1032, 618, 588.

The specific surface area of synthesised HAP was calculated according to the Brunauer–Emmett–Teller (BET) method. N_2 adsorption/desorption isotherms were measured at 77K using a Micrometrics Instrument Corp. Gemini VII 2385 after the samples were degassed and

dried overnight at 200℃. The surface area was calculated to be 77.14 m^2 g^{-1} which was 23 m^2 g^{-1} lower than the value reported in the literature the synthesis method was based on.

3.4 Preparation and Characterisation of Nanocatalysts

Techniques for the characterisation of the synthesised nanocatalysts, such as the direct imaging of the Au nanoclusters on the support surface (HAADF-STEM), elemental analysis (AAS), determining the structural and electronic properties of the deposited Au nanoclusters (XPS), and determination of the Au% content of the synthesised nanocatalysts (ICP-MS) were all considered. These techniques, however, were all unavailable at the time this study was conducted. The AAS instrument in the UC Department of Chemistry was unavailable due to it becoming inoperational. The ICP-MS instrument had also been shown inaccuracies in detecting concentrations of Au after a series of prepared standards showed an order of magnitude higher Au content than what was present. XPS capabilites are not available at UC.

The supports used for the preparation of the nanocatalysts were TiO2 (pure anatase), TiO_2 (Degussa, P-25), CeO_2 and HAP. Prior to deposition the supports were dried in an oven at 120℃ overnight then cooled to room temperature. Following this the support was added into a round bottomed flask with dry DCM (30 ml) to form a slurry and the flask sealed. The flask was then sonicated for 10 mins and then stirred (900 rpm) for 10 mins. A calculated amount of Au nanocluster equivalent to a 0.2% weight loading by Au weight (See Table 3.4) was dissolved in a minimum amount of dry DCM and injected into the slurry under stirring (1000 rpm).

Table 3.4. Calculated weight of Au_x nanocluster needed for 0.2% wt loading

Nanocluster	Au wt% of cluster	Nanocluster wt (g) per 1 g of support
$[Au_{19}(PhC{\equiv}C)_9(Hdppa)_3](SbF_6)_2$	59.59	0.00336
$[Au_{20}(PP_3)_4]Cl_4$	57.46	0.00348
$[Au_{22}(Dppee)_7]$	58.32	0.00343

The slurry was allowed to stir for 3 hrs with deposition being completed as indicated by the colourless supernatant. An aliquot was taken of the supernatant was taken and the absorption spectrum analysed on a Cintra 4040 UV-Vis spectrometer to detect the absence of characteristic Au nanoclusters peaks to confirm that deposition had been completed. The solvent was then removed using reduced pressure evaporation and the catalyst dried under vacuum for 6 hrs. The catalysts that utilised TiO2 (pure anatase), TiO_2 (Degussa, P-25), CeO_2 supports were then calcined in a tube furnace at 300℃ for 2 hrs under static air (HAP's post-deposition treatment will be detailed in section 3.4.1). The ramping rate for calcination was kept at 2℃/min for all catalysts and the furnace cooled naturally after calcination was complete. UV-Vis DRS was used to characterise the catalysts as-made. UV-Vis DRS and Powder XRD were used to characterise after calcination, and recovered after catalytic reactions.

Powder XRD was performed on all nanocatalysts using an Agilent Supernova SCXRD diffractometer with CuKα radiation. The sample was packed into a ~ 80 mm long piece of Rtx-50 GC column tubing and mounted on a sample needle and analysed using powder experiment mode.

By using the Scherrer equation (*Equation 3.1*) the crystallite size of Au nanoparticles can be estimated.

$$D = \frac{b\lambda}{\beta \cos\theta}$$

(*Eq 3.1*)

Where D is the crystallite size, b is the shape constant (generally between 0.89 and 0.94) λ is the wavelength of the X-rays, β is the full width at half the maximum of the peak, and θ the Bragg angle.[140] Due to a non-dedicated Powder XR diffractometer being used to characterise the nanocatalysts the resolution of obtained diffractograms was low due to poorly defined diffraction patterns (Figure 3.4). For this reason the Scherrer equation was unable to be used to qualitatively analyse the sintered Au nanoclusters in Chapter 7.

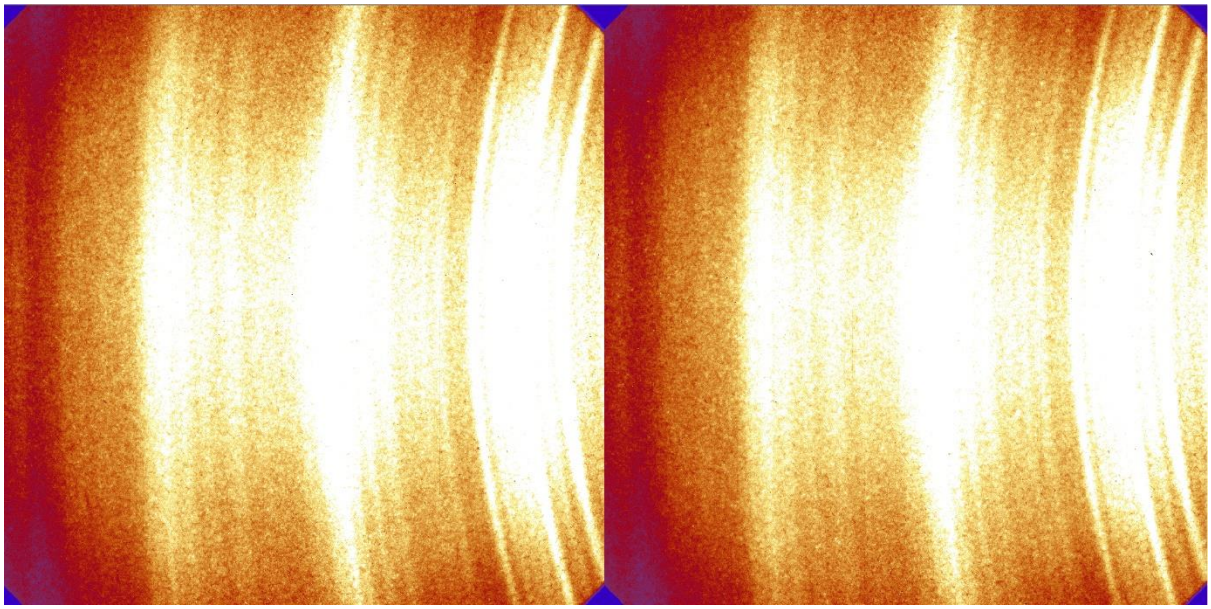

Figure 3.4. Obtained diffraction patterns of 2.5% Au_{22}/HAP-H_2 (left) and Au_{22}/HAP-H_2 recovered after hydrogenation of nitrobenzene (right)

Results will be discussed in Chapter 5.

3.4.1 Preparation of Au-based HAP nanocatalysts

The preparation of Au supported HAP nanocatalysts followed the same 0.2% weight loading deposition procedure as detailed in Section 3.4 with an additional series of nanocatalysts that were prepared with higher weight loadings by percentage of Au weight (Table 3.4.1).

Table 3.4.1 Calculated weights of Au_x nanoclusters to achieve target weight loading

Nanocluster	Weight Loading (%)	Nanocluster wt (g) per 1 g of support
$[Au_{19}(PhC{\equiv}C)_9(Hdppa)_3](SbF_6)_2$	0.5	0.00839
	1.0	0.01678
	2.5	0.04195
$[Au_{20}(PP_3)_4]Cl_4$	0.5	0.00870
	1.0	0.01740
	2.5	0.04351
$[Au_{22}(Dppee)_7]$	0.5	0.00857
	1.0	0.01715
	2.5	0.04287

Following deposition, the Au supported HAP nanocatalyst was calcined in a tube furnace at 400℃ for 2 hrs under static air with a ramp rate of 2℃/min for each nanocatalyst. The furnace cooled naturally after calcination was complete. Au supported HAP nanocatalysts were further reduced under pure H_2 using a gas-flow system attached to a furnace tube. The system was flushed for 15 mins with Ar to remove any O_2 in the system. H_2 was then flowed for 10 mins to flush the line before Ar was flowed for another 5 mins to flush the system again. The furnace program was then started with Ar flow continuing. The ramp rate was 2℃/min to 400℃ with Ar flow (190 sccm) being ceased at 390℃ and H_2 flow (15 sccm) started. The reduction of the catalysts was carried out for 2 hrs before the furnace was cooled naturally.

When the furnace reached 390℃ during cooling, the H_2 flow was ceased and Ar flow (190 sccm) begun again until the furnace had cooled to 30℃. UV-Vis DRS was used to characterise the catalysts as-made, after calcination, after reduction treatments and recovered after catalytic reactions. Powder XRD was used to characterise the catalysts after reduction treatments and recovered from reactions. Results will be discussed in Chapter 5.

3.5 Experimental Catalytic Tests

All catalytic hydrogenation reactions were carried out in a batch reactor (Parr-like) (Figure 3.5) with a 60 mL PTFE liner containing the reaction mixture. In a typical experiment the PTFE liner was charged with 15 mL EtOH, 0.1 g of nanocatalyst and 2 mmol of reactant for p-nitro-benzene, -toluene, and -phenol, and 0.297 mmol of 1,4-dinitrobenzene hydrogenation reactions. The liner was sonicated for 4 mins, then placed in the batch (Parr-like) reactor and the reactor was sealed. The reactor was flushed sequentially with N_2, H_2, and finally pressurised to 10 bar with H_2. The reaction mixture was stirred with a magnetic stirrer bar at 700 rpm with a set reaction temperature of 100 ℃. with the reaction time beginning after the reactor reached the set temperature. After 5 hours (unless stated otherwise) stirring and heating were ceased, and the reactor cooled in an ice bath. The reaction mixture was separated from the nanocatalyst with centrifugation (12000 rpm for 10 mins) and filtered through a 45 μm pore size PTFE filter. The recovered catalyst was washed 3 times 25 mL with EtOH (re-dispersion followed by centrifugation and separation) and dried under vacuum

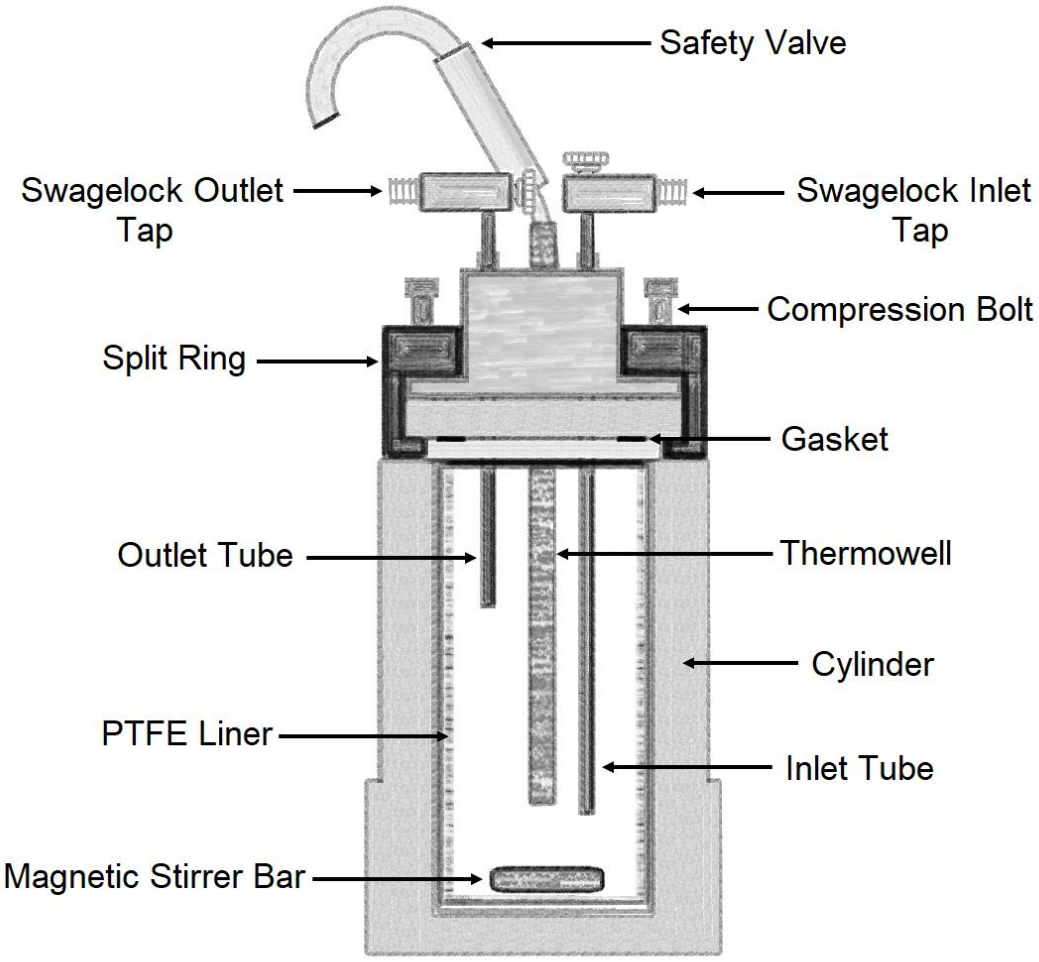

Figure 3.5. Diagram of the Parr-like batch reactor used in catalytic hydrogenation experiments.

The reaction mixtures from the catalytic hydrogenation reactions were qualitatively and quantitatively analysed by Gas Chromatography (GC) using a Shimadzu GC-2010 with a Restek Rtx-50 PMPS column installed and equipped with a Shimadzu AOC-20i auto injector and Flame Ionisation Detector (FID). The gas chromatographic conditions used to carry out the analyses of the reaction mixtures obtained from p-nitro-benzene, -toluene, -phenol, and 1,4-ninitrobenzene hydrogenation were specific for each of the reaction sets (Figure 3.6 - 7). The ideal chromatographic conditions to obtain ideal peak separation and resolution were determined using standard solutions containing relatively pure samples of reactants and the expected products from the reactions.

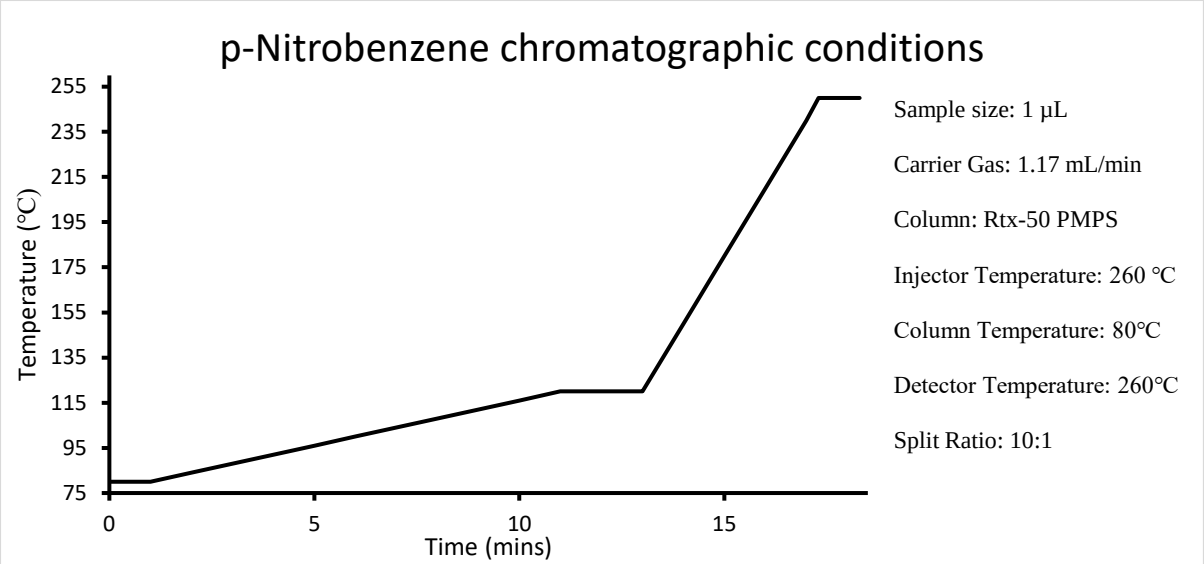

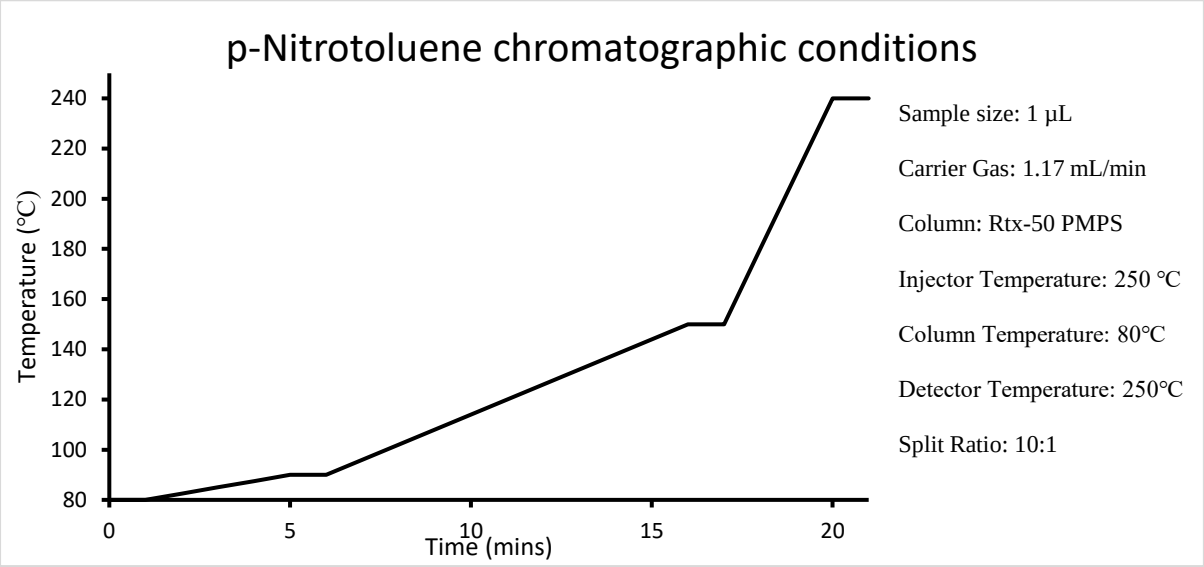

Figure 3.6. Gas Chromatographic Conditions for a given reaction set.

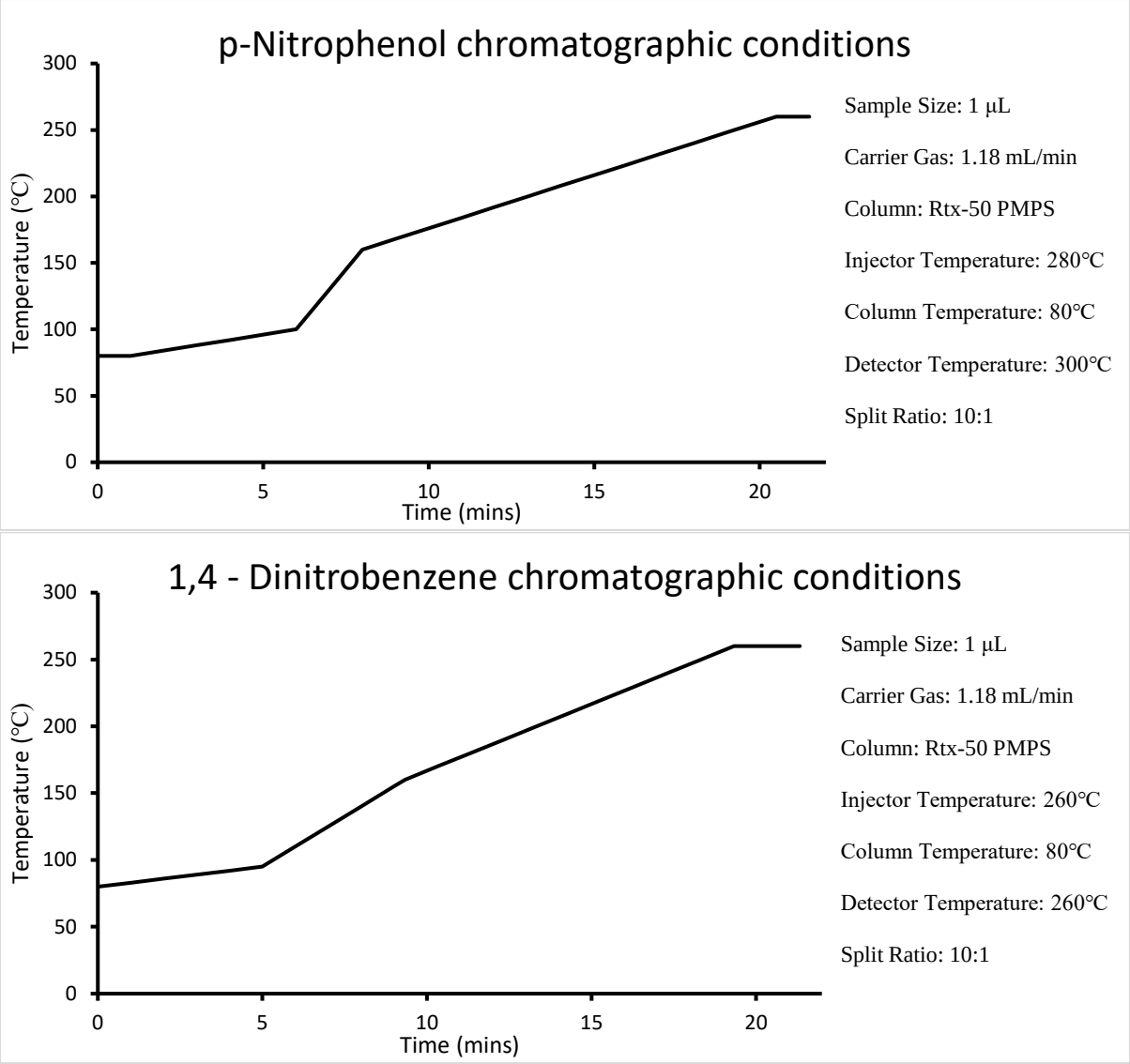

Figure 3.7. Gas Chromatographic Conditions for a given reaction set.

The standard solutions were also used to quantitatively analyse reaction mixtures obtained from catalytic hydrogenation reactions. Standard solutions were prepared containing known concentrations of reactants and products, along with 10 µL of an internal standard n-Decane. Typically, unless otherwise stated, a standard solution contained 2 mmol of analyte in 15 mL EtOH. 1.0 mL, 0.8 mL, 0.6 mL, 0.4 mL, and 0.2 mL aliquots of the standard solution were taken with sub-1.0 mL samples made up to a volume of 1.0 mL with the addition of EtOH. 10 µL of n-Decane was then added to each 1 mL sample. Given that the molar amount of analyte in each sample was known, the molar amount of analyte in a 1 µL sample injection into the GC-FID could be calculated.

Calibration curves were plotted in coordinates $n_{analyte}$ - $R_{analyte}/R_{decane}$, where $n_{analyte}$ is the molar value of the compound in the 1 μL injection of sample into the GC column for analysis, $R_{analyte}$ – peak area obtained from the chromatogram of the corresponding analyte, and R_{decane} – peak area peak area obtained from the chromatogram for n-Decane. Calibration coefficients were obtained from a linearization of plotted calibration curves.

The calibration coefficients were then used to calculate the molar amounts of analytes in reaction mixtures from the peak-area ratio of analyte/n-Decane. This was determined from chromatograms obtained from the analysis of 1 mL samples which contained 10 μL n-Decane as an internal standard. These molar amounts correlated to the amount of sample in 1 μL injection and by dividing by dilution factors, the molar amount contained in the reaction mixture could be calculated.

The reaction mixtures from the catalytic hydrogenation reactions that were found to contain azobenzene or substituted symmetric azobenzene's were qualitatively analysed using High Performance Liquid Chromatography (HPLC). This is due the azo-compounds thermal stabilities and high molecular weight which limited their detection using the GC oven temperature program used for detecting all other products from reactions in GC-FID analysis. HPLC was conducted using a Thermo Fisher Scientific Dionex Ultimate 3000 series equipped with a Luna C18(2) 100A column of 5.0 μm particle size (250 × 4.60 mm). Miliq H_2O containing 0.005% (v/v) trifluoroacetic acid and acetonitrile were the mobile phases A and C respectively. Gradient elution (Figure 3.6) was used to obtain the appropriate separation for compounds. UV-Vis analyses were conducted using a Thermo Fisher Scientific Dionex Ultimate 3000 Rapid Separation Diode Array Detector where scans were conducted over the 210 – 450 nm wave-range.

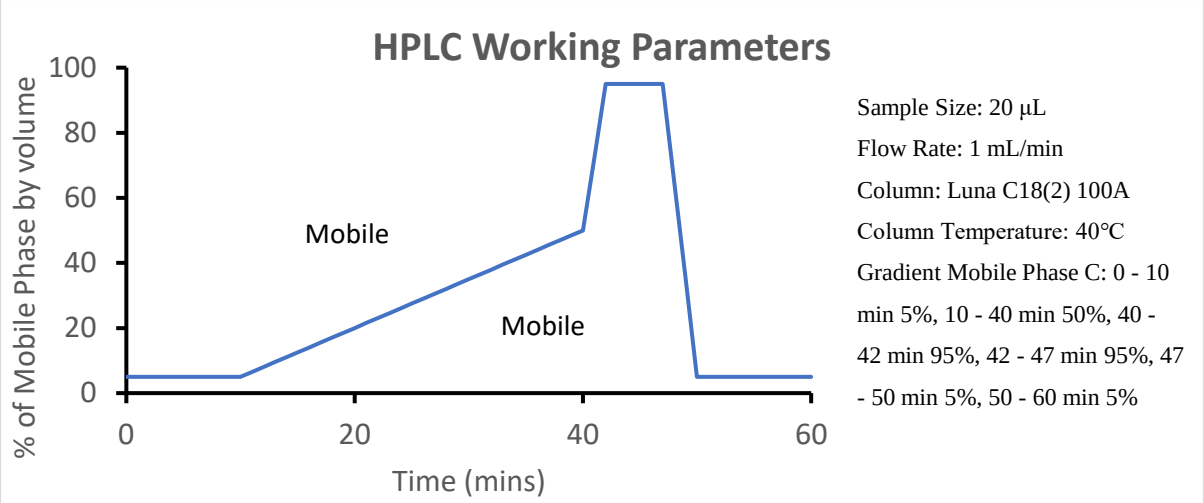

Figure 3.6. HPLC Working Parameters for Azo- and substituted symmetric Azobenzene detection.

Quantitative analysis was carried out in the same way as GC-FID analysis. Standard solutions were prepared containing known concentrations of reactants and products, along with 10 µL of an internal standard n-Decane. A standard solution contained 1 mmol of commercially available Azo-, Azoxy-, or Hydrazo-benzene in 15 mL EtOH. 1.0 mL, 0.8 mL, 0.6 mL, 0.4 mL, and 0.2 mL aliquots of the standard solution were taken with sub-1.0 mL samples made up to a volume of 1.0 mL with the addition of EtOH. 10 µL of n-Decane was then added to each 1 mL sample. Given that the molar amount of analyte in each sample was known, the molar amount of analyte in a 20 µL sample injection onto the HPLC column could be calculated.

Chapter 4 Effect of Support in Preventing Sintering of Supported Au Nanoclusters

4.1 Introduction

The importance of the support in preventing the sintering of Au nanoclusters deposited on the surface, after activation treatments, and during catalytic processes cannot be understated. The unique physical and chemical properties that atomically precise Au nanoclusters possess in terms of higher catalytic activity, quantum confinement effects, and a high number of uncoordinated sites are a result of their subnanometre size; the one consequence of this subnanometre size though is the lack of thermal stability at high temperatures and pressure which is one of the reasons limiting their use for industrial applications. The relatively low stability of Au-based catalysts has been attributed to Au's low Tammann temperature (395℃).[141] The Tammann temperature is the temperature at which the atoms of a solid have acquired sufficient energy for bulk mobility to become appreciable, which results in the sintering of Au nanoparticles as they approach this temperature.[142] While all chemically synthesised Au nano-clusters and -particles are stabilised by protecting groups, these generally decompose or get removed from the cluster core at high temperatures (around 250 ℃ and above) used in activating supported Au-based heterogeneous catalyst. The bare Au nanoclusters formed as a result of these treatments are left unprotected and are, thus, not averse to sintering and deactivation. To properly gain an insight into and understanding of their activity and selectivity, atomically precise Au nanoclusters must be prevented from sintering. While the properties affecting the interaction of Au nanoclusters with supports are often not well understood, there is a general agreement that the nature of the support is a determining factor that affects the stability of supported metal nanoparticles and Au nanoclusters as discussed in sections 1.3.4 and 1.3.5. Given that supported Au nanoclusters can demonstrate

varying thermal stability dependent on the support, three metal-oxides, titania TiO_2 (Degussa P25 and anatase), rare earth-based oxide CeO_2, and a nonoxide support, hydroxyapatite HAP were used in this work.

TiO_2 has been a very widely used support for Au-based heterogeneous catalysts as it provides a reasonable metal-support interaction with good chemical stability allowing some protection against the sintering of Au nanocluster under the right thermal conditions.[143] It has also been shown that the morphology and crystalline phase of TiO_2 can affect Au nanoparticle sintering, where during calcination at 300 ℃ the degree of sintering increased in the order of the mesoporous titania, rutile, anatase, and brookite crystalline phases.[144] CeO_2 has shown promise as a heterogeneous catalyst support given its high thermal stability[145] as well as strong metal-support bonding with supported Ag and Au nanoparticles.[57] The strong metal-support bonding on CeO_x nanoparticles showed a resistance to sintering upon calcination at 300 ℃, and the possibility of incorporation into the CeO_x support itself due to these strong interactions further enhancing stability.[146] Hydroxyapatite is part of the phosphate mineral apatite group, in the form of calcium apatite represented as $Ca_{10}(PO_4)_{6(}OH)_2$, with naturally occurring mineral forms found in bones and dental enamel.[147] It has recently attracted interest as a support for Au-based heterogeneous catalysts, that is in part due to the strong interaction between deposited Au nano-clusters and -particles and the PO_4^{-3} moieties of HAP which provides a good resistance to sintering.[148-149] Of even greater importance was the discovery in a recent study that HAP displays SMSI at a lower temperature *cf.* supports that demonstrate classical SMSI, which provided an explanation for the strong anti-sintering properties this substrate has on supported Au nano-clusters and particles (The concept of SMSI was discussed in detail in section 1.3.5.3). In the study by Tang *et al.* the reversible encapsulation of Au nanoparticles on HAP was demonstrated with respective oxidative and reductive treatments at 300 – 500 ℃ with minimal sintering observed at a relatively high Au wt% loading.[85]

4.2 Catalyst Preparation and Characterisation

All catalysts were prepared as detailed in Chapter 4, Sections 4.4 and 4.4.1. Powder XRD characterisation for all activated catalysts, and catalysts recovered after catalytic reactions, was performed using an Agilent Supernova SCXRD diffractometer with CuKα radiation. The sample was packed into a ~ 80 mm long piece of Rtx-50 GC column tubing and mounted on a sample needle and analysed using powder experiment mode. The UV-Vis DRS characterisation for all as-made, activated and recovered catalysts, was performed using a Cintra 4040 double beam, double monochromator spectrometer fitted with a GBC scientific equipment total integrating sphere fitted with a Spectralon reference. A baseline was recorded using a sample holder with respect to a Spectralon reference. The Kubelka-Munk Function was calculated using *Equation 2.4*.

4.3 Results and Discussion

4.3.1 Sintering Study on 0.2% Weight Loaded Au-Based Supported Nanocatalysts

Two characterisation methods, UV-Vis DRS and Powder XRD were utilised to detect the sintering of the Au nanoclusters deposited on the various supports used in this work. Au_{19}, $Au_{20,}$ and Au_{22} nanoclusters are smaller than *ca.* 1.7 nm, with a high uncoordinated surface to inner atom ratio, and excitonic (non-metallic) surface states due to quantum confinement effects. This means they do not possess localised surface plasmon resonances unlike larger nanoparticles in the transition size regime (1.7 – 2.3 nm) that exhibit a mixture of molecular and plasmonic behaviour, and metallic size regime (> 2.3 nm) that exhibit plasmonic behaviour. This shift to the plasmonic behaviour is characterised by the emergence of a surface plasmon resonance peak in optical absorption spectra.[150] This means that UV-Vis DRS is an ideal technique capable of qualitatively detecting the existence of sintering in Au nanoclusters

deposited on the surface of a support. Importantly, UV-Vis DRS is not suitable for the exact quantification of plasmonic particles on the support or providing evidence of the non-existence of the ultra-small non-plasmonic particles.[151]

Powder XRD is used to determine the emergence of the metallic state in Au nanoparticles as smaller Au_n (n = < 144) nanoclusters possess non-bulk molecule-like icosahedral structures and larger Au_n (n = > 144) possess bulk-like fcc structures. Smaller Au nanoparticles with fcc-like structures have generally been found to give a single peak at the (111) Bragg reflection. With increasing size, the (220) Bragg reflection begins to emerge due to diffraction at this plane as the geometric structure of Au nanoparticles changes from fcc to bulk-fcc Au planes.[109, 152] The bulk fcc-structure of larger Au nanoparticles gives characteristic (111), (200), (220), and (311) Bragg reflections.[153]

The catalyst activation treatments and Au wt% loadings used in this work were specifically chosen to help minimise the risk of sintering of the deposited Au nanoclusters. The Au wt% loading was kept low at 0.2% in accordance with previous studies conducted in my group and elsewhere which showed lower loadings were conducive to lowered sintering propensity of deposited metal nanoparticles.[151, 154] According to the thermogravimetric analysis (Figure 3.2) carried out on the phosphine protected Au_{19}, Au_{20}, and Au_{22} nanoclusters, the majority of the phosphine protecting ligands would be lost around 400 ℃. From a previous study conducted in my group it was found that smaller, atomically precise, phosphine protected Au nanoclusters would sinter on TiO_2 at around 200 ℃.[155] A scoping study conducted earlier in this work found that the severity of sintering increased at temperatures above 300 ℃ for the phosphine protected Au nanoclusters deposited on TiO_2 and CeO_2 supports. An example of the work from this study is given in Figure 4.1, shown by the red-shifting of the peaks in the UV-Vis DR spectra that emerged at 550 nm and broadened out with increasing calcination temperature. These results fit with earlier research that showed that as Au nanoparticle sizes

increase, the localised surface plasmon resonance (LSPR) band will broaden and cover the visible range.[156] For these reasons it was determined that 300 °C would be a reasonable temperature for the activation by calcination of the supported Au-based TiO_2 (anatase and Degussa P25) and CeO_2 catalysts which corresponded to a ~20 - 30% loss of ligands based on the thermogravimetric analysis.

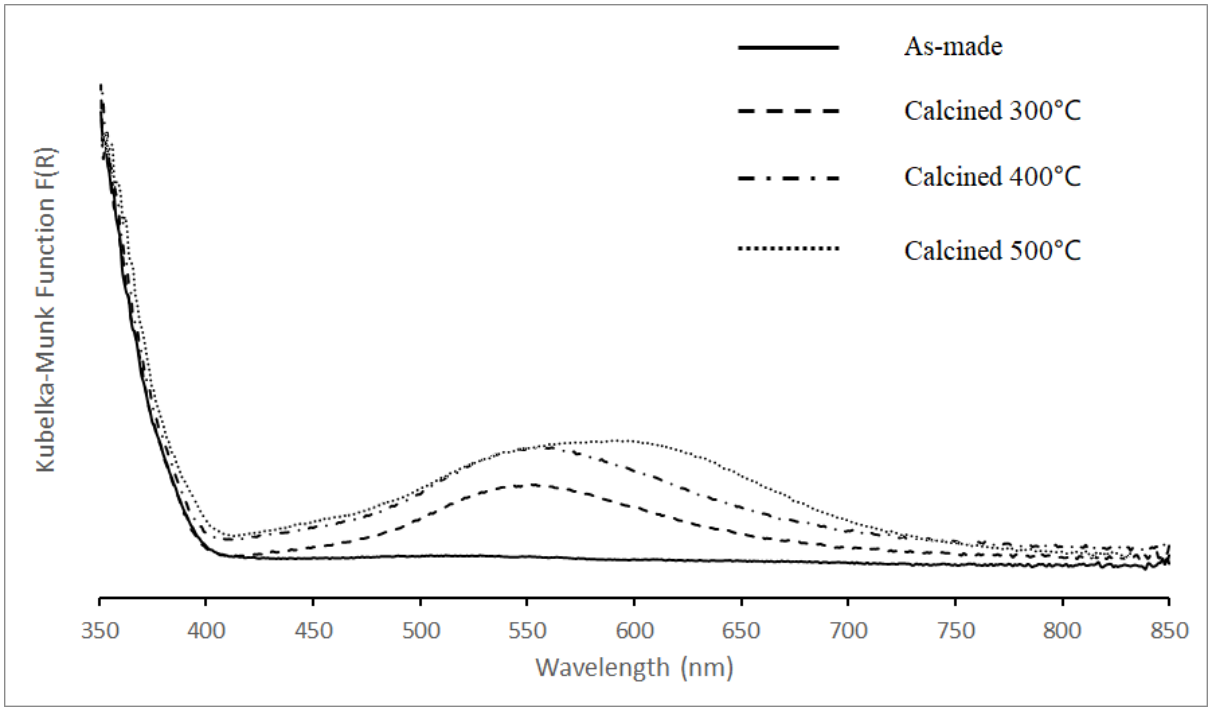

Figure 4.1. Example of the effect of increasing temperature on sintering for Au nanoclusters on the Au_{20}/Degussa P25 catalyst.

The UV-Vis DRS study (Figures 4.2 - 4) of the as-made catalysts showed a broad absorption from 400 nm to 850 nm with the absence of SPR bands in the spectra suggesting that most deposited clusters had retained their size and non-metallic state after deposition. After calcination the emergence of SPR bands with a peak maximum at ~550 nm indicates the formation of larger bulk-like Au nanoparticles, with sizes greater than 2.3 nm emerge within the supported Au_n/anatase and Degussa P25 catalysts (n = 19, 20, 22). After calcination, the spectra of the Au_n/CeO_2 (n = 19, 20, 22) showed little change apart from a rather low intensity broad peak at 500 nm – 600 nm in the visible light range. This broad

peak suggests the formation of Au nanoparticles larger than 2.3 nm but given its relatively intensity *cf.* the Au_n/Anatase and Degussa P25 catalysts (n = 19, 20, 22), it can be concluded that the sintering on the Au_n/CeO_2 catalyst was comparatively less severe or in other words a lower proportion of initially present clusters was consumed by the sintering.

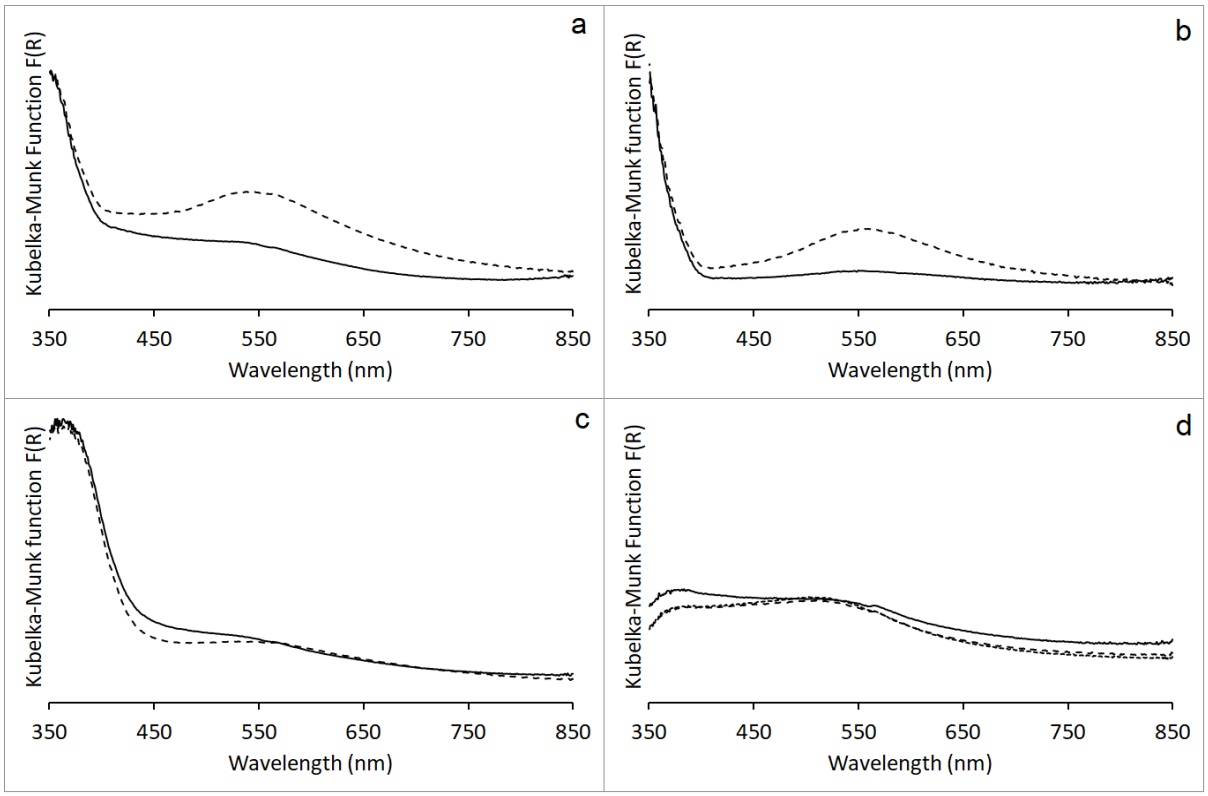

Figure 4.2. UV-Vis DR Spectra of (a) 0.2% Au_{19}/anatase, (b) 0.2% Au_{19}/Degussa P25, (c) 0.2% Au_{19}/CeO_2, (d) 0.2% Au_{19}/HAP.

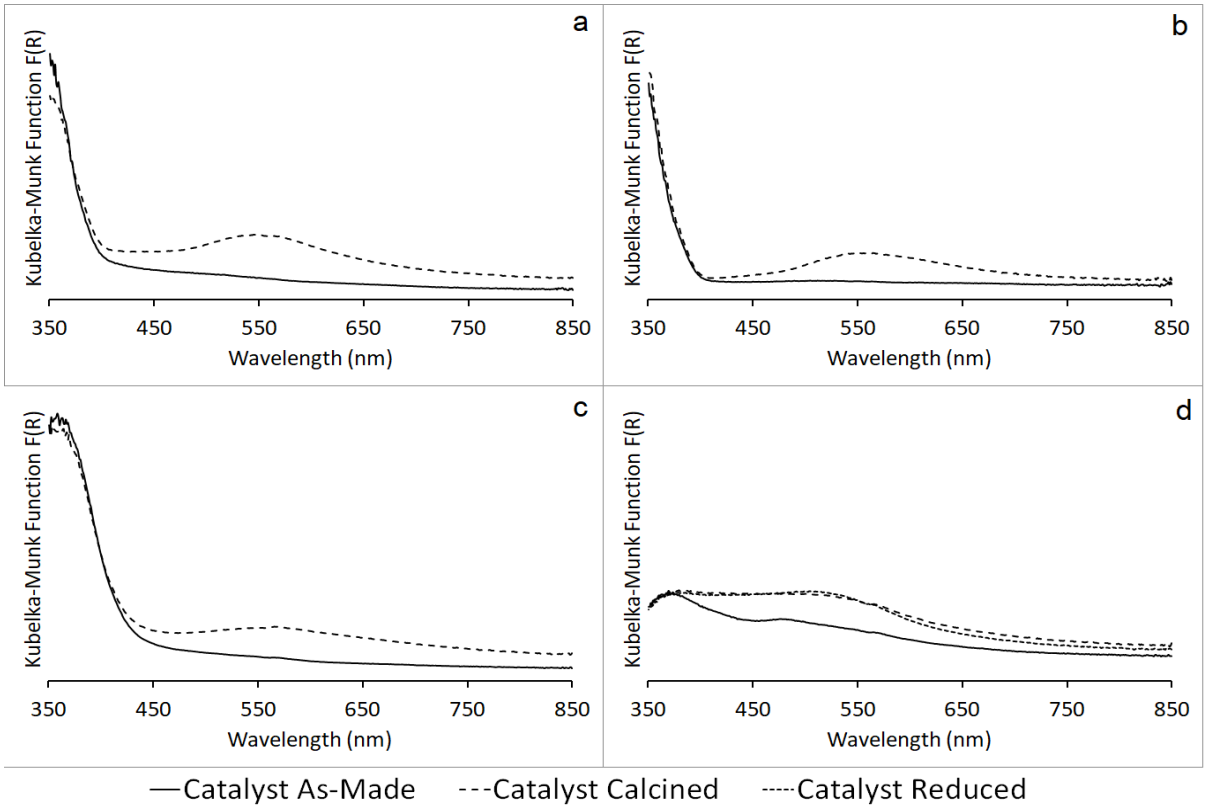

Figure 4.3. UV-VIS DR Spectra of (a) 0.2% Au_{20}/anatase, (b) 0.2% Au_{20}/Degussa P25, (c) 0.2%Au_{20}/CeO_2, (d) 0.2% Au_{20}/HAP.

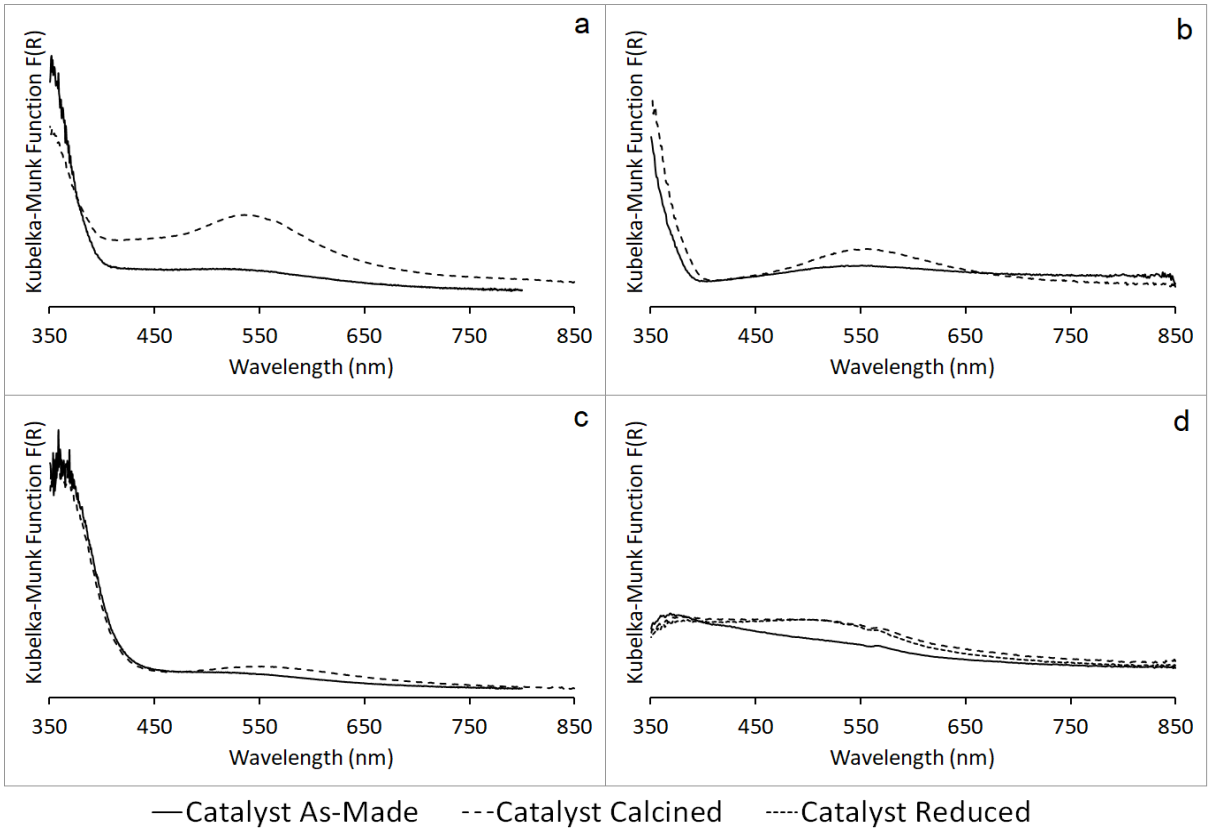

Figure 4.4. UV-VIS DR Spectra of (a) 0.2% Au_{22}/anatase, (b) 0.2% Au_{22}/Degussa P25, (c) 0.2% Au_{22}/CeO_2, (d) 0.2% Au_{22}/HAP.

After calcination the spectra of the Au_n/HAP catalysts (n = 19, 20, 22) also show little change compared to the as-made catalysts apart from a weak broad peak in the 400 – 500 nm visible region. The spectra from after the reduction of these catalysts showed almost no change when compared to the spectra after the calcination treatment. In a previous study Liu *et al*., it was proposed that a structural rearrangement of the atomically precise Au_{25} nanocluster core deposited on HAP occurred as a result of the calcination treatment at 300 ℃. It was the change from the original cluster core morphology of the deposited Au nanoclusters which was attributed to the formation of the weak band observed in the UV-Vis DR spectrum. Due to the HAADF-STEM data this factor was suggested to be more likely than the formation of larger Au nanoparticles given Au's strong interaction with HAP.[149]

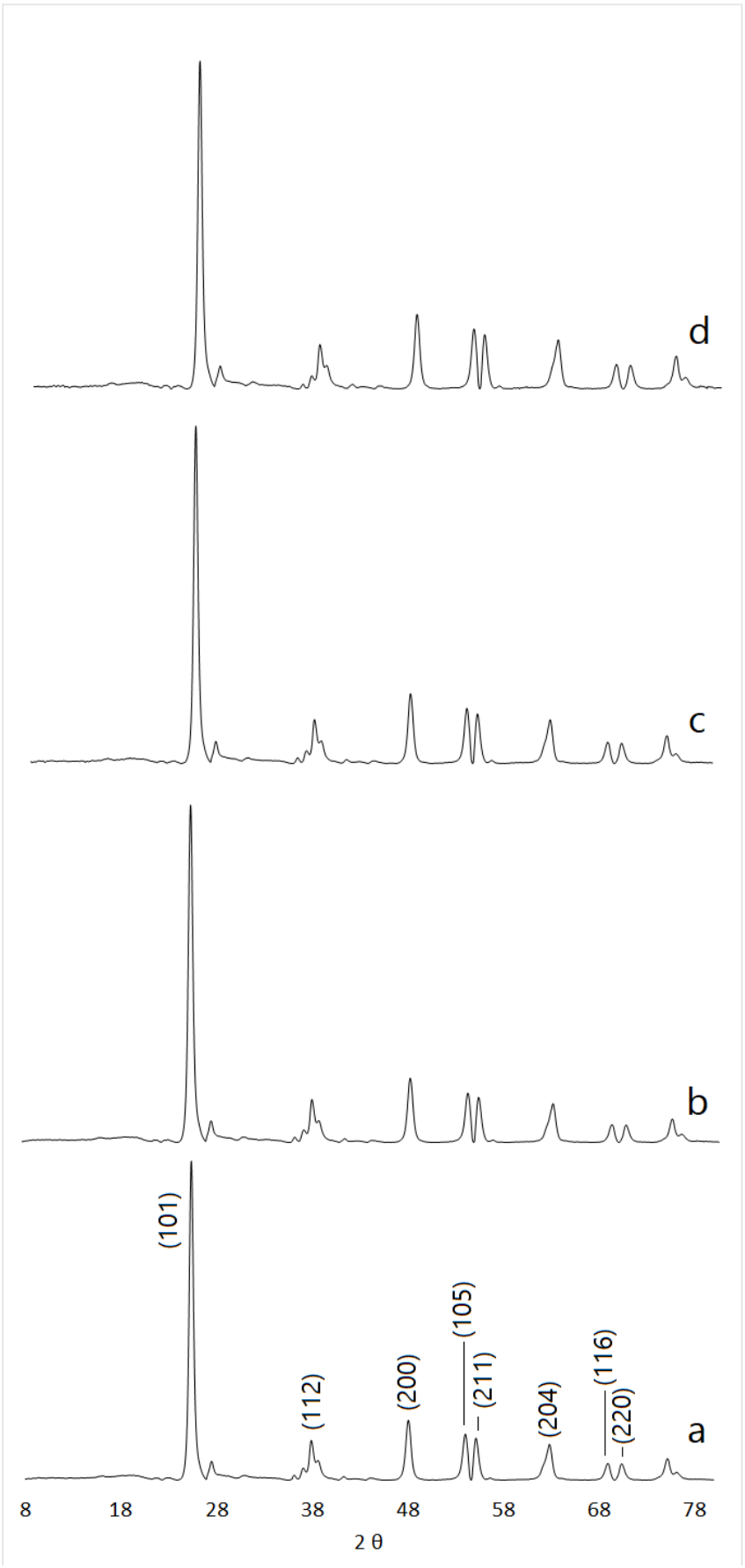

Figure 4.5. PXRD diffractograms of (a) anatase, (b) 0.2% Au_{19}/anatase, (c) 0.2% Au_{20}/anatase, (d) 0.2% Au_{22}/anatase.

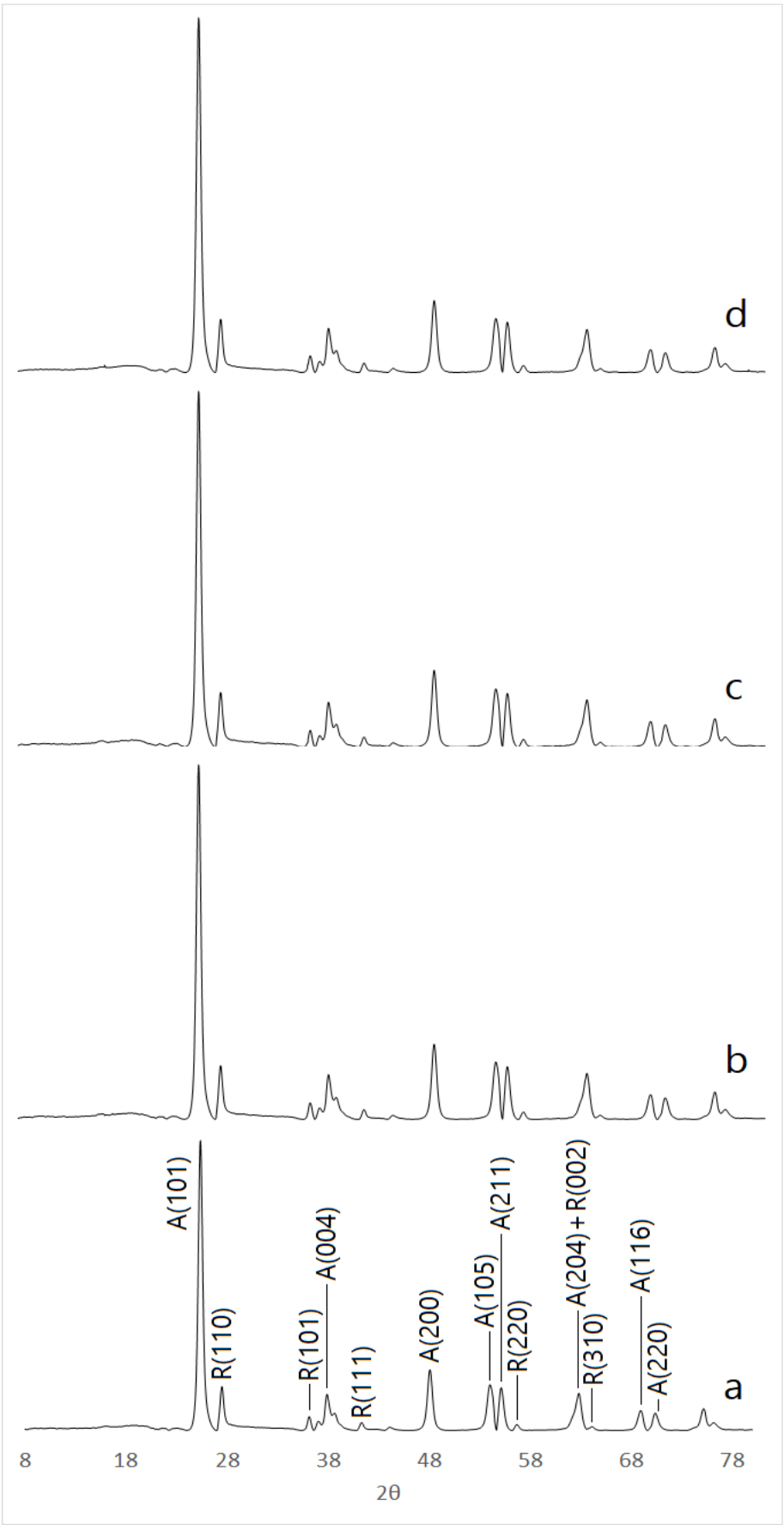

Figure 4.6. PXRD diffractograms of (a) Degussa P25, (b) 0.2% Au_{19}/Degussa P25, (c) 0.2% Au_{20}/Degussa P25, (d) 0.2% Au_{22}/Degussa P25. A denotes anatase planes. R denotes rutile planes.

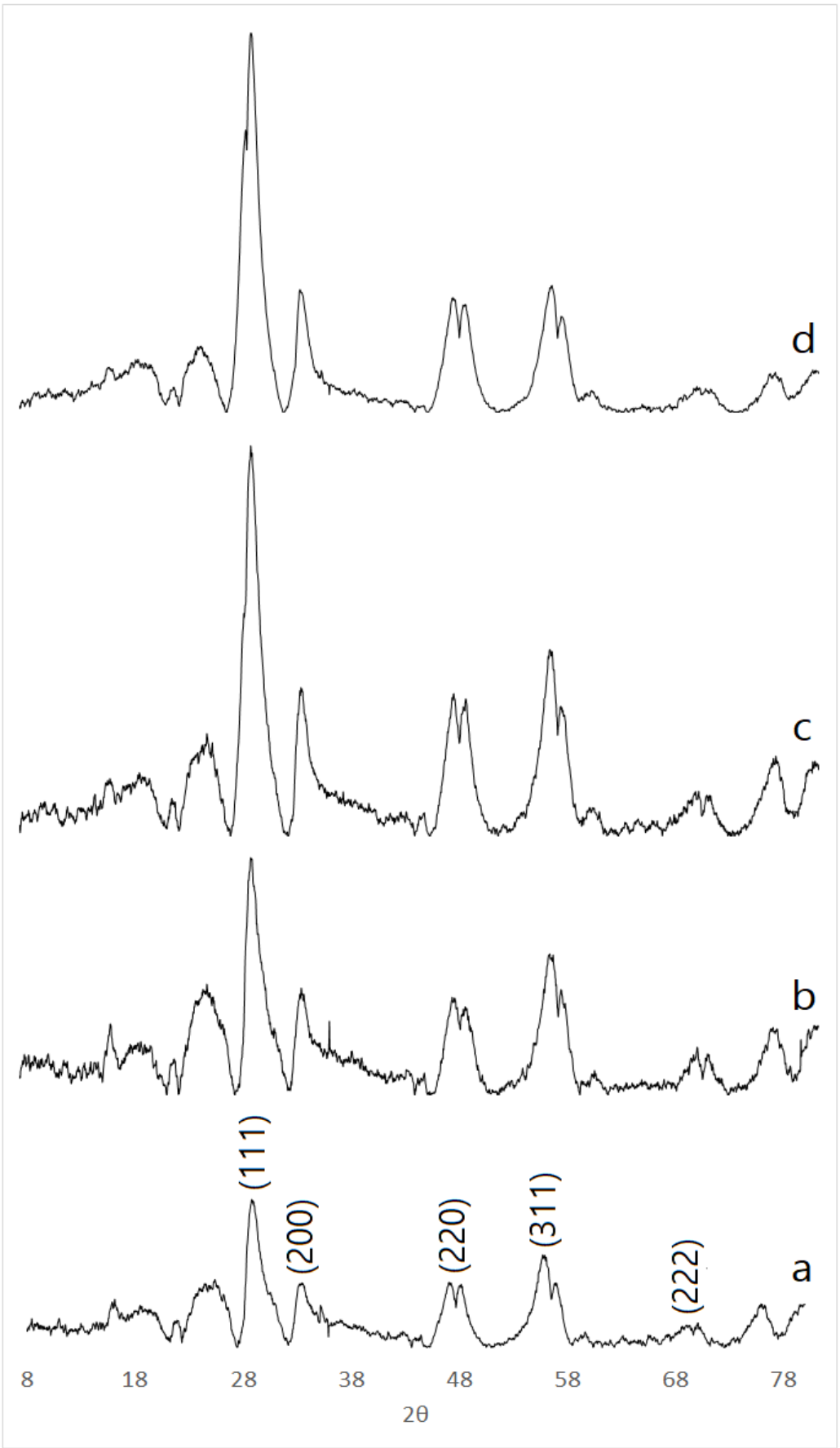

Figure 4.7. PXRD diffractograms of (a) CeO2, (b) 0.2% Au_{19}/CeO2, (c) 0.2% Au_{20}/CeO2, (d) 0.2% Au_{22}/CeO2

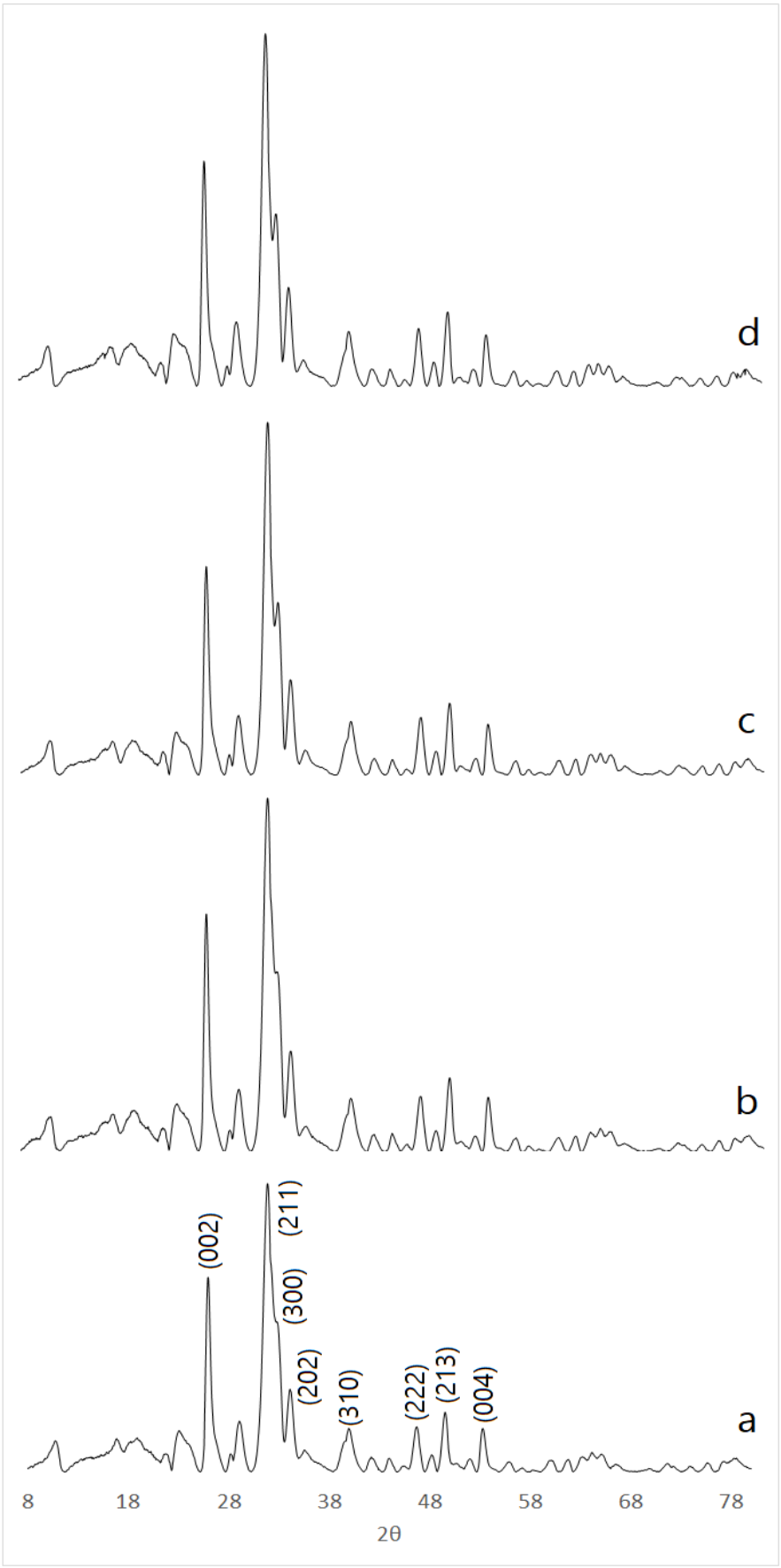

Figure 4.8. PXRD of diffractograms (a) HAP, (b) 0.2% Au_{19}/HAP-H_2, (c) 0.2% Au_{20}/HAP-H_2, (d) 0.2% Au_{22}/HAP-H_2

The Powder XRD study (Figures 4.5 - 8) of the as-made catalysts showed almost no variation in the spectra from the unmodified supports. The -H_2 prefix used in this section denotes that the catalyst had been treated under reductive conditions (Section 3.4.1). None of the peaks associated with the metallic phase of Au given by the Bragg reflections of the (111) plane (2θ ~38.2), (200) plane (2θ ~44.5), (220) plane (2θ ~64.9), or (311) plane (2θ ~77.9), could be identifed in the Powder XR diffractograms. Given the appearance of plasmonic features in the UV-Vis DR spectra for the Au clusters supported on anatase, and Degussa P25, it would be expected that some of the Bragg reflections might be visible in the Powder XR diffractograms. This was not the case and could be attributed to the fact the Bragg reflections for the Au(111), anatase (112), and Degussa P25 A(004) planes are located around the same 2θ values. A low population density of sintered Au nanoparticles which would result in the low intensity peak, or a minimal average size of sintered Au nanoparticles that give weak, broad peaks at a given Bragg reflection could also be reasons why no discernible peaks are observed for any of the catalysts.

4.3.2 Sintering Study on the Higher Weight % Loaded Au-Based HAP Nanocatalysts

Due to the strong interaction between Au_n nanoclusters and HAP, and the high catalytic activity demonstrated in the reduction of substituted nitroaromatics by the 0.2% weight Au_n-based HAP catalysts, the decision was made to increase the weight % loading of Au_n nanoclusters on this specific support. Where the spectra for the 0.2% Au_n/HAP-H_2 (n = 19, 20, 22) catalysts showed little change upon activation (*cf.* as-made catalysts) apart from a weak broad peak in the 400 – 500 nm visible region, the higher weight % Au_n/HAP-H_2 (n = 19, 20, 22) catalysts showed some evidence of aggregation (Figures 4.9 - 11). This was seen in the emergence of SPR peaks with absorption maxima in the 515 – 530 nm range of the visible

region. Lower intensities are observed in the 0.5% by Au weight loaded catalysts *cf.* the 1.0% and 2.5% Au weight loaded catalysts.

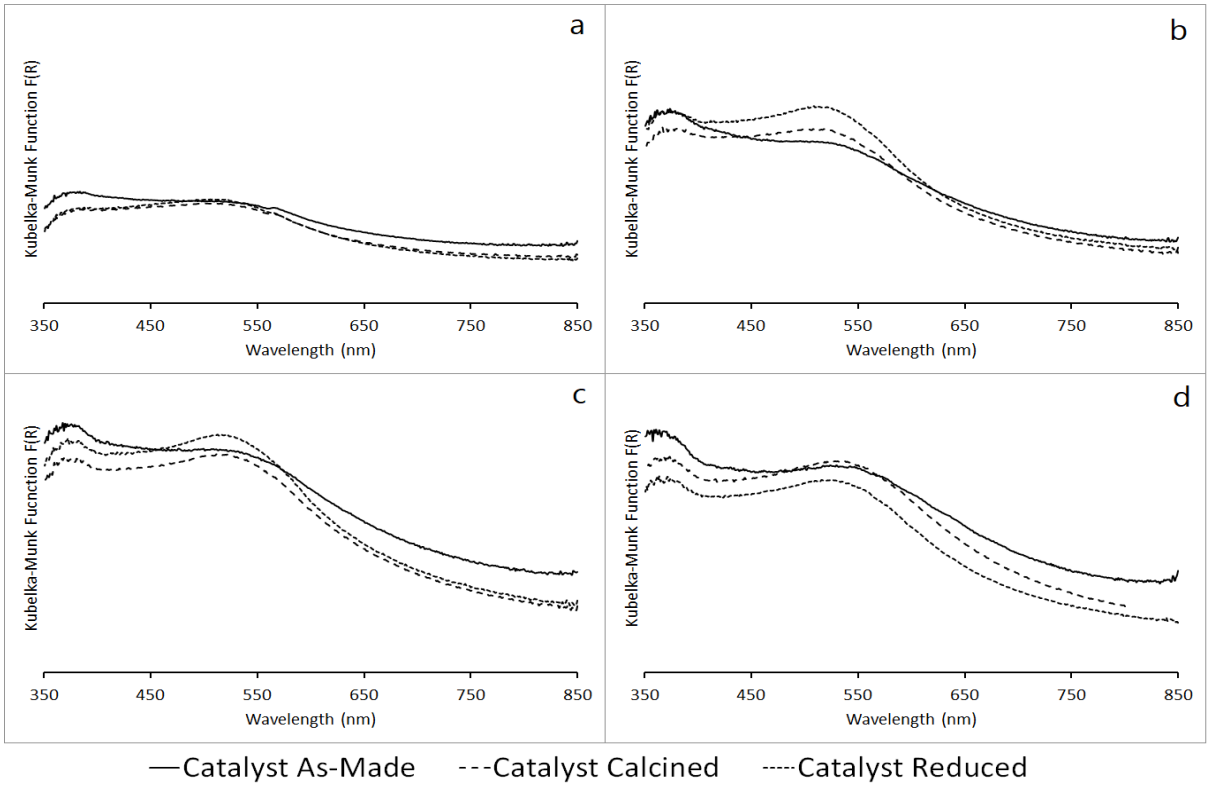

Figure 4.9. UV-Vis DRS Spectra of (a) 0.2% Au_{19}/HAP, (b) 0.5% Au_{19}/HAP, (c) 1.0% Au_{19}/HAP, (d) 2.5% Au_{19}/HAP.

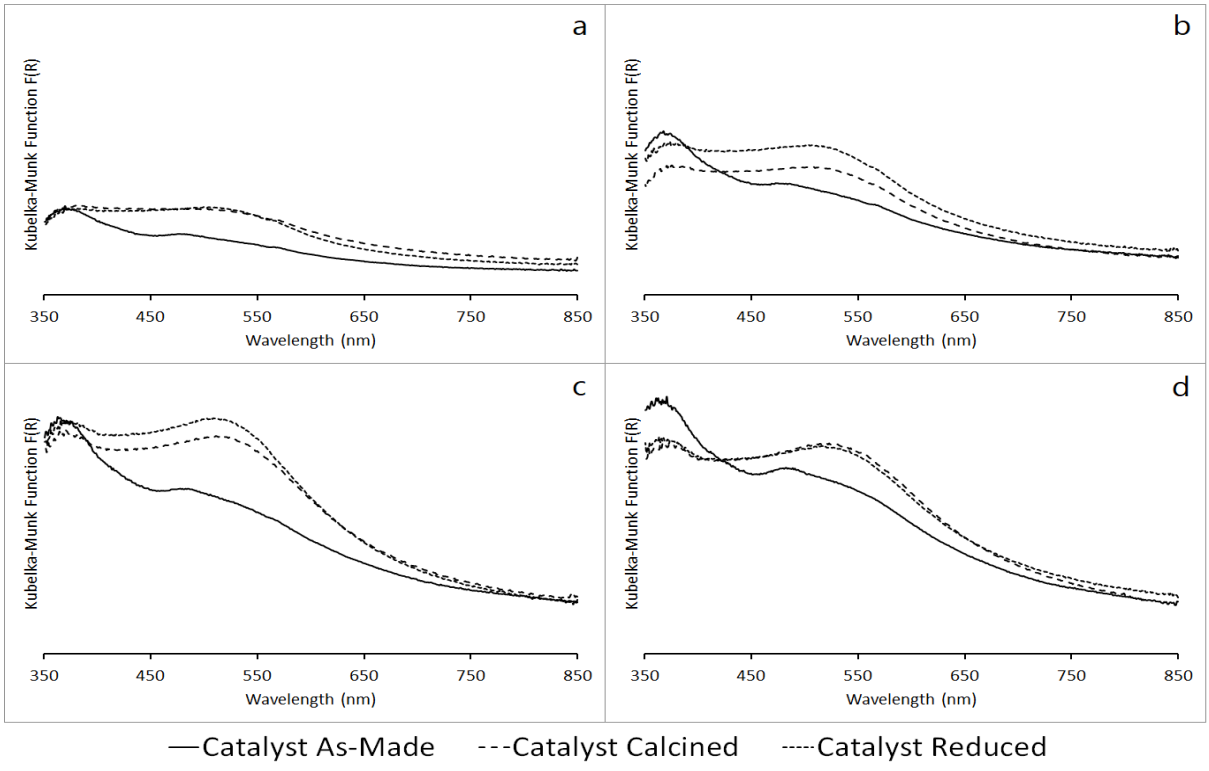

Figure 4.10. UV-Vis DRS Spectra of (a) 0.2% Au_{20}/HAP, (b) 0.5% Au_{20}/HAP, (c) 1.0% Au_{20}/HAP, (d) 2.5% Au_{20}/HAP.

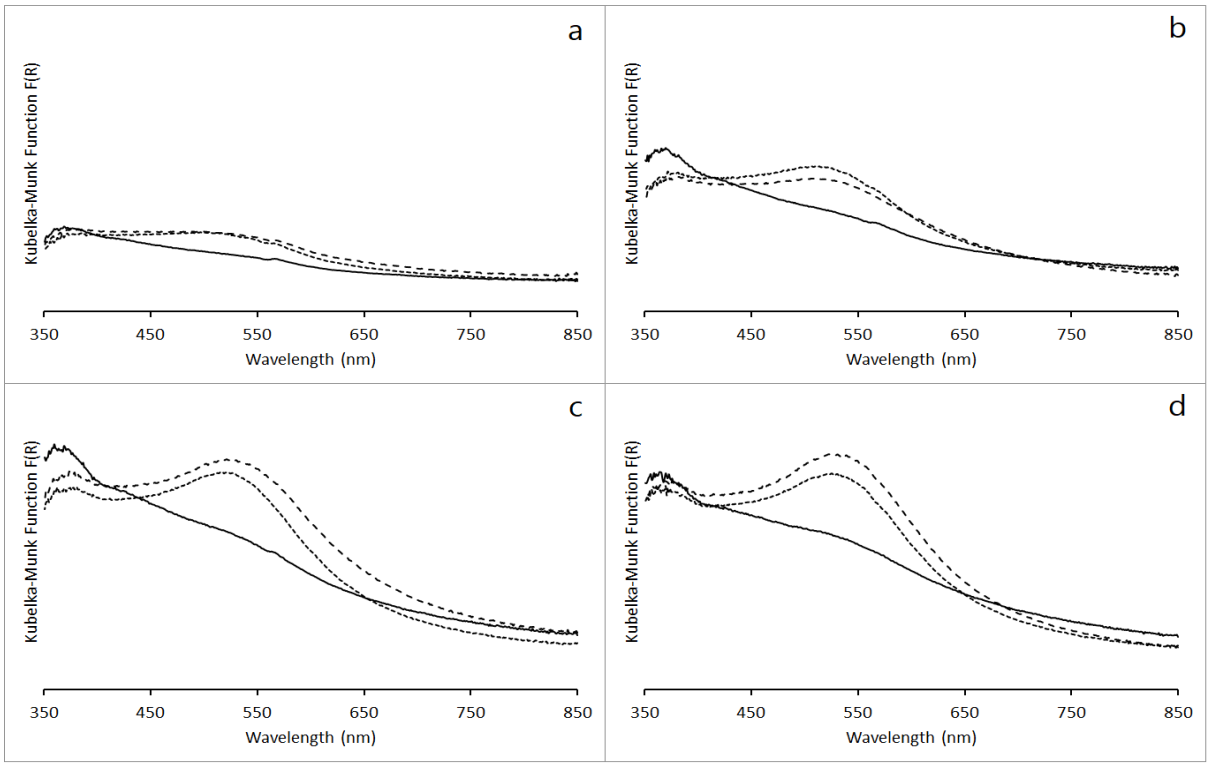

Figure 4.11. UV-Vis DRS Spectra of (a) 0.2% Au_{22}/HAP, (b) 0.5% Au_{22}/HAP, (c) 1.0% Au_{22}/HAP, (d) 2.5% Au_{22}/HAP.

Given the position of the absorption maxima it can be concluded that the degree of sintering is not as severe as in the case of catalysts based on Au_n clusters on anatase and Degussa P25. From previous studies where TEM was used in conjunction with UV-Vis DRS[157-158] it can be concluded that the average Au nanoparticle size on these catalysts is ~ 3 nm.

The Powder XRD study of the 0.5% Au_n/HAP-H_2 (n = 19, 20, 22) catalyst showed no deviation in the diffractograms compared to the 0.2% Au_n/HAP-H_2 (n = 19, 20, 22) catalysts (Figure 4.8). The diffractograms for the 1.0% Au_n/HAP-H_2 (n = 19, 20, 22) catalysts (Figure 4.12) showed the emergence of the Bragg reflection peak for the Au(111) plane (2θ = 38.2). This peak was even better defined for the 2.5% Au_n/HAP-H_2 (n = 19, 20, 22) catalysts (Figure 4.13). This appearance of this peak is characteristic of the formation of metallic Au nanoparticles larger than 2.3 nm which is in agreement with the data from the UV-Vis DRS study. The increase in intensity of this peak with higher loading can be explained by the formation of a higher proportion of ~ 2.5 nm sized Au nanoparticles. The root cause of this is most likely the lower degree of dispersity and higher surface density or smaller inter-cluster distances inherent for deposited Au nanoclusters in the higher loading catalysts, which increases the population of sintered nanoparticles upon activation.[159] With increasing Au nanoparticle size, the next peak to be observed would be the Bragg reflection from the Au(200) plane. It should be noted that the Bragg reflection for the HAP(203) plane (2θ = 44.2) is in very close proximity to the the Bragg reflection for the Au(200) plane (2θ = 44.5). Thus, even if the latter is present, it could be masked by the peak from the HAP(203) plane peak.

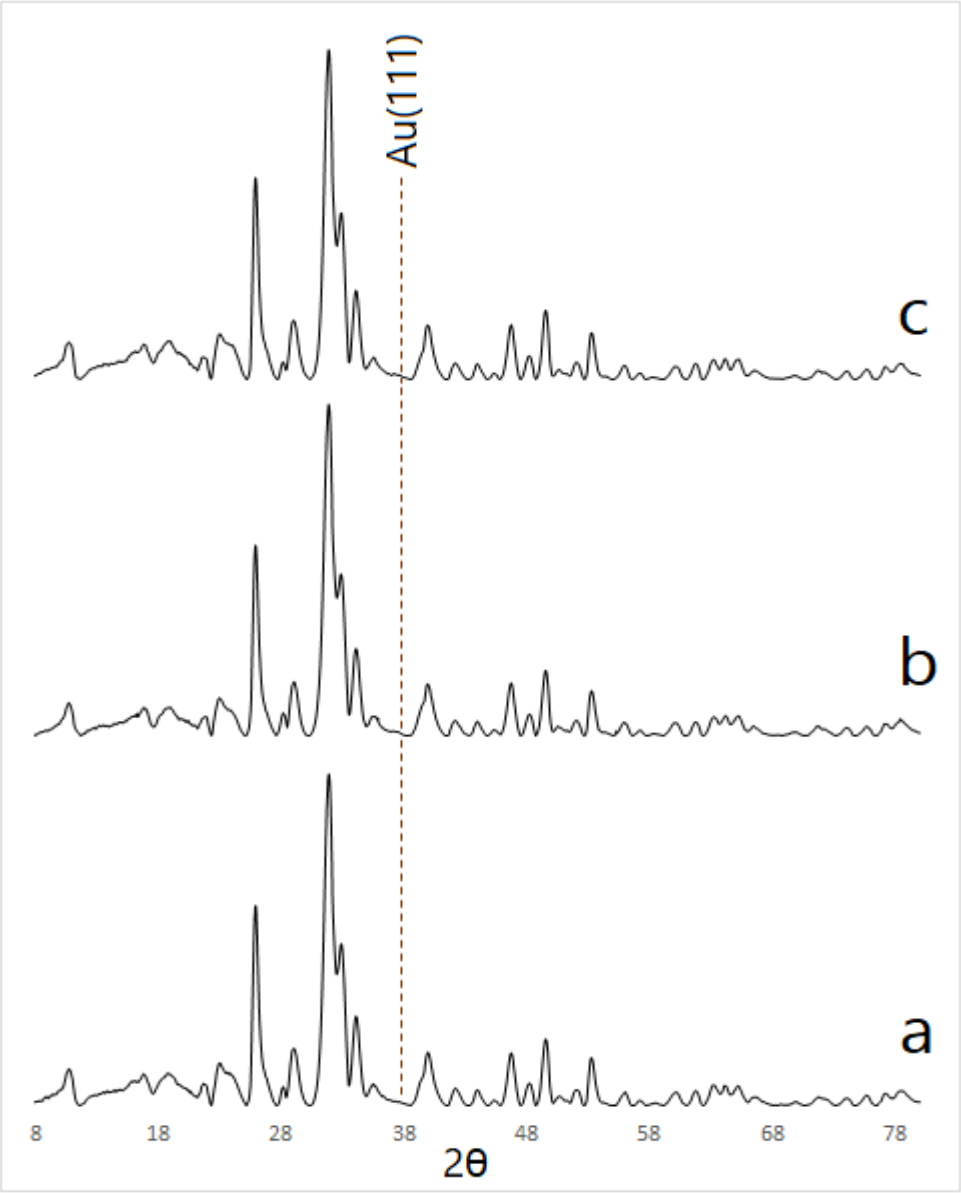

Figure 4.12. PXRD diffractograms of (a) 1.0% Au_{19}/HAP-H_2, (b) 1.0% Au_{20}/HAP-H_2, (c) 1.0% Au_{22}/HAP-H_2.

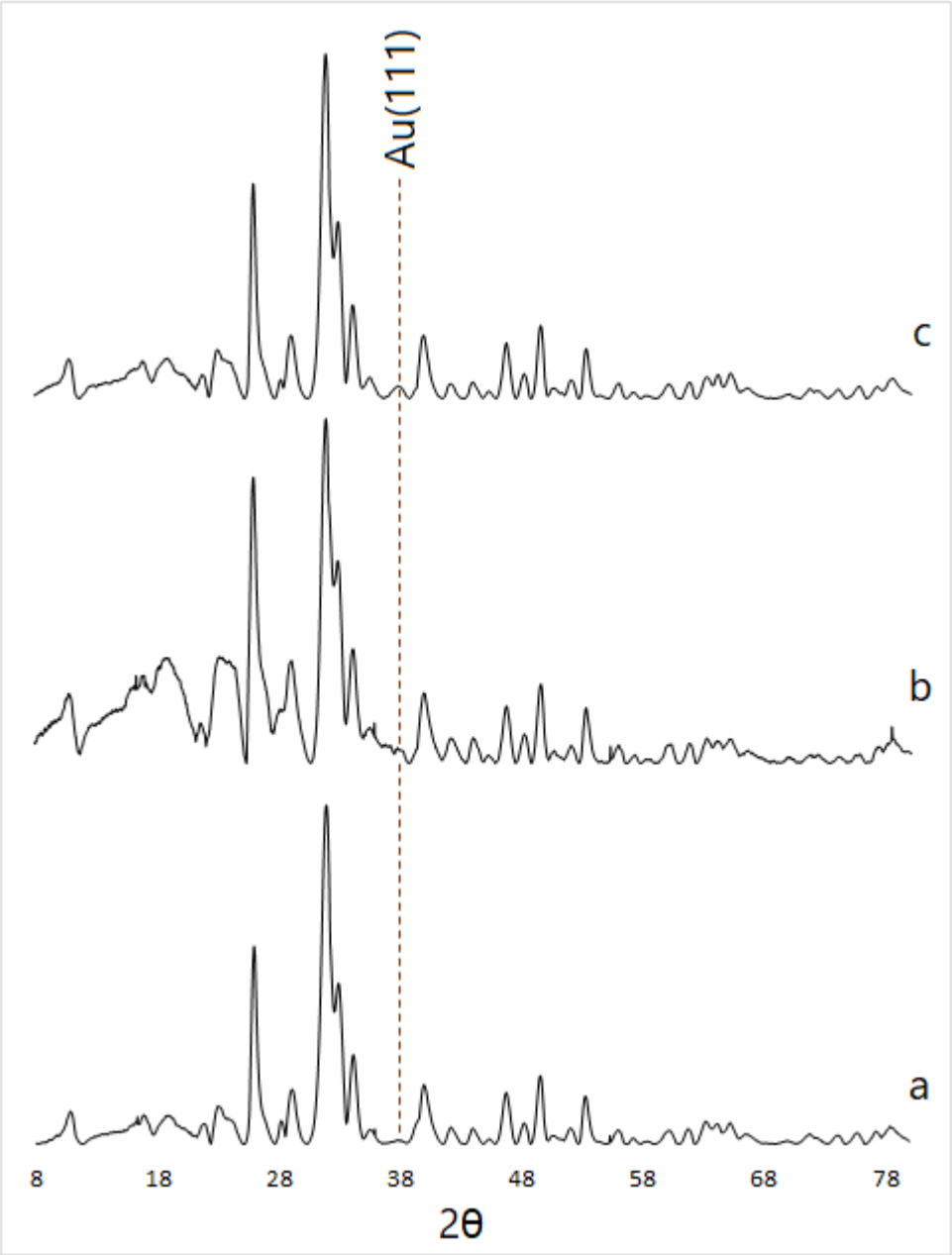

Figure 4.13. PXRD diffractograms of (a) 2.5% Au_{19}/HAP-H_2, (b) 2.5% Au_{20}/HAP-H_2, (c) 2.5% Au_{22}/HAP-H_2.

4.3.3 Sintering Study on Au Nanocatalysts Recovered from Reactions

UV-Vis DRS studies showed that the Au_n/anatase, Degussa P25, CeO_2 and HAP-H_2 (n = 19, 20, 22) catalysts recovered after catalytic tests changed little compared to the catalysts activated prior to catalytic reactions (Figures 4.14 - 16). The only system that showed a

significant change compared to the spectra of the activated catalyst before reaction was the Au_n/CeO_2 (n = 19, 20, 22) series. This series showed large shifts in the intensity of absorption which was hypothesised to be caused by the reduction of the support itself under catalytic hydrogenation reaction conditions. To test this hypothesis, the unmodified CeO_2 support was calcined at 300 °C and used in catalytic hydrogenation tests for each reagent under the same experimental conditions as for the Au-based catalysts (see Section 3.1. Almost identical spectra were obtained for each of the CeO_2 materials recovered after the blank hydrogenation reactions as compared to spectra of the corresponding recovered Au_n/CeO_2 (n = 19, 20, 22) catalysts. This led to the conclusion that it was the reduction of the CeO_2 support itself under the reaction conditions used, and not the evolution of the deposited Au nanoclusters that resulted in observed changes in spectra. Powder XRD study was performed on all the recovered catalysts but there was no noticeable difference between the activated and recovered catalysts.

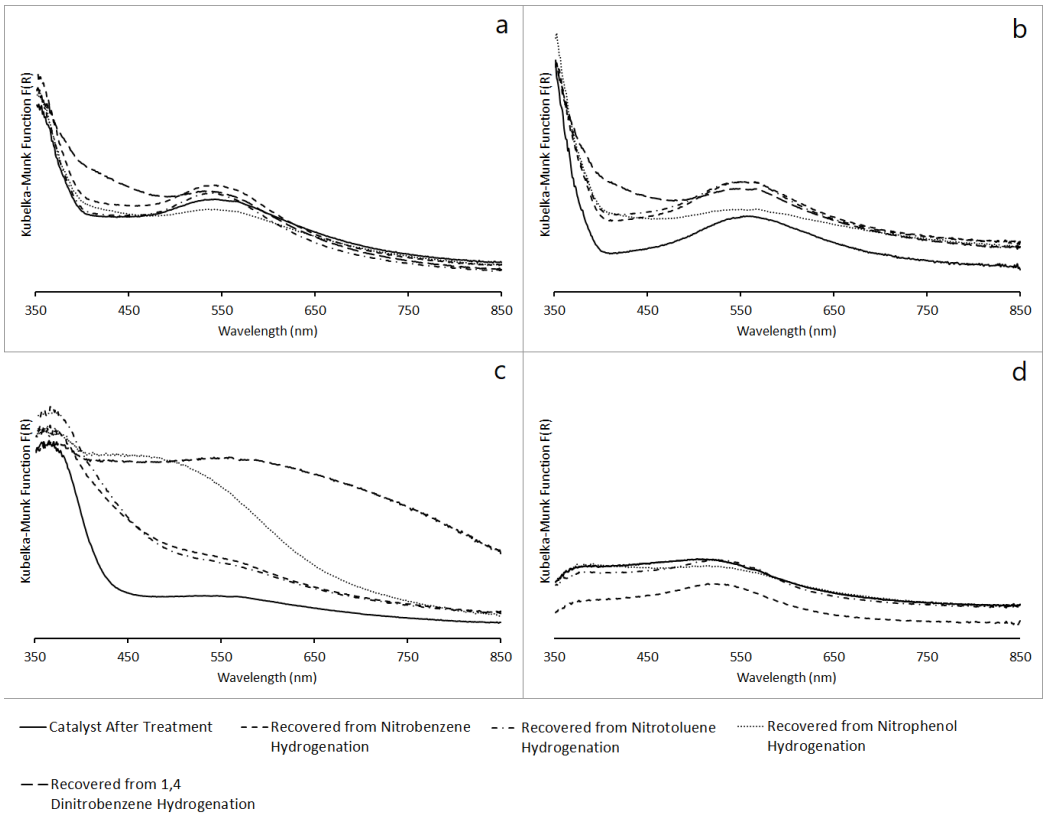

Figure 4.14. UV-Vis DR Spectra of (a) 0.2% Au_{19}/anatase, (b) 0.2% Au_{19}/Degussa P25, (c) 0.2% Au_{19}/CeO_2, (d) 0.2% Au_{19}/HAP after recovery from catalytic hydrogenation reactions.

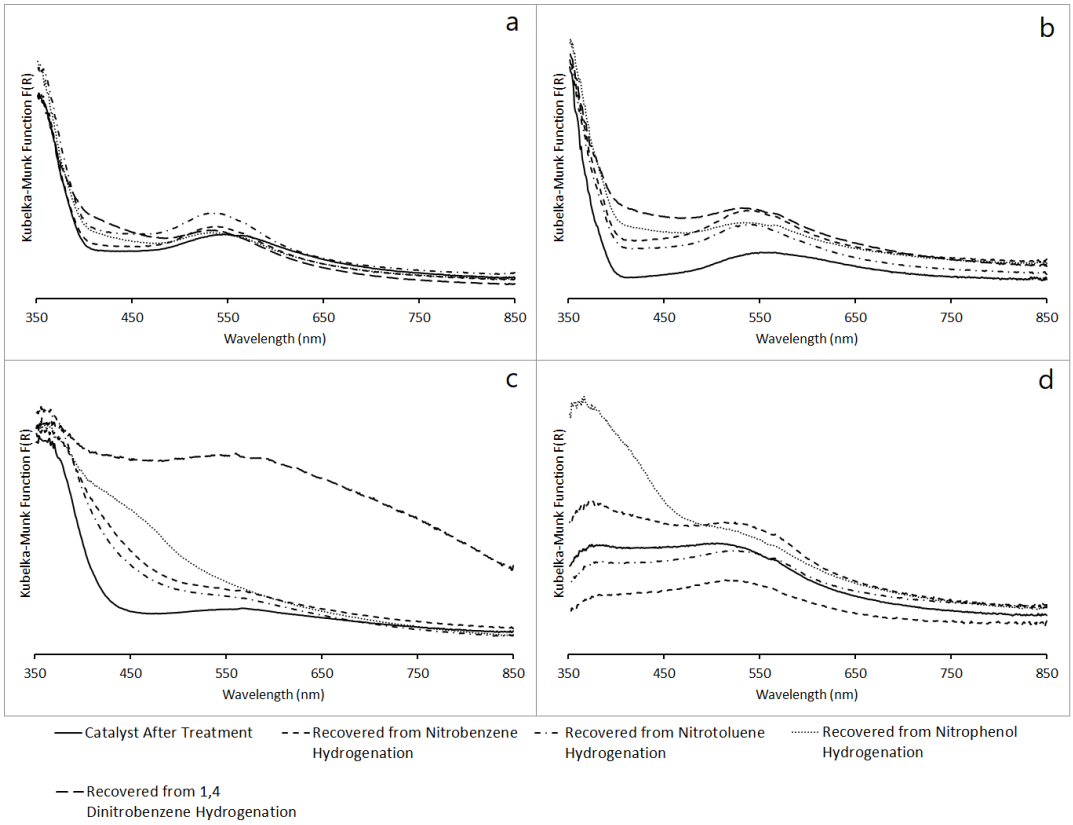

Figure 4.15. UV-Vis DRS Spectra of (a) 0.2% Au_{20}/Anatase, (b) 0.2% Au_{20}/Degussa P25, (c) 0.2% Au_{20}/CeO_2, (d) 0.2% Au_{20}/HAP after recovery from catalytic hydrogenation reactions

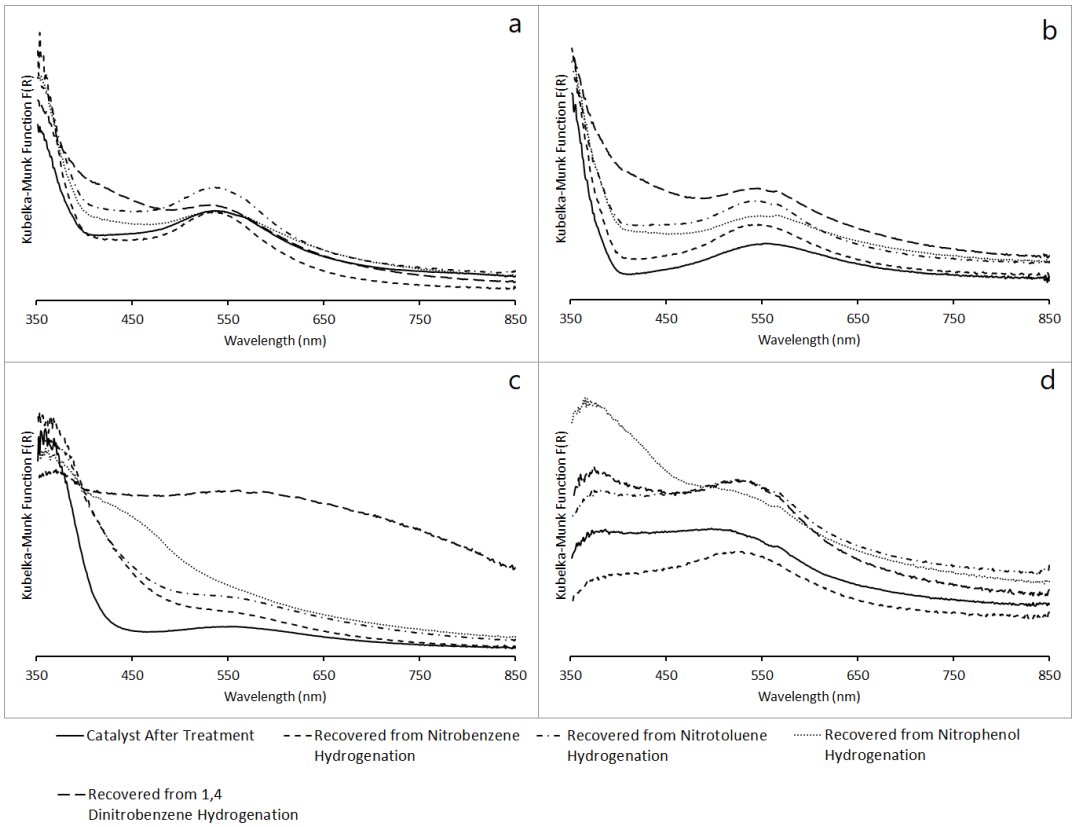

Figure 4.16. UV-Vis DRS Spectra of (a) 0.2% Au_{22}/Anatase, (b) 0.2% Au_{22}/Degussa P25, (c) 0.2% Au_{22}/CeO_2, (d) 0.2% Au_{22}/HAP after recovery from catalytic hydrogenation reactions

4.4 Conclusions

In conclusion the nature of the interaction of the support with deposited Au nanoclusters is an important determinant for the occurrence of sintering due to catalyst activation treatments or during the catalytic reactions. In this study the supports HAP, and CeO_2, that had shown strong interactions with deposited Au nanoparticles in previous studies showed little evidence of severe sintering of the Au nanoclusters deposited on their surface. This does not mean that sintering was completely absent on these supports, just that the size or proportion of larger Au nanoparticles formed was not sufficient to give a discernible fingerprint within limitations of the methods used here. The anatase and Degussa P25 supports that had shown weaker interactions with deposited Au nanoparticles in previous studies, had shown evidence of cluster sintering in my UV-DRS study too. Given that no direct imaging techniques (such as aberration corrected HRTEM or HAADF-STEM) were available at UC, the average size of Au nanoparticles formed and the relative proportions of the total nano-cluster *vs.* nanoparticle population had to be estimated. The increasing surface density of the deposited nanoclusters due to the gradually increasing Au weight loadings series on HAP resulted in a more pronounced sintering of clusters with increase in Au content. Specifically, while the 0.2% Au_n/HAP-H_2 catalysts (n = 19, 20, 22) showed no evidence of sintering the 0.5%, 1.0% and 2.5% by Au weight did. While the sizes could only be very roughly estimated based on the UV-Vis DRS study the emergence of the Au(111) plane Bragg reflection helped confirm the average Au nanoparticle size on the 1.0% and 2.5% HAP catalysts to be *ca.* 2.5 nm.

Chapter 5 Catalytic Hydrogenation of Nitrobenzene and Substituted Nitro-Aromatics Using Supported Au Nanocatalysts

5.1 Introduction

Substituted anilines are one of the most important building blocks in industrial chemical processes as they are valuable intermediates in the production of pharmaceuticals, agrochemicals, rubber processing chemicals, isocyanates, pigments, and dyes. Historically the reduction of substituted nitroaromatics was performed using iron powder or iron(II) chloride in the Béchamp process, as well as using sulfides.[160] The amination of phenol has also been utilised to a limited extent industrially[161] and the direct amination of benzene was investigated, but never developed for use in an industrial capacity.[162] The direct amination of benzene requires very high temperatures, pressures and an excess of ammonia which abrogated it's use as an industrially viable method,[163] with nitro-aromatics (produced from the nitration of substituted benzenes) used by all major chemical producers as the precursors in the production of substituted anilines. The Béchamp process had the disadvantage of forming Fe oxide sludges that were problematic due to issues with the separation of adsorbed reaction product and disposal given their detrimental effects on the environment.[164] The sulphide reduction process had disadvantages with the formation of sulfur containing by-products, elemental sulfur, and use of highly toxic reagents.[165] The number of other problems associated with the early methods for the synthesis of substituted anilines in terms of the formation of un-wanted by-products, high-energy requirements, low-product quality and intensive processing to obtain the product necessitated the development of improved methods for the synthesis of substituted anilines.

This introduction will focus on the catalytic liquid phase rather than the gas-phase hydrogenation of substituted nitro-aromatics. The heterogeneous catalysts used in the catalytic gas phase hydrogenation of substituted nitro-aromatics are similar to the ones used in the liquid-phase and are usually supported Cu- or Pd- based catalysts on carbon or metal-oxides, with other metals such as Cr, Pd and V, used as promoters and modifiers. A distinction will also be made here between by-products and intermediates. By-products in catalysed reactions are the final are species in a cascade of the (catalytic) reactions that form at the same time as the main product(s) due to conditions that result in a secondary reaction pathway being followed as well and are often of lower economic importance to the main product. They can also be toxic, carcinogenic, or detrimental to the catalytic process with the most common outcomes being the reduction of a catalysts' life or the poisoning of the catalyst itself.[166] Intermediates in the catalysed reactions are species produced during various steps of a catalytic cycle in a chemical process that are not final products per se but are the feedstocks for the continuation of the reaction along the (desired) pathway to its completion. Like by-products, some intermediates can be undesirable depending on the reaction pathway that is followed.[167]

The earlier industrial synthesis methods have mostly been supplanted with the use of superior heterogeneous catalysts based on supported nobel-metal nanoparticles for the selective hydrogenation of substituted nitro-aromatic compounds in the industrial production of anilines. The hydrogenation process is normally carried out in the liquid or vapor phases, with the reaction conditions, such as temperature and pressure in these media being the major factors defining the activity and selectivity of the catalyst. The reaction mechanism suggested by Haber[168] for the electrochemical reduction of nitrobenzene to aniline holds true for the heterogeneously catalysed hydrogenation of nitrobenzene and other substituted nitroaromatics (Figure 5.1); the direct and condensation routes have been confirmed experimentally as being

relatively the same for obtaining aniline, substituted aniline, and symmetric and asymmetric azo-aromatics from the catalytic hydrogenation of nitroaromatics.

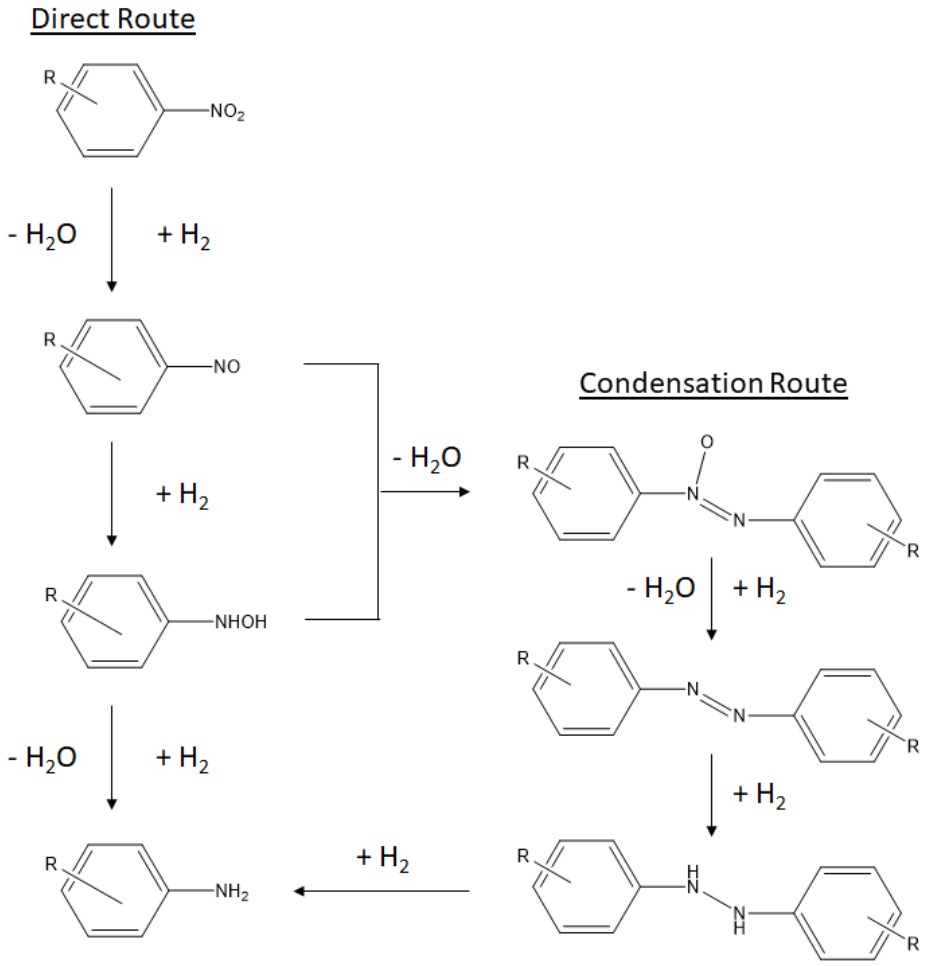

Figure 5.1. Reaction pathways based on those proposed by Haber for the reduction of a nitroaromatic compound to the corresponding aniline

Issues still remain with the supported nobel-metal catalysts, such as Pt- or Pd-based, used traditionally in the industrial synthesis of anilines and substituted anilines. Inorganic and organic modifiers (also known as promoters) such as metals, metal salts, *e.g.* alkali metal carbonates or hydroxides, as well as organic bases are needed to alter the properties of these heterogeneous catalysts primarily to improve selectivity. The secondary purpose is to prevent accumulation of harmful intermediates, unwanted reduction of other reducible functional

groups when they are present, and to improve reaction rates. Without these modifiers supported Pt- and Pd-based catalysts are more selective for the hydrogenation of alkene and carbonyl functional groups than nitro functional groups. Dupont utilises a Pd- or Pt- based catalyst supported on an activated carbon support with Cr, Fe, or Ni (up to ten percent by metal weight) added as modifiers to prevent the hydrogenation of the aromatic ring and improve activity[169] while BASF use a supported Pt- based catalyst on an active carbon support with Fe(III) hydroxide as a modifier to improve selectivity.[170] Although Pt is more selective in this reaction than Pd, the formation of unwanted by-products such as phenylcyclohexyl amine was considered to be high as a percentage of the total yield even in the case of pure Pt-based catalysts.[170] The metal and modifier content of these supported catalysts is considered excessive, especially when taking into account the modifiers blocking of active sites leading to a low atom economy of the supported noble metals; it has been estimated that only a small percentage of the total metal surface (and even lower % of the loading) is active during the catalytic reaction.[171]

Apart from improving selectivity and activity, modifiers are employed to prevent the formation and accumulation of harmful N-aryl hydroxylamine intermediates. Such intermediates are carcinogenic, result in a lower quality product and are detrimental to the catalytic process itself. Modifiers achieve abovementioned prevention by catalysing the disproportionation of N-aryl hydroxylamine intermediates to either the desired aniline product or nitroso-intermediate which consequently re-enters the catalytic cycle.[172] The decomposition of N-aryl hydroxylamine intermediates is strongly exothermic, and while the activation energy for initiating the decomposition is high, under the right conditions the self-accelerated process can become more facile. The decomposition process can result in not only the decomposition of the reaction mixture including desired synthesised products, but also give rise to a severe

safety problem as an excessive amount of heat can accumulate in the reactor if vital cooling systems fail potentially leading to explosion.[173]

Since the discovery of supported Au-based heterogeneous catalysts for the chemo-selective hydrogenation of nitro-aromatics to their corresponding aniline compounds[174-175] there was a renewed interest in conducting research with these catalytic systems given their potential to overcome the problems inherent in the traditionally utilised catalysts for such reactions. The problems, as discussed earlier was the difficulty in selectively reducing nitro functional groups in the presence of other reducible functional groups, particularly, when the ideal reductant is the industrially preferred gas H_2. Other issues include the difficulty in controlling the reduction pathways to afford the fully hydrogenated aniline compound or a desired reaction intermediate; achieving high activity, since activity is often sacrificed to obtain greater selectivity. Perhaps the greatest difficulty lies in achieving all of these aims while developing an environmentally friendly, heterogeneous catalyst that operates under mild reaction conditions (relatively low temperature and pressures), using a relatively 'green' reaction medium, and without the requirement of expensive, and often toxic, modifiers and promoters.

The subsequent, but limited research into Au-based catalysts for use in the catalytic hydrogenation of nitro-aromatics[8, 176-177] has shown that these catalytic systems offer high chemo-selectivity for the reduction of the nitro functional group in the presence of reducible functional groups; the chemo-selectivity remains unchanged when reductants like H_2 and $NaBH_4$ are used. The accumulation of N-aryl hydroxylamines, and other partially reduced intermediates (depending on the support), is not observed during the catalytic hydrogenation of nitro-aromatics using Au-based heterogeneous catalysts which shows their great potential for use in industrial applications. Au-based catalysts have shown a propensity towards catalysing the disproportionation of N-aryl hydroxylamine intermediates to either the nitroso-

intermediate or the desired aniline product. The problems associated with the exothermic decomposition of these compounds are mitigated too, as the need to use modifiers and promoters otherwise employed to circumvent this issue. The Au-based heterogeneous catalysts have also demonstrated activity for the catalytic hydrogenation of nitro-aromatics under mild reaction conditions in relatively 'green' reaction media. The only downside that comes with the use of Au-based heterogeneous catalysts is their low catalytic activity for nitro-aromatic hydrogenation in comparison to the traditionally utilised noble metal-based catalysts. Of interest is the drastic increase in the catalytic activity over the Au-based catalysts as the supported particle size decreases approaching the nanocluster size regime (*e.g.* below ~ 3 nm). Most studies that have attributed an increase in catalytic activity to the smaller Au nanoparticle sizes have used relatively simple catalyst fabrication methods, such as the impregnation and deposition-precipitation method using $HAuCl_4$ to prepare catalysts.[178-182] These methods commonly give polydisperse Au nanoparticles where the particle size range can be as wise as 1 to 8 nm which corresponds to the difference from tens to thousands of Au atoms per between atomically precise nano-clusters and larger particles. Any activity attributed in these studies to smaller Au particle sizes is more an average across the entire size population of Au particles with wide size distribution rather than a reflection of the catalytic activity given by specific, well-defined particle sizes. As of writing this Thesis, only two studies have been conducted utilising supported atomically precise nanoclusters in the catalytic hydrogenation of nitro-aromatics.[158, 183] The first study, conducted by Fang *et al.* studied the catalytic hydrogenation of nitrobenzene over thiolate-protected Au_{25} nanoclusters supported on HAP, TiO_2, pyrolysed graphene oxide, activated carbon and SiO_2 at 1% Au weight loadings. The prepared catalysts were all activated by calcination at 300 °C. The second study conducted by Li *et al.* studied the catalytic hydrogenation of 4-nitrobenzaldehyde over thiolate-protected Au_{99} nanoclusters supported on CeO_2, TiO_2, and SiO_2 at 1% Au weight loadings. Thiolate-protected Au_{25} and

Au_{36} were also supported on CeO_2 at 1% Au weight loadings. The prepared catalysts were activated by annealing at 150 °C. The hydrogenation of substituted nitro-aromatic compounds is an ideal catalytic system for studying the size effects of sub-nanometre atomically precise Au nanoclusters, which could ultimately pinpoint how the difference of only an atom changes catalytic activity. This is due to the fact that hydrogen dissociation has been shown to be the rate-limiting step in this reaction over supported Au-based heterogeneous catalysts.[184] This study will show how the activity of atomically precise Au nanoclusters supported on anatase, Degussa P25 and HAP changes as a function of nanocluster size.

5.2 Catalyst Preparation and Experimental Catalytic Procedure

The detailed catalyst preparation protocol is given in Section 3.4. The detailed experimental catalytic test procedure is given in Section 3.5 and is reiterated here for the convenience of the reader. Very briefly, in a typical experiment, a PTFE liner was charged with 15 mL EtOH, 0.1 g of nanocatalyst and a calculated amount of reactant (Table 5.2). The liner was sonicated for 4 mins, then placed in the batch (Parr-like) reactor and the reactor was sealed. The reactor was flushed sequentially with N_2, H_2, and finally pressurised to 10 bar with H_2. The reaction mixture was stirred with a magnetic stirrer bar at 700 rpm with a set reaction temperature of 100 °C. After 5 hours (1 hour in the induction time study) stirring and heating were ceased, and the reactor was cooled in an ice bath. The reaction mixture was separated from the nanocatalyst by centrifugation (12000 rpm for 10 mins) and filtered through a 45 μm pore size PTFE filter. The recovered catalyst was washed 3 times 25 mL with EtOH (re-dispersion followed by centrifugation and separation) and dried under vacuum. Each experiment was reproduced at least 2 times. The typical standard errors of independent catalytic tests were below 1.5%. The reproducibility between each reaction set varied with < 2% difference between the nitrobenzene and nitrotoluene catalytic hydrogenation results, < 3% for the 1,4-dinitrobenzene catalytic hydrogenation results and < 5% between the nitrophenol

catalytic hydrogenation results. Analysis of the reaction mixtures was performed using GC-FID as detailed in Section 3.5.

Table 5.2 Amounts of reagents used in catalytic hydrogenation reactions

Reagent	Mass (g)	Volume (mL)	Amount (mmol)
Nitrobenzene	0.246	0.205	2
p-Nitrotoluene	0.274	0.197	2
p-Nitrophenol	0.276	0.197	2
1,4-Dinitrobenzene	0.05	0.031	0.297

TOF values in this chapter were calculated according to the following equation:

$$TOF(h^{-1}) = \frac{n_f\ product}{reaction\ time(h) \times n_{Au}}$$

(*Eq 5.2*)

Where n_f *product* is the number of moles of the substituted nitroaniline produced from the reaction, after reaction time (h) and n_{Au} is the assumed number of moles of Au contained on the catalyst. TOF values were calculated for the production of substituted anilines for all reactions. The method of calculating the TOF in this work from the moles is justifiable given the high surface to volume ratio of smaller gold nanoclusters (*e.g.* Au_{20}'s surface area to volume ratio is 1.00). This means a high proportion of the atoms in gold nanocluster are possible active sites. In larger nanoparticles the surface to volume ratio decreases as the nanoparticles size increases (*e.g.* a 10 nm diameter Au nanoparticles' surface area to volume ratio is 0.60).[185]

It must noted that the activity and selectivity of only the Au_n/anatase, Degussa P25 and HAP (n = 19, 20, 22) nanocatalysts will discussed in this section. The activity and selectivity of Au_n/CeO_2 (n = 19, 20, 22) nanocatalysts will be discussed in Chapter 6.

5.3 Determination of Ideal Catalytic Hydrogenation Conditions

The reaction conditions used in this study were based on parameters commonly used in the literature when reactions are performed in the liquid phase using batch type reactors utilised in research on the hydrogenation of substituted nitro-aromatics by supported heterogeneous catalysts.[186-188] These reaction conditions were ideal given the limited pressure (15 bar) the liquid phase batch type reactors used here could operate at and taking into account that this study intentionally aimed for the hydrogenation of substituted nitro-aromatics under mild conditions. It must be noted that the pressure of H_2 used in this study for the catalytic hydrogenation reactions comes with a caveat; the TOF for the hydrogenation of substituted nitro-aromatics shows a marked increase as the H_2 pressure is increased from 10 to 40 bar with the only downsides being a slight decrease in selectivity for substituted anilines and the formation of a small percentage of N-aryl hydroxylamine.[189]

Solvent type is also an important factor in liquid phase catalytic hydrogenation reactions given that the solvent can affect reaction kinetics, optimal adsorption of reactants onto the active site, and H_2 mass transfer. Polar protic alcohols are commonly used in the catalytic hydrogenation of nitroaromatics given that they possess high H_2 solubility and relatively low cost.[190] While methanol would seem suitable for this work, given its greater H_2 solubilising ability and increased activity in the catalytic hydrogenation reactions, compared with ethanol, it was not considered as the ideal choice.[191] It has been shown that while the catalytic hydrogenation of substituted nitroaromatics showed a slightly higher conversion rate in methanol than ethanol, yields of the substituted aniline compounds were lower in methanol .[192] The solubility of substituted aromatics (dependent on the functional group) is also generally lower in methanol than in ethanol. This is an important factor, since the reaction rates in catalytic hydrogenation can decrease as the solubility of the reagent or intermediates formed in

the liquid phase during the catalytic process is decreased.[193] For the reasons above, ethanol was chosen as the solvent to be used for the liquid phase catalysis in this work.

5.4 Results and Discussion

5.4.1 Induction Time Study

The majority of catalytic tests performed in this chapter had a duration of 5 hours. However, it was important to establish presence or absence of the induction period (*i.e.* onset of catalytic activity with time of reaction). Hence, a shortened catalytic test study was conducted to find the initial activity of the Au nanocatalysts to determine if there was an induction period. An induction period can help give an idea of what is responsible for the activity observed in a reaction over a catalyst. Some catalysts require a transformation to occur under reaction conditions to activate the catalyst or in the case of nanocatalysts such a period can help elucidate the particle size responsible for catalytic activity.[151]

The study on the induction time was conducted only for the hydrogenation for nitrobenzene over the period of 1 hour with the results summarised in Table 5.3. It was found that there seemed to be no induction period in this reaction. The TOFs obtained using Au nanocatalysts are relatively close to those calculated for the 5 hour reactions with at most a 20% difference between the initial and final TOFs for the 1 and 5 hour reactions respectively. This observation supports the smaller size of the Au nanoclusters deposited on the surface of the catalysts are responsible for this activity, but that this size regime of the catalytically active species is maintained on the catalyst surface with minimal sintering during the reaction. This conclusion is also backed-up by the UV-Vis DRS data which showed little indication that sintering had occurred within the Au nanocatalysts, but it should be noted that sintering on the Au nanocatalysts may not have been entirely absent.

Table 5.3 Induction time study on nitrobenzene hydrogenation

Nanocatalyst	Conversion (%)	Selectivity (%)		TOF(h^{-1})
		Nitrosobenzene	Aniline	
Au_{19}/Anatase	4.4	1.5	98.5	104.6
Au_{19}/Degussa P25	9.9	3.5	96.5	186.5
Au_{19}/HAP-H_2	14.8	26.9	73.1	200.5
Au_{20}/Anatase	0.5	3.2	96.8	8.8
Au_{20}/Degussa P25	1.4	4.5	95.5	27.9
Au_{20}/HAP-H_2	15.0	21.0	79.0	244.6
Au_{22}/Anatase	3.4	2.0	98.0	68.1
Au_{22}/Degussa P25	4.7	2.2	97.8	86.1
Au_{22}/HAP-H_2	17.3	28.6	71.4	248.5

Reaction conditions: nitrobenzene (0.205 mL, 2 mmol), ethanol (15 mL), nanocatalyst (0.1 g), H_2 (10 bar), 100℃, 1 hour

5.4.2 Catalytic Hydrogenation of Substituted Nitro-aromatics

Tables 5.3 – 5.6 and Figures 5.2 - 5 summarise the catalytic activity of Au_{19}, Au_{20}, and Au_{22} deposited on TiO_2 (anatase and Degussa P25), and HAP at 0.2% weight loadings in the catalytic hydrogenation of nitrobenzene, p-nitrotoluene, p-nitrophenol and 1,4-ninitrobenzene. Blank reactions using the reactor itself, charged with standard reaction mixture and unmodified supports were carried out for each reagent. These tests all showed a < 1% conversion of each reagent meaning that any catalytic activity in the hydrogenations could only be attributed to the presence of the Au nanocatalyst. TOF values were only calculated for the production of aniline and functionalised anilines.

The concentration used in the catalytic hydrogenation of 1,4-dinitrobenzene is less than that used in the other hydrogenation reactions. At 2 and 1 mmol amounts the total conversion was less than 5% for the catalytic hydrogenation which was most likely due to the poor solubility of 1,4-Dinitrobenzene in ethanol. Once the amount was lowered to the value adjusted for solubility for 1,4-dinitrobenzene in alcohols (*ca.* 1 g in 300 mL) provided by the manufacturer (Sigma-Aldrich) appreciable catalytic activity was observed. As discussed in Section 5.3, this is an example of why reagent solubility in the liquid phase employed in catalytic hydrogenation reactions is an important factor

Table 5.3 Performance of Au nanocatalysts in catalytic nitrobenzene hydrogenation

Nanocatalyst	Conversion (%)	Selectivity (%)		TOF(h^{-1})
		Nitrosobenzene	Aniline	
Au_{19}/Anatase	18.6	< 1	99.0	73.0
Au_{19}/Degussa P25	35.6	< 1	99.0	154.0
Au_{19}/HAP-H_2[a]	45.5	12.6	87.3	136.8
Au_{20}/Anatase	2.2	< 1	99.0	7.5
Au_{20}/Degussa P25	4.5	< 1	99.0	17.8
Au_{20}/HAP-H_2[a]	53.0	13.8	86.2	166.8
Au_{22}/Anatase	12.0	< 1	99.0	45.7
Au_{22}/Degussa P25	10.5	< 1	99.0	37.8
Au_{22}/HAP-H_2[a]	57.4	13.4	86.6	209.9

Reaction conditions: nitrobenzene (0.205 mL, 2 mmol), ethanol (15 mL), nanocatalyst (0.1 g), H_2 (10 bar), 100°C, 5 hours a: Trace amounts of azoxybenzene detected < 1%

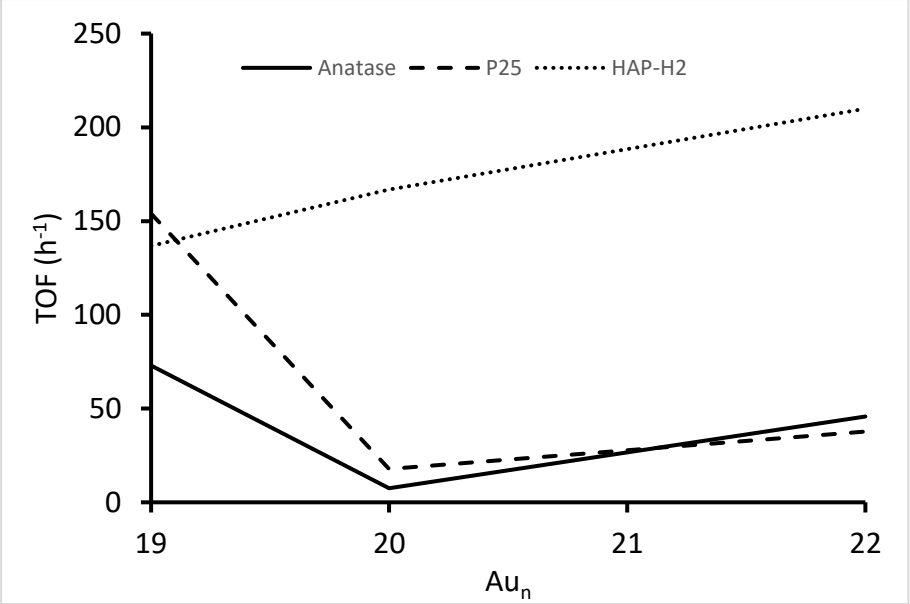

Figure 5.2. TOF(h^{-1}) as a function of size (n) Au_n clusters in nitrobenzene hydrogenation.

Table 5.4 Performance of Au nanocatalysts in catalytic p-nitrotoluene hydrogenation

Nanocatalyst	Conversion (%)	Selectivity (%)		TOF(h^{-1})
		p-Nitrosotoluene	p-Toluidine	
Au_{19}/Anatase	16.5	< 1	99.0	68.8
Au_{19}/Degussa P25	39.6	< 1	99.0	143.7
Au_{19}/HAP-H_2[a]	32.2	4.1	95.9	112.0
Au_{20}/Anatase	1.6	< 1	99.0	5.8
Au_{20}/Degussa P25	3.2	< 1	99.0	11.8
Au_{20}/HAP-H_2[a]	42.7	4.3	95.7	154.1
Au_{22}/Anatase	8.5	< 1	99.0	31.7
Au_{22}/Degussa P25	10.0	< 1	99.0	33.8
Au_{22}/HAP-H_2[a]	47.6	3.8	96.1	177.5

Reaction conditions: 4-nitrotoluene (0.2743 g, 2 mmol), ethanol (15 mL), nanocatalyst (0.1 g), H_2 (10 bar), 100°C, 5 hours Trace amounts of 4,4'-azoxytoluene detected < 1%

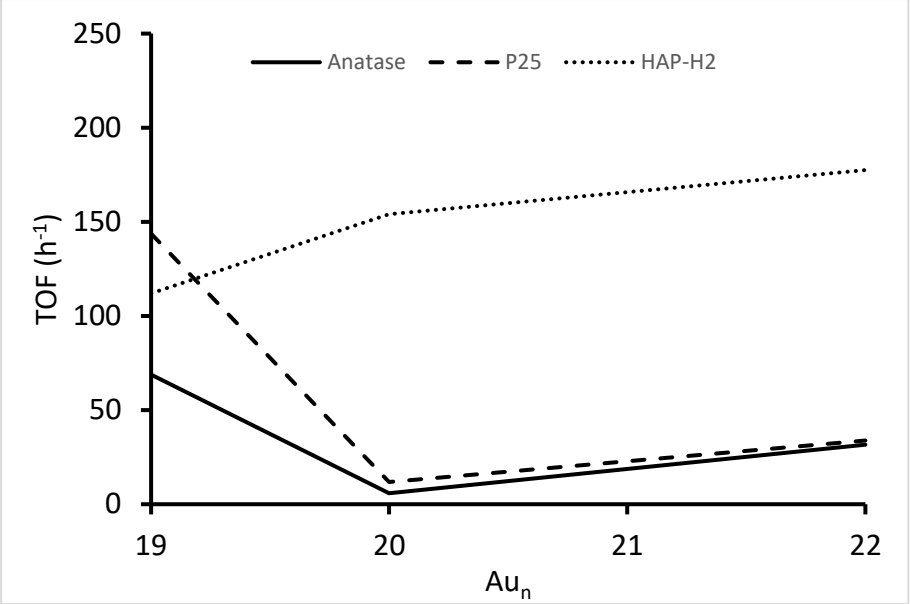

Figure 5.3. TOF(h^{-1}) as a function of size (n) Au_n in 4-nitrotoluene hydrogenation.

Table 5.5 Performance of Au nanocatalysts in catalytic p-nitrophenol hydrogenation

Nanocatalyst	Conversion (%)	Selectivity (%)		TOF(h^{-1})
		p-Nitrosophenol	p-Aminophenol	
Au_{19}/Anatase	11.5	< 1	99.0	39.9
Au_{19}/Degussa P25	21.3	< 1	99.0	74.6
Au_{19}/HAP-H_2[a]	10.7	2.1	97.9	37.9
Au_{20}/Anatase	1.2	< 1	99.0	4.3
Au_{20}/Degussa P25	4.0	< 1	99.0	14.5
Au_{20}/HAP-H_2[a]	19.2	1.2	98.7	63.7
Au_{22}/Anatase	7.2	< 1	99.0	28.0
Au_{22}/Degussa P25	5.9	< 1	99.0	22.3
Au_{22}/HAP-H_2[a]	23.2	1.2	98.7	79.8

Reaction conditions: 4-nitrophenol (0.2762 g, 2 mmol), ethanol (15 mL), nanocatalyst (0.1 g), H_2 (10 bar), 100°C, 5 hours Trace amounts of 4,4' azoxyphenol detected < 1%

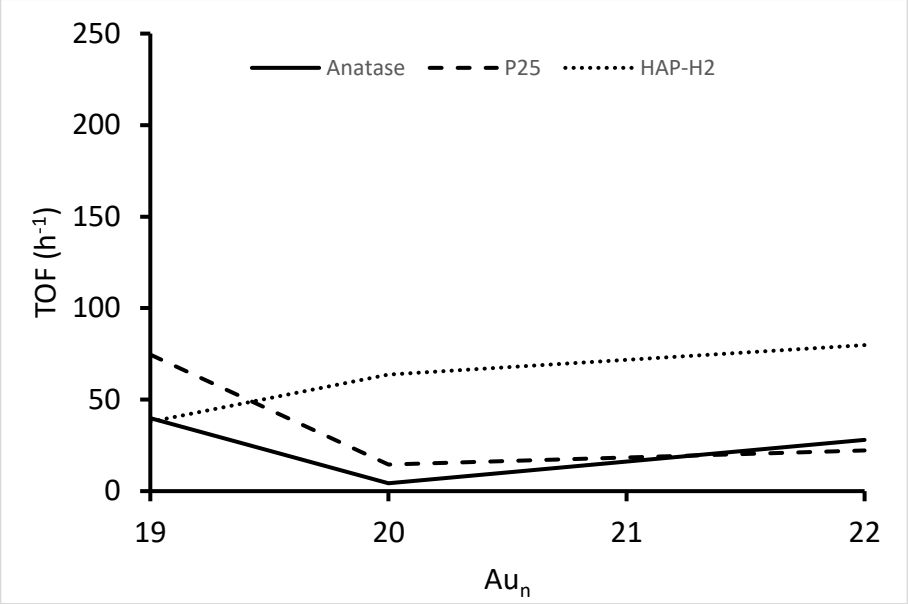

Figure 5.4. TOF(h^{-1}) as a function of size (n) Au_n in 4-nitrophenol hydrogenation.

Table 5.6 Performance of Au nanocatalysts in catalytic 1,4-dinitrobenzene hydrogenation

Nanocatalyst	Conversion (%)	Selectivity (%)			TOF(h^{-1})
		1-Nitro-4-Nitrosobenzene	4-Nitroaniline	Phenylenediamine	
Au_{19}/Anatase	4.6	< 1	99.0	nd	2.5
Au_{19}/Degussa P25	28.2	< 1	99.0	nd	15.1
Au_{19}/HAP-H_2	> 99.0	nd	95.2	4.8	31.5
Au_{20}/Anatase	1.4	< 1	99.0	nd	0.9
Au_{20}/Degussa P25	5.0	< 1	99.0	nd	3.1
Au_{20}/HAP-H_2	> 99.0	nd	94.4	5.6	29.7
Au_{22}/Anatase	4.5	< 1	99.0	nd	2.9
Au_{22}/Degussa P25	6.6	< 1	99.0	nd	3.6
Au_{22}/HAP-H_2	> 99.0	nd	80.5	19.5	28.5

Reaction conditions: 1,4-dinitrobenzene (0.05 g, 0.297 mmol), ethanol (15 mL), nanocatalyst (0.1 g), H_2 (10 bar), 100°C, 5 hours nd = not detected

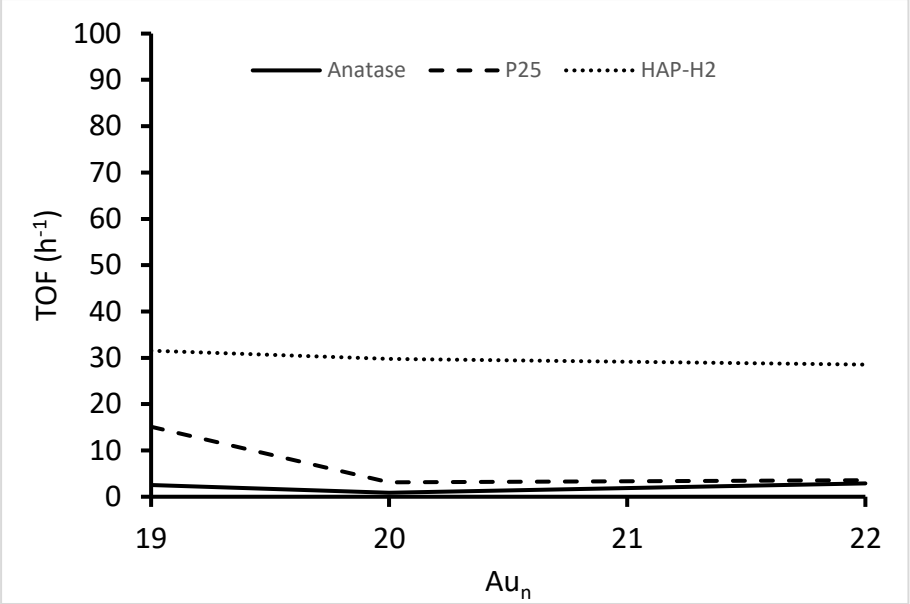

Figure 5.5. TOF(h^{-1}) as a function of size (n) Au_n in 1,4-dinitrobenzene hydrogenation.

The Au_n/anatase and Degussa P25 (n = 19, 20, 22) nanocatalysts are highly selective for anilines and substituted anilines in the catalytic hydrogenation reactions investigated in this study with minimal amounts of the nitroso compounds detected. While selectivity is roughly the same over these nanocatalysts, the activity over the Au_{19}/Degussa P25 catalyst is around double that of the Au_{19}/anatase catalyst in all reactions. This suggests a support effect is present for the Au_{19}/Degussa P25 nanocatalyst given its much higher activity than the Au_{19}/Anatase nanocatalyst. The support effect for supported Au_{19} nanoclusters is most likely a result of the improved stability afforded by the mixture of the anatase and rutile phases present in Degussa P25 which has been shown to offer an improved interaction with Au nanoparticles.[194-195] Given the slightly higher degree of sintering over the anatase support *cf.* the Degussa P25 support prior to the catalytic reaction it could be reasonably concluded that this more pronounced sintering occurring over the Au_{19}/anatase resulted in Au nanoclusters of a larger size regime. This could be a factor in the resulting decreased catalytic activity as Au/anatase supported catalysts have shown relatively high levels of activity in the catalytic hydrogenation of nitro-

aromatics.[196] Similar cluster core size effects also seems to be present in the case of these catalyst systems, given similar rates observed over the Au_{22}/anatase and Degussa P25 nanocatalysts. For comparability the Au_{22}/Degussa P25 catalyst reported in this work had a slightly higher aniline production rate (37.8 h^{-1}) in the nitrobenzene hydrogenation reaction than a Au_{25}/Degussa P25 nanocatalyst (rate of 37.7 h^{-1}) prepared under similar conditions and used under similar catalytic test reaction conditions reported by Fang *et al*. It is to be noted that the pressure of H_2 was higher (40 bar) in their study compared to the 10 bar of H_2 used in this work [158] It should be noted that the studies referenced used higher weight loadings in the ~1 – 2% range which is notably higher than the 0.2% weight loading used in this study.

The Au_{20}/anatase and Degussa P25 nanocatalysts showed the lowest activity of all the catalysts used in this chapter. This low activity could be ascribed to the Au_{20} nanoclusters unique electronic properties best described by the spherical jellium model where the charge from the valence electrons is distributed evenly over the clusters' surface. The valence electrons behave as nearly free electrons confined by the positively charged cluster core. In such a spherical potential well the angular and radial parts of the wavefunctions give rise to discrete electronic shells surrounding the cluster core.[197] According to this model the bare Au_{20} nanocluster is considered to have a closed electronic shell, formed from its 20 valence electrons with the configuration $(1S)^2(1P)^6(1D)^{10}(2S)^2$ and has been experimentally shown to have a relatively large HOMO-LUMO gap of 1.77 eV.[137] The bare Au_{20} nanocluster also has a unique close-packed tetrahedral pyramid structure, where every atom is located at the surface as it lacks a core atom. These properties have been predicted to result in a nanocluster with enhanced stability while at the same time rendering it chemically inert with severely reduced catalytic activity.[198] For reference the ligand protected $[Au_{20}(PP_3)_4]^{4+}$ nanocluster used to synthesise the Au_{20}/anatase and Degussa P25 nanocatalysts has been calculated to have only 16 valence electrons and a HOMO-LUMO gap of 1.33 eV.[135] The free Au_{20} nanocluster, with 20 valence

electrons, was found to be catalytically inactive, while the anionic form of the bare Au_{20} nanocluster was found to be catalytically active in the gas phase.[199] This suggested that chemically inert nanoclusters could be made catalytically active with excess electron donation. A DFT based study found that Au_{20} clusters supported on metal-oxides would show little change in their catalytic activity in the case of weak metal-support interaction, possessing relatively the same electronic structure as that found with free Au_{20} nanoclusters. Even placing the nanocluster at an F^+ centre, generally considered the most likely adsorption site for deposited Au nanoparticles, would do little to change its electronic structure and improve catalytic activity. It was theorised that the charge transfer from the F^+ centre site would only be localised at the Au atom at the interface with support; with the energy bending down towards the nanoclusters valence band.[200] A weak interaction between Au_{20} and the anatase and Degussa P25 supports , the presence of a higher proportion of F^+ than F^{2+} centres or a combination of both seem likely reasons given Au_{20} poor activity when compared to the performance of the Au_{19} and Au_{22} supported on both anatase and Degussa P25.

The highest activity for the catalytic hydrogenation of substituted nitro-aromatics in this work was observed over the Au_n/HAP-H_2 (n = 19, 20, 22) nanocatalysts in this work. In a scoping study conducted earlier in this work it was found that the catalytic activity over the Au_n/HAP (n = 19, 20, 22) nanocatalysts calcined at 400 ℃ before the reductive treatment resulted in a ~ 10% conversion of nitrobenzene to products. After the reductive treatment at 400℃ the conversion increased dramatically giving 45%, 53%, and 57% conversion of nitrobenzene to products for the Au_{19}, Au_{20}, and Au_{22}/HAP-H_2 nanocatalysts respectively. The HAP support has been shown to display a non-classical SMSI which was discussed in detail in Section 1.3.5.3. A study by Tang *et al.* had found that Au nanoparticles deposited on the surface of HAP had undergone encapsulation by a partially oxidised layer of substrate under an oxidative treatment. This encapsulation was then reversed under the reductive treatment

leaving exposed Au nanoclusters. The degree of the encapsulation and reversibility over the Au nanoparticles had depended on the treatment temperatures with minimal sintering observed at 300 – 500 °C, with decreased catalytic activity observed after oxidative treatment, which subsequently increased after the second reductive treatment.[85] Given the above results it could be concluded that the Au_{19}, Au_{20}, and Au_{22}/HAP-H_2 nanocatalysts used in this work are exhibiting the same SMSI as in the case study discussed above, which would account for the high level of stability and lack of sintering observed over these nanocatalysts.

The Au_n/HAP-H_2 (n = 19, 20, 22) nanocatalysts clearly showed how a difference in cluster size of 1 to 2 atoms could affect the catalytic activity in the hydrogenation of substituted nitroaromatics. The observed catalytic activity demonstrated an almost linear increase as the Au nanocluster size increased. The TOF was also much higher than in the case of nanoclusters supported on the anatase and Degussa P25. This suggests that the Au nanocluster size is a key factor defining catalytic activity in these series. This observation is in agreement with previous literature reports that nanoclusters with an average size range of 1 – 1.5 nm were more active in the catalytic hydrogenation of substituted nitroaromatics than nanoparticles with an average size range of 2.5 – 3 nm.[179] It should be noted that the reduction of the TOF in the case of 1,4-dinitrobenzene from the Au_{19}/HAP-H_2 to the Au_{22}/HAP-H_2 nanocatalyst was due to the more pronounced further reduction of 4-nitroaniline to phenylenediamine in the case of larger clusters. The strong metal-support interaction also seems to play a key role, as the stronger interaction of the deposited Au nanoclusters was most likely responsible for the improved catalytic activity *cf.* that observed for anatase and Degussa P25 supported nanoclusters. Of note, a similar trend of the increasing catalytic activity with increasing Au nanocluster size has been demonstrated in a study by Liu *et al.* using atomically precise Au nanoclusters deposited on HAP for the aerobic oxidation of cyclohexane.[139] The study found that catalytic activity increased as a function of Au nanocluster size from Au_{10}, Au_{18}, Au_{25}, and Au_{39}. The Au_{39}

nanocluster displayed the highest catalytic activity with a drop-off in activity observed after this.

The catalytic activity displayed by the Au_{20}/HAP-H_2 nanocatalyst is in contrast with earlier observations. Where this cluster demonstrated a minimum of the activity in series when deposited on anatase and Degussa P25, it showed an increased activity compared to Au_{19}/HAP-H_2 when deposited on HAP. This likely means that the HAP support provides a unique synergistic effect with this cluster as a result of strong metal-support interactions, resulting in an increase of charge transfer from the support to the Au_{20} nanocluster.[85] Another reason could be theorised, where the higher temperature activation treatments led to the improved de-protection of cluster cores, exposing more Au atoms in a systematic fashion across the series. The Au_{20} nanocluster was possibly less active as it was more stable under the lower activation temperatures to de-ligation and hence less Au surface was exposed.

5.4.3 Hammett Correlation in the Hydrogenation of Para-Substituted Nitro-aromatics

To find the effect that electron withdrawing functional groups at the *para*-position on the nitro-aromatic ring had on the catalytic activity during hydrogenation, the Hammett relationship was applied to the catalytic activity observed in this study. While the *para*-substituted -NO_2 1,4-dinitrobenzene was planned to be included in this study it was subsequently left out as the reaction was not carried out under the same conditions (due to solubility issues mentioned above) as the other para-substituted -CH_3, and -OH nitro-benzenes. For this approach, the reaction rate, derived as a function of the decrease in nitro-benzene concentration (mol L^{-1}) over time (seconds), for the case of nitrobenzene hydrogenation to the aniline was recorded as a reference (R_0). The reaction rate for the hydrogenation of the

substituted nitroaromatics to their corresponding anilines (*Ri*) was then related to (R_0) according to *Equation 5.4*:

$$\log\left(\frac{R_i}{R_0}\right) = \rho \times \sigma$$

(*Eq 5.4*)

Where ρ is the reaction constant and σ the Hammett substituent constant. The σ substituent constant is an empirical factor based on the polarity of the specific substituent. The stronger the electron withdrawing behaviour of a substituent the more positive its σ value; the opposite is true for electron donating substituents with stronger donating behaviour resulting in more negative σ values. It is generally found that *para* σ constants correspond to the influence of inductive and resonance effects while *meta* σ constants represent the inductive effects of the substituent. The reference values of *p*-CH_3 σ = -0.17 and *p*-OH σ = -0.37 were obtained from the literature.[201] The reaction constant, ρ, allows the establishment of a quantitative relationship between catalytic activity and the electronic effects of the electron withdrawing or donating functional groups.

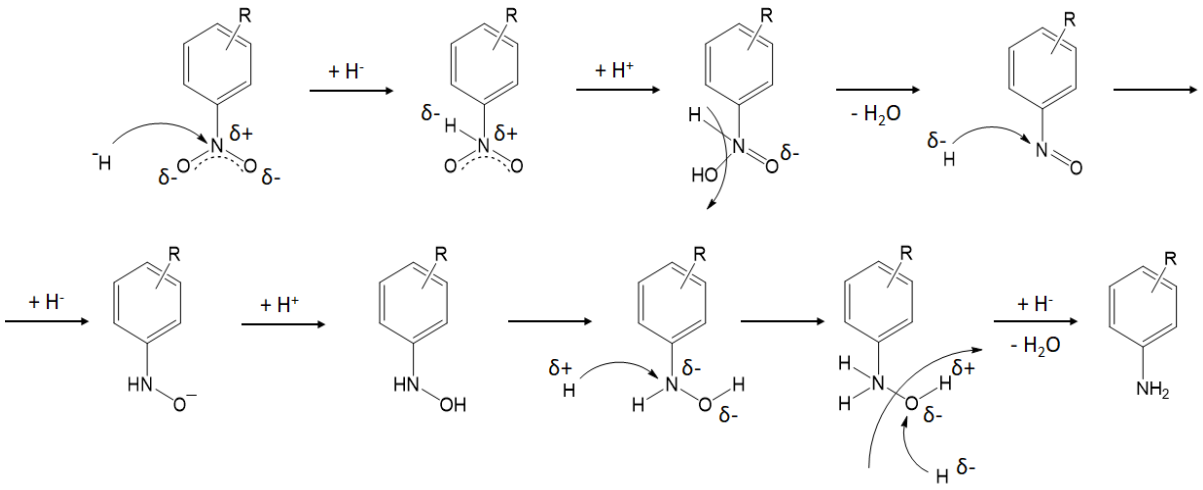

Scheme 5.1. Nucleophilic reaction pathway for the hydrogenation of nitrobenzene [adapted from 190].

With the presence of a negatively charged transition state (see Scheme 5.1), the reaction is slowed by electron-donating substituents and the reaction constants' value is found to be greater than zero. The slope of the line in Figure 5.6, which corresponds to ρ gives it a positive value, which means the catalytic hydrogenation reactions over catalysts studied in this work likely proceed consistent *via* a nucleophilic mechanism such as that proposed in earlier studies.[202-203] The introduction of electron-donating substituents at the *para*-position results in the stabilisation of the $-NO_2$ functional group through resonance and inductive effects. In the mechanism provided in Scheme 5.1, the $-NO_2$ group needs to be activated to form a negatively charged intermediate, which can then be attacked by hydrogen acting as a nucleophile. If destabilised the $-NO_2$ group is more easier to activate for the hydrogenation reaction thus increasing the reaction rate as the electron withdrawing ability of the *para*-substituent increases.

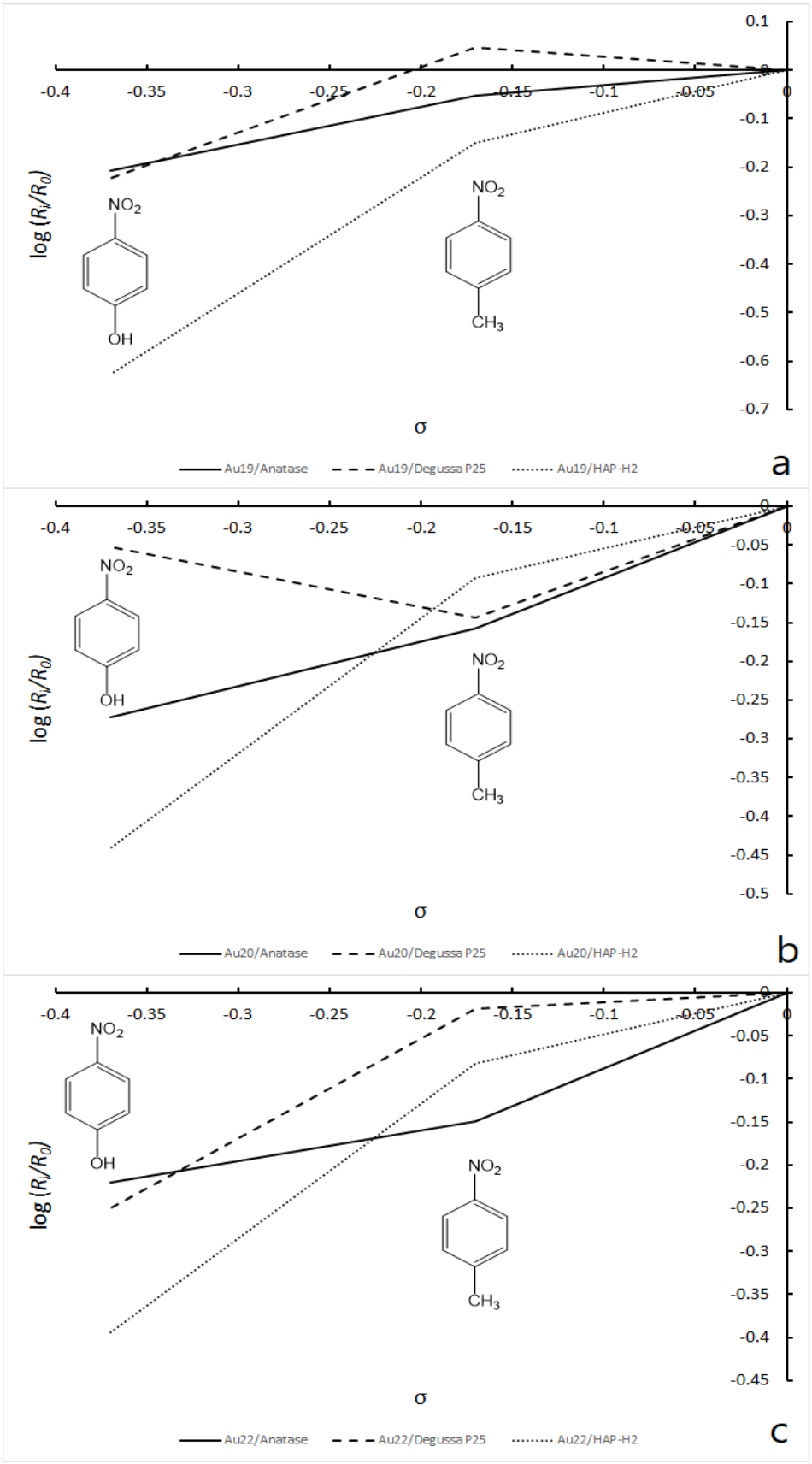

Figure 5.6. Hammett plots for the -NO_2 group reduction on para-substituted nitrobenzene using (a) Au_{19} nanocatalysts, (b) Au_{20} nanocatalysts, (c) Au_{22} nanocatalysts.

5.4.4 Reaction Mechanism for the Catalytic Hydrogenation of Substituted Nitroaromatics

Given the product distributions obtained in the catalytic hydrogenation it can be concluded that the reaction mechanism occurring in the case of the nanocatalysts supported on anatase and Degussa P25 is different than the one over the HAP- supported nanocatalysts. The reaction mechanism over the anatase and Degussa P25 nanocatalysts seems to follow the direct route (Figure 5.1) detailed in Haber's proposed reaction scheme given that no azo compounds were detected in the reaction products. Given that no N-aryl hydroxylamines were detected in the reaction products either, the most likely reaction pathway is given in Figure 5.7. These findings match closely with previously reported findings on the reaction mechanism over Au nanoparticles supported on TiO_2.[204]

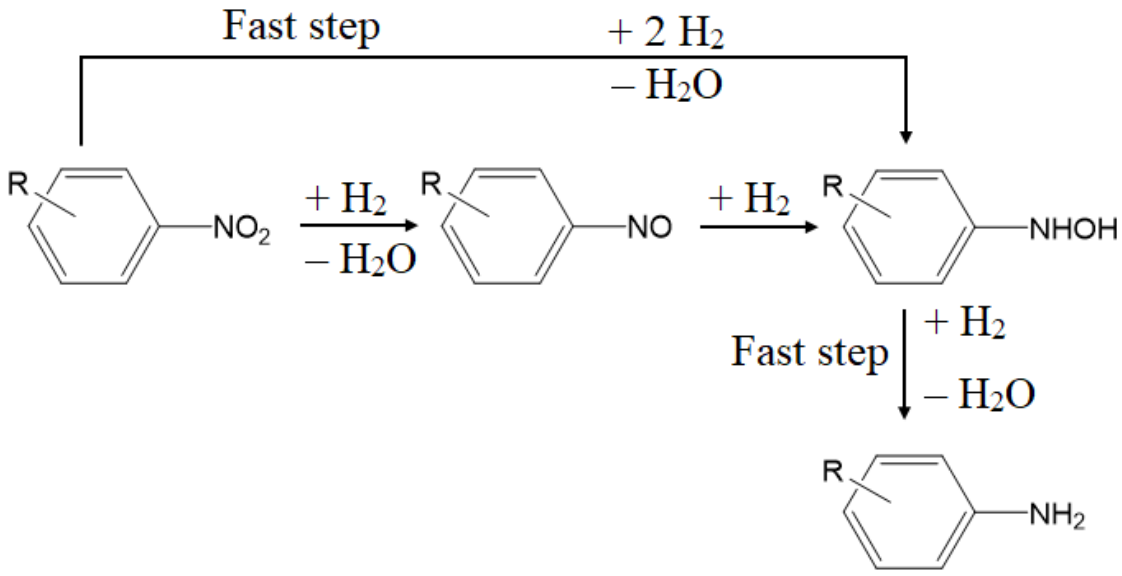

Figure 5.7. Reaction pathway for hydrogenation of substituted nitro-aromatic over Au/anatase and Degussa P25 nanocatalysts.

From the product distribution observed over the HAP-based nanocatalysts, nitrosobenzene and trace amounts of substituted azo-compounds were detected suggesting that the hydrogenation of substituted nitroaromatics occurs through the direct and to a minor extent the condensation pathways detailed in Haber's reaction scheme (Figure 5.1). Given the amount of substituted nitrosobenzene (21 – 28% of total conversion) obtained in the product mixture after 1 hour, it is not surprising that the condensation of the nitroso intermediates occurs with N-aryl hydroxylamines to form azobenzene (at conversions not exceeding 1.0%). The fact that N-aryl hydroxylamines were not detected, most likely means that the hydrogenation of nitrosobenzene is somewhat slower, compared to the relatively fast hydrogenation of these compounds. Azo-compounds were not detected in the 1,4-dinitrobenzene reaction which had reached > 99.0% conversion meaning that they are also further hydrogenated to give substituted nitro-aromatics.

5.5 Conclusions

In conclusion a size effect has been demonstrated for supported Au nanocatalysts with a cluster core size difference of only one or two Au atoms. This size effect changed with the support used. In the case of titania, the smaller Au_{19}/anatase and Degussa P25 showed higher reactivity compared with the Au_{20} and A_{22} supported clusters. The Au_{20}/anatase and Degussa P25 nanocatalysts had the lowest activity which was ascribed to the Au_{20} nanoclusters unique electronic properties and rather high stability. The trend significantly changed for the HAP-H_2 nanocatalyst series, with the Au_{22}/HAP-H_2 demonstrating the highest activity. The TOFs for these catalysts were higher (200 – 248 h^{-1}) than the TOFs (< 170 h^{-1}) for conventional Au nanocatalysts in the catalytic hydrogenation of nitroaromatics.[184] These high TOF were also achieved at relatively low 0.2% by Au weight loadings compared to the commonly used 1.0 – 2.0% by Au weight loadings used in previous studies. These results fit with previously reported findings that Au nanoclusters in the 1 – 3 nm size range display the highest catalytic

activity. Unfortunately, it is not known exactly to what extent sintering affected the Au nanocluster supported Anatase and Degussa P25 catalysts.

From the Hammett plot study, it was shown that the introduction of electron donating substituents in the *para*-position decreased the catalytic activity in the hydrogenation of substituted nitroaromatics as observed in previous studies. The introduction of electron-donating substituents at the *para*-position results in the stabilisation of the $-NO_2$ functional group through resonance and inductive effects. Due to this stabilisation the $-NO_2$ group is more difficult to activate for the hydrogenation reaction thus slowing the reaction rate as the electron donating ability of the *para*-substituent increases.

Chapter 6 Study of the Activity of the Au/CeO_2 Nanocatalysts in the Catalytic Hydrogenation of Substituted Nitro-aromatics

6.1 Introduction

The aromatic azo-compound intermediates formed in the condensation route that makes up the reaction pathway for the catalytic hydrogenation of substituted nitrobenzene to anilines (Figure 5.1) were often thought of as undesirable intermediates in the catalytic hydrogenation of nitro-aromatics. The majority were historically used in the production of dyes for the polymer, textile and food industries but were of little economic and material value for other processes in the chemical industry.[205] Further research into azo-compounds has furthered their application to the production of pharmaceuticals and radical reaction initiators, with promising applications in the area of materials science such as use in liquid crystal displays, optical media storage and as chemosensors.[206]

There are a number of processes available for the production of aromatic azo-compounds including diazotization and coupling, the condensation of nitro-aromatics with aromatic-amines, reduction of nitro-aromatics, and the oxidation of aromatic-amines.[206-207] The main synthetic industrial procedure for the synthesis of aromatic azo-compounds is the coupling of aryl diazonium salts *via* an electrophilic substitution reaction with electron-rich aromatic compounds. The diazonium salt is formed *in-situ via* a diazotization method which involves oxidation of the aromatic amine with a concentrated mineral acid and nitrite (generally sodium nitrite) solution.[208] The Mills reaction involves the formation of nitroso-functionalised aromatics from the oxidation of aniline, which are subsequently coupled to aromatic-amines in glacial acetic acid.[209] The Wallach reaction involves the rearrangement of a functionalised azoxy-aromatic, obtained from the reduction of the corresponding nitro-aromatic, that is

subsequently transformed into the 4-hydroxy substituted azo-derivative with the treatment of concentrated acid at high temperature.[210] While these methods allow for the synthesis of desired azo-aromatic compounds they also have the drawbacks such as the use of stoichiometric amounts of concentrated and sometimes toxic acids, multiple reaction steps, and the generation of a large amount of environmentally harmful by-products and waste from the multiple reaction processes involved and post-treatments.[211] The supported Au catalysts have shown the ability to yield substituted azo-compounds under relatively mild conditions, without the use of modifiers or stoichiometric amounts of nitrites or transition metals. Au/TiO_2 catalysts have been used in the synthesis of azo-compounds by coupling substituted anilines under oxidative conditions.[212] Of interest, though, is the activity displayed by Au nanoparticles supported on CeO_2, which were able to catalyse synthesis of substituted azo-compounds from substituted nitroaromatics in a one-step hydrogenation reaction.[213] In this chapter, the catalytic hydrogenation of substituted nitro-aromatics was investigated to determine if the nanocatalysts based on the atomically precise Au clusters supported on CeO_2 exhibited the same selectivity as was seen in previous studies.

6.2 Catalyst Preparation and Experimental Catalytic Procedure

The detailed catalyst preparation protocol is given as detailed in Section 3.4. The experimental catalytic procedure is the same as detailed in Section 3.5. The amount of reagent used in catalytic reactions was same as detailed in Table 5.2. Briefly, in a typical experiment a PTFE liner was charged with 15 mL EtOH, 0.1 g of Au_n/CeO_2 nanocatalyst (n = 19, 20, 22) and a calculated amount of reactant (Table 5.2). The liner was sonicated for 4 mins, then placed in the batch (Parr-like) reactor and the reactor was sealed. The reactor was flushed sequentially with N_2, H_2, and finally pressurised to 10 bar with H_2. The reaction mixture was stirred with a magnetic stirrer bar at 700 rpm with a set reaction temperature of 100℃. After 5 hours (1 hour in the induction time study) stirring and heating were ceased, and the reactor cooled in an ice

bath. The reaction mixture was separated from the nanocatalyst by centrifugation (12000 rpm for 10 mins) and filtered through a 45 μm pore size PTFE filter. The recovered catalyst was washed 3 times with 30 mL of EtOH (re-dispersion followed by centrifugation and separation) and dried under vacuum. Reactions were repeated 3 times. The typical standard errors of independent catalytic tests were below 1.5%. Reproducibility varied with a < 3% difference between the nitrobenzene and *p*-nitrotoluene catalytic hydrogenation results, < 5% for the 1,4-Dinitrobenzene catalytic hydrogenation results and < 7% between the *p*-nitrophenol catalytic hydrogenation results. Analysis of the reaction mixtures was performed using a combination of GC-FID and HPLC as detailed in Section 3.5. TOFs were calculated for the substituted aniline products only according to *Equation 5.2*.

6.3 Results and Discussion

6.3.1 Induction Time Study

The study on the induction period was performed at the beginning of these experiments similarly to that described at the beginning of Chapter 5, but conducted only for the hydrogenation of nitrobenzene over the Au/CeO_2 nanocatalysts over the period of 1 hour (in comparison to longer test durations discussed later in this chapter). The obtained results are summarised in Table 6.6. It was found that there seemed to be no significant induction period in this reaction with all catalysts demonstrating appreciably high conversions. The TOF's calculated based on the production of aniline over the Au/CeO_2 nanocatalysts are, however, twice as high for 1 hour reactions as those calculated for the 5 hour reactions. The conversion % of nitrobenzene was also only roughly half that of the conversion % in the 5 hour reactions. The UV-Vis DRS data suggested that the small size of the Au nanoclusters deposited on the surface of the catalysts was maintained during reaction, which is indicative that ultra-small clusters are the most likely species responsible for the catalytic activity. Apart from the onset

of the reagent mass-transfer/diffusion limitations during late stages of reaction, there are not that many other factors that could be easily identifiable as responsible for apparent decrease in TOF. The one such factor could be the reduction of the CeO_2 support itself during reaction; this phenomenon will be discussed further in the results and discussion section of this chapter. Given that the UV-Vis DRS data showed little indication that cluster sintering had occurred within the Au nanocatalysts, it still cannot be assumed however that sintering was entirely absent on the Au/CeO_2 nanocatalysts.

Table 6.6 Induction Time Study on Au/CeO_2 Nanocatalysts in Catalytic Nitrobenzene Hydrogenation

Nanocatalyst	Conversion (%)	Selectivity (%)			TOF(h^{-1})
		Nitrosobenzene	Aniline	Azoxybenzene	
Au_{19}/CeO_2	23.5[a]	1.4	42.5	56.1	129.9
Au_{20}/CeO_2	16.1[a]	1.2	32.5	66.3	79.4
Au_{22}/CeO_2	16.2[a]	2.5	20.5	77.0	86.1

Reaction conditions: nitrobenzene (0.2051 mL, 2 mmol), ethanol (15 mL), nanocatalyst (0.1 g), H_2 (10 bar), 100°C, 1 hour a: trace amounts of azobenzene detected

6.3.2 Catalytic Hydrogenation of Substituted Nitro-aromatics over CeO_2 Nanocatalysts

Standard catalytic tests over 5 hours were performed for a wider range of substituted nitro-aromatics using Au clusters supported and activated on ceria. Tables 6.7 – 6.10 summarise the catalytic activity of Au_{19}, Au_{20}, and Au_{22} deposited on CeO2, at 0.2% weight loadings, in the catalytic hydrogenation of nitrobenzene, *p*-nitrotoluene, *p*-nitrophenol and 1,4-dinitrobenzene. Blank reactions of the reactor itself, and unmodified supports were carried out for each reagent.

These tests all showed a < 1% conversion of each reagent, meaning that any catalytic activity in the hydrogenations could only be attributed to the presence of the Au/CeO_2 nanocatalyst. TOF values were only calculated for the production of aniline and functionalised anilines. The reduced amount of 1,4-dinitrobenzene used in catalytic tests was due to the same reasons as discussed in Section 5.4.2.

Table 6.7 Catalytic Performance of Au/CeO_2 Nanocatalysts in Catalytic Nitrobenzene Hydrogenation

Nanocatalyst	Conversion (%)	Selectivity (%)			TOF(h^{-1})
		Nitrosobenzene	Aniline	Azoxybenzene	
Au_{19}/CeO_2	40.7[a]	< 1	35.3	64.6	65.8
Au_{20}/CeO_2	40.8[a]	< 1	23.5	76.4	39.9
Au_{22}/CeO_2	33.6[a]	< 1	19.1	80.8	30.0

Reaction conditions: nitrobenzene (0.2051 mL, 2 mmol), ethanol (15 mL), nanocatalyst (0.1 g), H_2 (10 bar), 100℃, 5 hours a: trace amounts of azobenzene detected

Table 6.8 Catalytic Performance of Au/CeO_2 Nanocatalysts in Catalytic p-Nitrotoluene Hydrogenation

Nanocatalyst	Conversion (%)	Selectivity (%)			TOF(h^{-1})
		Nitrosotoluene	p-Toluidine	4,4'-Methylazoxybenzene	
Au_{19}/CeO_2	52.6[a]	< 1	37.1	62.8	83.9
Au_{20}/CeO_2	37.0[a]	< 1	32.4	67.5	55.5
Au_{22}/CeO_2	45.7[a]	< 1	23.5	76.4	51.9

Reaction conditions: p-nitrotoluene (0.2743 g, 2 mmol), ethanol (15 mL), nanocatalyst (0.1 g), H_2 (10 bar), 100℃, 5 hours a: trace amounts of azobenzene detected

Table 6.9 Catalytic Performance of Au/CeO_2 Nanocatalysts in Catalytic p-Nitrophenol Hydrogenation

Nanocatalyst	Conversion (%)	Selectivity (%)			TOF(h^{-1})
		Nitrosophenol	Aminophenol	4,4' Hydroxyazoxybenzene	
Au_{19}/CeO_2	15.5	2.5	97.5	nd	61.2
Au_{20}/CeO_2	6.0	5.2	94.9	nd	22.5
Au_{22}/CeO_2	10.5	4.3	95.8	nd	36.6

Reaction conditions: p-nitrophenol (0.2762 g, 2 mmol), ethanol (15 mL), nanocatalyst (0.1 g), H_2 (10 bar), 100℃, 5 hours nd = not detected

Table 6.10 Catalytic Performance of Au/CeO_2 Nanocatalysts in Catalytic 1,4-Dinitrobenzene Hydrogenation

Nanocatalyst	Conversion (%)	Selectivity (%)			TOF(h^{-1})
		1-Nitro-4-nitrosophenol	4-Nitroaniline	4,4'-Dinitrozobenzene	
Au_{19}/CeO_2	90.9[a]	< 1	4.0	96.0	2.3
Au_{20}/CeO_2	85.6[a]	< 1	1.5	98.4	0.4
Au_{22}/CeO_2	88.4[a]	< 1	1.8	98.1	0.5

Reaction conditions: 1,4-dinitrobenzene (0.05 g, 0.297 mmol), ethanol (15 mL), nanocatalyst (0.1 g), H_2 (10 bar), 100°C, 5 hours a: trace amounts of azoxybenzene detected

The Au/CeO_2 nanocatalysts generally showed the same size effect trend as the other metal-oxide catalysts with the Au_{19}/CeO_2 catalyst giving the highest activity and Au_{20}/CeO_2 catalyst giving the lowest activity for the production of anilines. However, it is noteworthy that the Au_{20} nanocluster shows reasonable activity when supported on CeO_2 *cf.* the anatase and Degussa P25 supports. Like in the case of HAP support, this is most likely due to the stronger support-interaction that Au has when deposited on CeO_2 supports.[214] Overall the conversion of substituted nitro-aromatics was higher over the Au_{19}/CeO_2, suggesting that the smaller Au nanocluster is responsible for an increase in the catalytic activity. Of interest, though, was the increase in selectivity for the substituted azoxy-aromatic that increased with the size of the Au nanoclusters supported on CeO_2. This could be a result of the smaller Au_{19} clusters catalysing the hydrogenation of the nitroso-compounds through the direct route, in the reaction pathway for the hydrogenation of substituted nitro-aromatics, faster than on the Au_{20} and Au_{22} CeO_2 nanocatalysts. For the condensation route to occur it has been proposed that a high surface concentration of nitroso-compounds is needed. This is a reason why the condensation route is

not favoured over the Au/TiO_2 catalysts as the nitroso-compounds are quickly converted to N-aryl phenylhydroxylamines, which then form the corresponding anilines. Because the hydrogenation rate over CeO_2 is relatively slower compared to that over Au/TiO_2 catalysts the condensation route, the reaction pathway for the hydrogenation of substituted nitroaromatics, is favoured.[204] Thus, the conversion rate of substituted nitro- and nitroso-aromatics is slower which allows the condensation of nitroso-compounds to the corresponding azoxy-aromatics as they accumulate on the catalyst surface. The decomposition of N-aryl phenylhydroxylamines has also been found to be relatively fast over CeO_2.[204]

The selectivity in these reactions towards the substituted azoxy-aromatic compounds and not the substituted azo-aromatic compounds can be explained by the faster rate of condensation to the azoxy-aromatic compound at the catalysts surface (Figure 6.1). This means it is not further hydrogenated to the substituted azo-aromatic compound due to the accumulation of nitroso-compounds at the catalysts surface. It has been shown that the hydrogenation of the substituted azoxy-aromatic compounds occurs only once a high proportion of the nitro-aromatic precursor has reacted.[213] At this point the substituted azoxy-aromatic compound undergoes further hydrogenation to the substituted azo-aromatic compound. Hydrogenation of the azo-aromatic compounds to their respective anilines only occurs once all the substituted azoxy-aromatic compounds have been hydrogenated due to their preferential adsorption at the catalyst surface. This is evidenced in the reaction of 1,4-dinitrobenzene, where reaction did proceed further down the catalytic pathways due to the reagent being at the lower concentration yielding 4,4'-dinitroazobenzene rather than 4,4'-dinitroazoxybenzene. After the 1,4-dinitrobenzene catalytic hydrogenation reaction was completed, a small amount of 4,4'-dinitroazobenzene crystallised out of all the reaction mixtures after cooling in the freezer. The details of characterisation of obtained products can be found in Section 3.3.

The presence of electron withdrawing or donating functional groups in the *para*-position had a varied effect on the reaction activity in the hydrogenation of the substituted nitroaromatics over the Au/CeO_2 nanocatalysts. While the hydrogenation of *p*-nitrophenol had the lowest conversion rate, it was found that the hydrogenation of *p*-nitrotoluene had the highest conversion rate. These observations are a notable contrast as both substituents are electron donating functional groups, although the hydroxy group has a stronger electron donating ability (*p*-OH σ value = 0.37, -*p*-CH_3 σ value = 0.17). Enhancement of the activity by the methyl group has been observed in a previous study by Liu *et al.* which found that the -CH_3 electron donating functional group increased the rate of reaction when compared with electron withdrawing functional groups.[215]

Another observed trend is the variation in production of the substituted azo-compounds as the functional group at the para-position of the nitroaromatic changes. Similarly, to the effect that electron withdrawing and donating groups have on the catalytic hydrogenation reaction rate, the condensation reaction between the substituted nitroaromatics is also affected via resonance and inductive effects. The condensation reaction rate between the substituted nitroso-compounds and N-aryl hydroxylamines is reduced by the presence of functional group in the para-position in the order -NO_2 > -H > -CH_3 > -OH.[211] For this reason, the variation in selectivity towards the substituted azoxyaromatics in the catalytic hydrogenation reactions of the substituted nitro-aromatics is observed due to the increased condensation reaction rate. The selectivity towards azoxybenzene for all catalysts was slightly higher than for 4,4'-methylazoxybenzene with 4,4'-dinitroazobenzene the main product in the hydrogenation of 1,4-dinitrobenzene hydrogenation. It is also for these reasons that the corresponding azoxy- or azo-compound is not observed in the hydrogenation of *p*-nitrophenol as has been shown before in previous studies. In this case, the condensation rate is outcompeted by the hydrogenation of nitroso-compound.[181] As the catalytic hydrogenation reaction of the 1,4-dinitrobenzene

reached close to 100% conversion it is probable that the azo-product distribution would change little from the initial conversion distributions seen in the other reactions. The comparability of this work to previous studies is difficult given larger particle sizes, the higher Au weight loadings used by others (~1 – 1.5%) and the range of solvents, such as toluene, and reductants, such as $NaBH_4$ used.[181, 204, 213, 216]

6.3.3 Deactivation of the Au/CeO_2 Nanocatalysts

Due to the reduction of the ceria support in the Au/CeO_2 nanocatalysts during the first catalytic test according to the UV-Vis DRS studies (Figures 4.3.14-16 (c)) the recovered nanocatalysts were reused for the catalytic hydrogenation of nitrobenzene to see if their catalytic activity would be different in a subsequent catalytic test. The results of this study are summarized below in Table 6.11.

Table 6.11 Catalytic Performance of Recovered Au/CeO_2 Nanocatalysts in Catalytic Nitrobenzene Hydrogenation

Nanocatalyst	Conversion (%)	Selectivity (%)			TOF(h^{-1})
		Nitrosobenzene	Aniline	Azoxybenzene	
Au_{19}/CeO_2	8.1	1.4	42.5	56.0	13.6
Au_{20}/CeO_2	9.6	1.2	32.5	66.2	12.2
Au_{22}/CeO_2	6.7	2.5	20.5	77.0	5.4

Reaction conditions: nitrobenzene (0.2051 mL, 2 mmol), ethanol (15 mL), recovered nanocatalyst (0.1 g), H_2 (10 bar), 100℃, 5 hours

It was found that the catalytic activity was severely reduced when compared to the first catalytic test (Table 6.7). However, the relative trends as a function of cluster size with respect to the conversion rate and selectivity remained almost the same over these catalysts. The metal-

support interfacial region in Au/CeO2 is very important for defining the catalytic activity over these catalysts, and any alteration to the support could have a detrimental effect on the synergistic interactions at this interface.[217] What is proposed in this study is that the reduction of the CeO_2 support to CeO_{2-x} is responsible for the loss of activity observed over the recovered catalysts given CeO_2's facile reducibility.[218] A study on the adsorption of nitrosobenzene on the surface found that in addition to the σ-N interaction at the Au metal site, a band indicating σ-O interaction emerged. This observation was attributed to the interaction between the N=O functional group and the surface oxygen ions on the CeO_2 support.[213] With the reduction of CeO_2 to CeO_{2-x} it is most likely that the concentration of oxygen atoms at the surface would decrease. With the reduction of oxygen atoms at the surface (and in particular, in proximity to Au clusters) it is probable that the rate of adsorption of nitrosobenzene would decrease with the loss of sites responsible for favourable interaction.

6.3.4 Reaction Mechanism

Overall the reaction mechanism for the hydrogenation of substituted nitroaromatics seems to follow the one shown in Figure 6.1. Given the detection of substituted nitrosobenzene intermediates in the reaction mixture and not any N-aryl phenylhydroxylamine compounds it can assumed that the condensation of these intermediates proceeds through the "route b". While this has been found to be the most likely mechanism the self-condensation of the substituted nitrosobenzene intermediates through the "route a" cannot be ruled out. Due to aniline being detected in the reaction mixture the direct route must also be catalysed over Au/CeO_2 nanocatalysts but at a much-reduced rate. There was also a size effect with the Au_{19}/CeO_2 catalyst showing a higher aniline production indicating that higher catalytic activity could be responsible for hydrogenating N-aryl phenylhydroxylamines at an increased rate *via* the direct route. Given that it has been shown to aniline is not formed until the substituted azoxy

intermediates have been hydrogenated to the corresponding azo compounds this is the most likely reason.

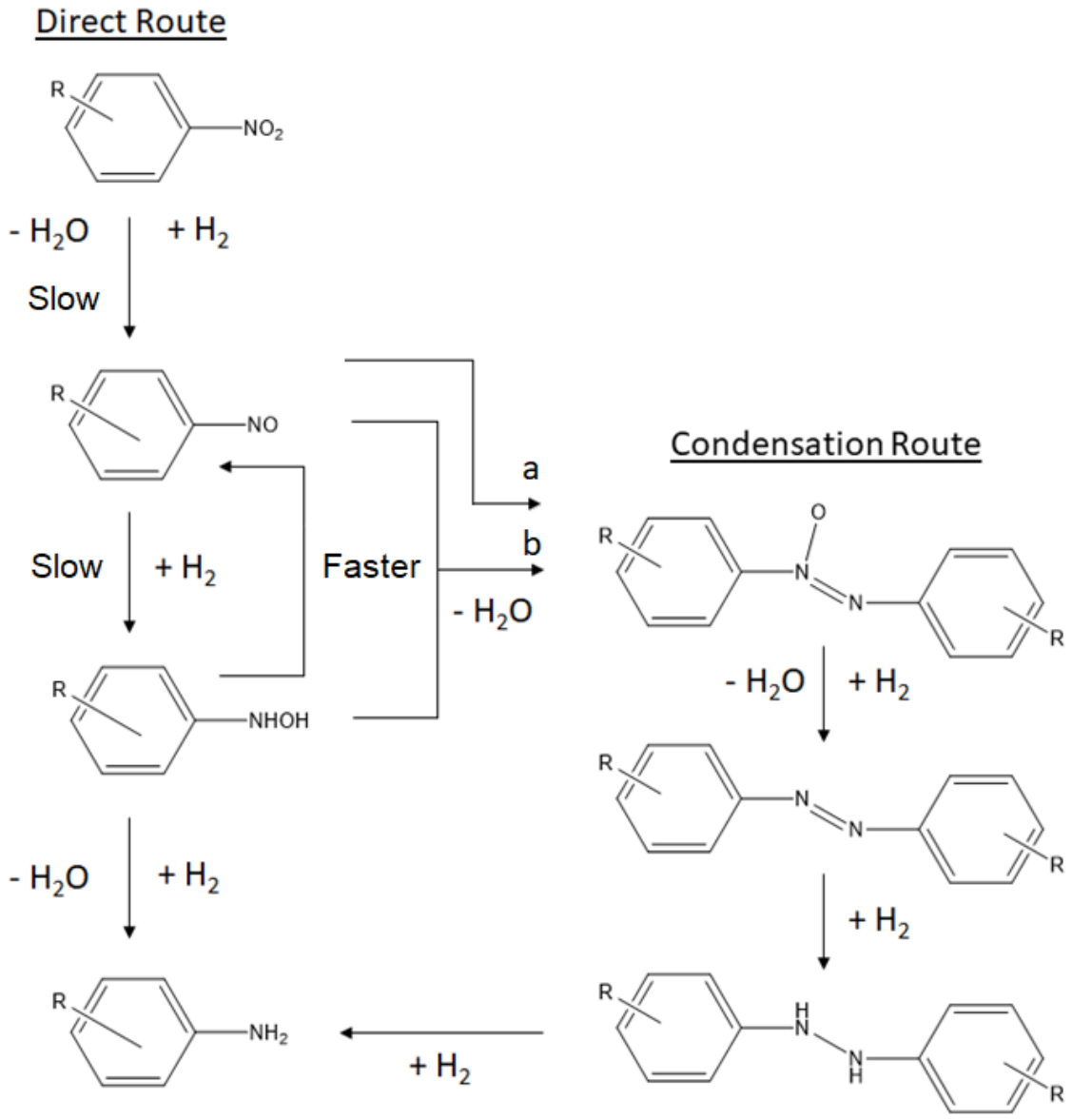

Figure 6.1. Reaction mechanism for the catalytic hydrogenation of substituted nitro-aromatics over the Au/CeO_2 nanocatalysts

6.4 Conclusions

In conclusion, the selectivity observed in the hydrogenation of substituted nitro-aromatics over Au/CeO_2 was much different to that observed over the other supports used in this reaction. This is due to the Au/CeO_2 nanocatalyst, catalysing the condensation route in the catalytic hydrogenation of substituted aromatics. While the size effect of the individual nanoclusters is not as pronounced as in the case of other supports previously reported in this work it still had some effect on catalytic activity, especially on the higher activity over the Au_{19}/CeO2 nanocatalyst that was also seen on the anatase and Degussa P25 supports. The Au_{20} and Au_{22} nanoclusters, however, catalysed the conversion of nitro-aromatics down the condensation route at a greater rate than the Au_{19}/CeO_2 nanocatalyst. Of note is role the substituents in affecting the activity and selectivity in these reactions. While the *para*-CH_3 functional group slowed the conversion of *p*-nitrotoluene over the anatase and Degussa P25 supports it increased the conversion over the Au/CeO_2 supports. The substituents also had effects on the catalytic activity through the condensation route with electron donating ones slowing the conversion to the azoxy-compounds. In the catalytic hydrogenation of *p*-nitrophenol the corresponding azoxy-compound was not formed at all – finding which aligns well with earlier reports. The recovered Au/CeO_2 nanocatalysts displayed interesting activity but low activity as a result of probable reduction under catalytic reaction conditions. Given CeO_2's reducibility this suggests that this support might not be ideal for certain catalytic reactions.

Chapter 7 Study of the Effect of Higher Au Weight Loadings on the Catalytic Activity

7.1 Introduction

The weight loadings of the supported Au nanoclusters used in this work are relatively low at 0.2%, compared to those typically used in previous studies on the catalytic hydrogenation of nitroaromatics. Weight loadings by Au weight on synthesised catalysts, of between 1% and 2.5% are commonly used in earlier studies. Weight loadings at these values however are disadvantageous for Au based nanocatalysts synthesised with atomically precise nanoclusters. The higher coverage density of Au clusters on the surface tends to lead to more pronounced sintering even on supports with strong metal-support interactions.[139] Given the high activity over the Au/HAP-H_2 nanocatalysts and strong support interaction between the Au nanoclusters used in this work and HAP it was decided that this would be an ideal system to study the effect of higher weight loadings on the catalytic activity of nitrobenzene hydrogenation.

7.2 Catalyst Preparation and Experimental Catalytic Procedure

The detailed catalyst preparation protocol is given as detailed in Section 3.4. and 3.4.1. The experimental catalytic procedure is the same as detailed in Section 3.5. The amount of nitrobenzene used in catalytic reactions was same as detailed in Table 5.2. Briefly, in a typical experiment a PTFE liner was charged with 15 mL EtOH, 0.1 g of Au_n/HAP-H_2 nanocatalyst (n = 19, 20, 22) of various Au% weight loadings and a calculated amount of reactant (Table 5.2). The liner was sonicated for 4 mins, then placed in the batch (Parr-like) reactor and the reactor was sealed. The reactor was flushed sequentially with N_2, H_2, and finally pressurised to 10 bar with H_2. The reaction mixture was stirred with a magnetic stirrer bar at 700 rpm with a set reaction temperature of 100℃. After 1, 2 and 5 hours stirring and heating were ceased, and the

reactor cooled in an ice bath. The reaction mixture was separated from the nanocatalyst by centrifugation (12000 rpm for 10 mins) and filtered through a 45 μm pore size PTFE filter. The recovered catalyst was washed 3 times with 30 mL of EtOH (re-dispersion followed by centrifugation and separation) and dried under vacuum. Each experiment was reproduced at least 2 times. The typical standard errors of independent catalytic tests were below 1.5%. The reproducibility between each reaction set varied with < 1% difference for the catalytic hydrogenation reactions of nitrobenzene. Analysis of the reaction mixtures was performed using GC-FID as detailed in Section 3.5. TOFs were calculated for the substituted aniline products only according to *Equation 5.2*.

7.3 Results and Discussion

7.3.1 The Effect of the Higher Au% Weight Loadings on the Catalytic Activity

The trends in the catalytic activity as the Au% weight loading was increased as summarised in Tables 7.1-3. It will be noted here, as well as indicated on Tables 7.1-3, that some samples had undergone further sintering due to being misplaced during the move to a new lab since these were not properly stored in a freezer. The results obtained using such slightly more sintered catalysts (denoted with *) in the catalytic hydrogenation of nitrobenzene were recorded for posterity. The 1 and 2 hour reactions were performed to give indication of the catalytic activity for the reaction significantly away from the completion, given that a number of the Au/HAP-H_2 catalysts had reached nearly complete nitrobenzene conversion after 5 hours. The general effect that the increase of Au% weight loadings has, is an increase in the conversion of nitrobenzene to aniline. This is to be expected, as the higher concentration of Au nanoclusters on the surface of the support will mean a higher concentration of active sites to facilitate catalytic hydrogenation. While the conversion rate increased, the catalytic activity as given by the TOF values decreased as the Au weight loading % increased. In the 5 hour reaction

the higher than 0.2% weight loaded catalysts exhibited an almost linear decrease in activity. From the 1 to 2 hour reactions, a trend in the 0.5%, 1.0% and 2.5% weight loaded nanocatalysts can also be seen where the relatively high TOFs decrease by around 50%. This can be attributed to further sintering occurring within these nanocatalysts as evidenced by the UV-Vis DRS spectra of the nanocatalysts recovered after the 5 hour reactions (Figure 7.1 - 3). These spectra show more pronounced peaks emerging at 530 – 540 nm indicating the increase of the average size of Au nanoclusters on the catalyst surface to ~ 2.5 - 3 nm.

Table 7.1 Performance of Au/HAP-H_2 Nanocatalysts in Catalytic Nitrobenzene Hydrogenation After 1 hour

Nanocatalyst	Conversion (%)	Selectivity (%)		TOF(h^{-1})
		Nitrosobenzene	Aniline	
Au_{19}/HAP-H_2 0.2%	14.8[a]	26.9	73.1	200.5
Au_{19}/HAP-H_2 0.5%	51.3[a]	6.8	93.2	417.4
Au_{19}/HAP-H_2 1.0%	47.1[a]	6.4	93.6	173.2
Au_{19}/HAP-H_2 2.5%	86.8[a]	4.4	95.6	145.3
Au_{20}/HAP-H_2 0.2%	15.0[a]	21.0	79.0	244.6
Au_{20}/HAP-H_2 0.5%	30.5[a]	9.2	90.8	249.2
Au_{20}/HAP-H_2 1.0%	31.6[a]	0.5	99.5	134.5
Au_{20}/HAP-H_2 2.5%	76.0[a]	5.8	94.2	117.9
Au_{22}/HAP-H_2 0.2%	17.3[a]	28.6	71.4	248.5
Au_{22}/HAP-H_2 0.5%	48.6[a]	7.2	92.8	378.5
Au_{22}/HAP-H_2 1.0%	55.3[a]	7.1	93.0	210.5
Au_{22}/HAP-H_2 2.5%	58.1[a]	6.3	93.7	84.6

Reaction conditions: nitrobenzene (0.2051 mL, 2 mmol), ethanol (15 mL), nanocatalyst (0.1 g), H_2 (10 bar), 100°C, 1 hour a: Trace amounts of azobenzene detected < 1%

Table 7.2 Performance of Au/HAP-H_2 Nanocatalysts in Catalytic Nitrobenzene Hydrogenation After 2 hours

Nanocatalyst	Conversion (%)	Selectivity (%)		TOF(h^{-1})
		Nitrosobenzene	Aniline	
Au_{19}/HAP-H_2 0.2%	21.0[a]	6.9	93.1	182.0
Au_{19}/HAP-H_2 0.5%	67.2 [a]	4.8	95.2	259.0
Au_{19}/HAP-H_2 1.0%	64.6 [a]	1.9	98.1	115.6
Au_{19}/HAP-H_2 2.5%	97.6	1.1	98.9	68.5
Au_{20}/HAP-H_2 0.2%	1.5[a]	14.8	85.2	12.0*
Au_{20}/HAP-H_2 0.5%	38.5 [a]	0.6	99.4	108.9 *
Au_{20}/HAP-H_2 1.0%	36.4 [a]	1.1	98.9	56.9 *
Au_{20}/HAP-H_2 2.5%	98.2	1.2	98.8	79.9 *
Au_{22}/HAP-H_2 0.2%	29.4 [a]	1.4	98.6	289.7
Au_{22}/HAP-H_2 0.5%	63.4 [a]	2.9	97.1	210.3
Au_{22}/HAP-H_2 1.0%	77.3 [a]	1.8	98.2	123.5
Au_{22}/HAP-H_2 2.5%	90.5 [a]	0.3	99.7	53.9

Reaction conditions: nitrobenzene (0.2051 mL, 2 mmol), ethanol (15 mL), nanocatalyst (0.1 g), H_2 (10 bar), 100°C, 2 hours a: Trace amounts of azobenzene detected < 1% *: Further sintering due to improper storage

This explains the higher initial activity over the 0.5% weight loaded nanocatalysts in the 1 hour reaction which then dropped to similar TOFs as observed in the 0.2% weight loaded nanocatalysts. This suggests that there is an ideal size regime for larger Au nanoclusters to give increased catalytic activity over supported HAP nanocatalysts. Sintering had already been observed over these catalysts during their calcination and reduction treatments before their use in the catalytic hydrogenation of nitrobenzene. The loss activity as further sintering occurred during the catalytic test suggests the size regime for higher catalytic activity may be quite

narrow, with the difference of only a few distinct sized Au nanoclusters in this range having a sizeable effect. Sintering had the greatest effect on the 2.5% weight loaded nanocatalysts.

Table 7.3 Performance of Au/HAP-H_2 Nanocatalysts in Catalytic Nitrobenzene Hydrogenation After 5 hours

Nanocatalyst	Conversion (%)	Selectivity (%)		TOF(h^{-1})
		Nitrosobenzene	Aniline	
Au_{19}/HAP-H_2 0.2%	45.5 [a]	12.6	87.3	136.8
Au_{19}/HAP-H_2 0.5%	93.0 [a]	2.9	97.1	161.2
Au_{19}/HAP-H_2 1.0%	83.7 [a]	2.0	98.0	76.8
Au_{19}/HAP-H_2 2.5%	97.5	1.6	98.5	29.0
Au_{20}/HAP-H_2 0.2%	53.0 [a]	13.8	86.2	166.8
Au_{20}/HAP-H_2 0.5%	72.5 [a]	4.3	95.7	122.0
Au_{20}/HAP-H_2 1.0%	86.1 [a]	2.3	97.7	72.2
Au_{20}/HAP-H_2 2.5%	98.1	<1.0	99.0	34.3
Au_{22}/HAP-H_2 0.2%	57.4[a]	13.4	86.6	209.9
Au_{22}/HAP-H_2 0.5%	98.6	1.4	98.7	168.3
Au_{22}/HAP-H_2 1.0%	98.9	<1.0	99.0	85.2
Au_{22}/HAP-H_2 2.5%	98.5	<1.0	99.0	37.5

Reaction conditions: Nitrobenzene (0.2051 mL, 2 mmol), Ethanol (15 mL), Nanocatalyst (0.1 g), H_2 (10 bar), 100°C, 5 hours a: Trace amounts of azobenzene detected < 1%

This is to be expected due to the larger concentration of Au nanoclusters on the catalyst surface, then the greater feedstock for the sintering of nanoclusters to even larger sizes. This was seen in the UV-Vis DRS and Powder XRD data (Section 4.3.2) for the synthesised 2.5% weight loaded nanocatalysts that had a higher average nanocluster size emerge after calcination and reduction treatments.

The catalytic experimental conditions further increased sintering over these catalysts during the hydrogenation reactions. Finally, in the case of 2.5% weight loaded nanocatalysts, reactions did proceed close to complete conversions (97+%) after 2 hour reactions implying significant reactant diffusion limitation towards the late stages of reaction, significantly affecting the TOF values. This explains the low TOFs in relation to the other nanocatalysts. The catalysts that underwent severe aggregation due to improper storage before they were used in 2 hour reactions (only) also backs up the above hypothesis regarding effect of sintering given their relatively low TOFs. Over all the nanocatalysts displayed very high selectivity towards aniline, especially when the reaction neared completion.

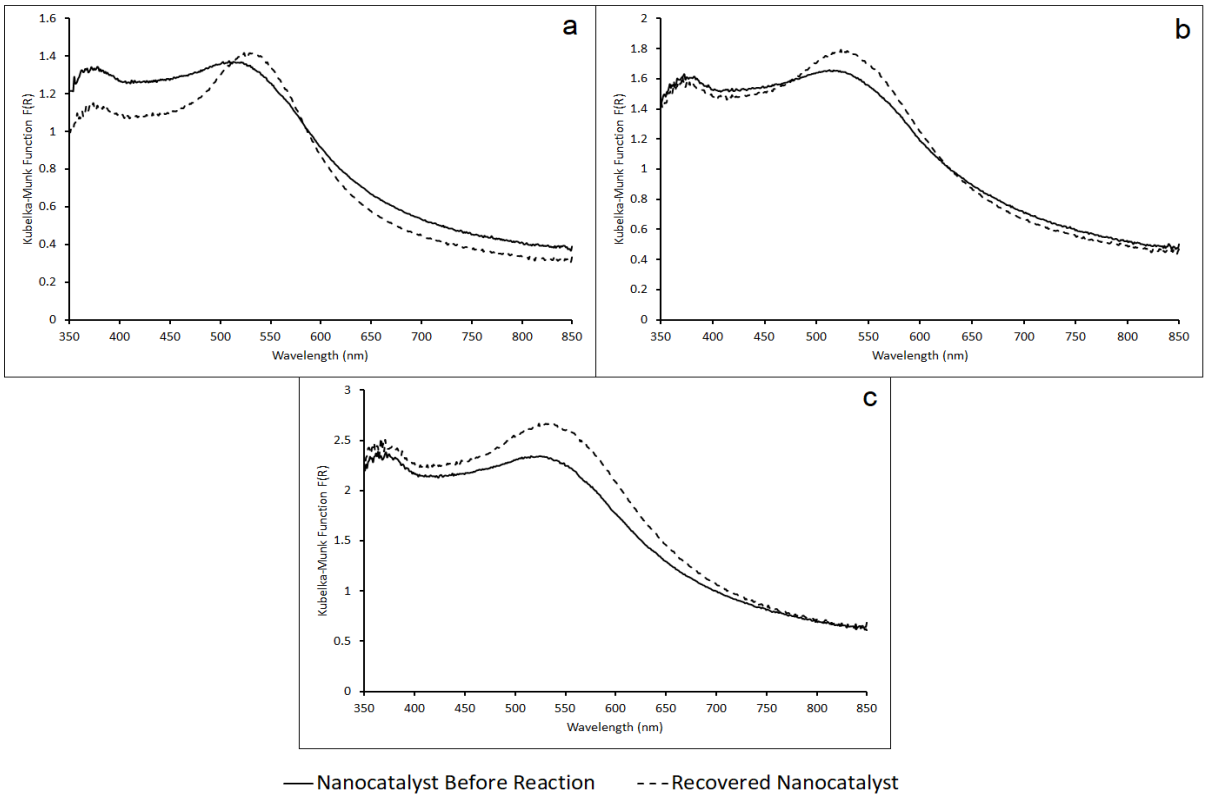

Figure 7.1. UV-Vis DR spectra of Au_{19}/HAP-H_2 nanocatalysts before and after 5 hour reaction (a) Au_{19}/HAP-H_2 0.5% (b) Au_{19}/HAP-H_2 1.0% (c) Au_{19}/HAP-H_2 2.5%.

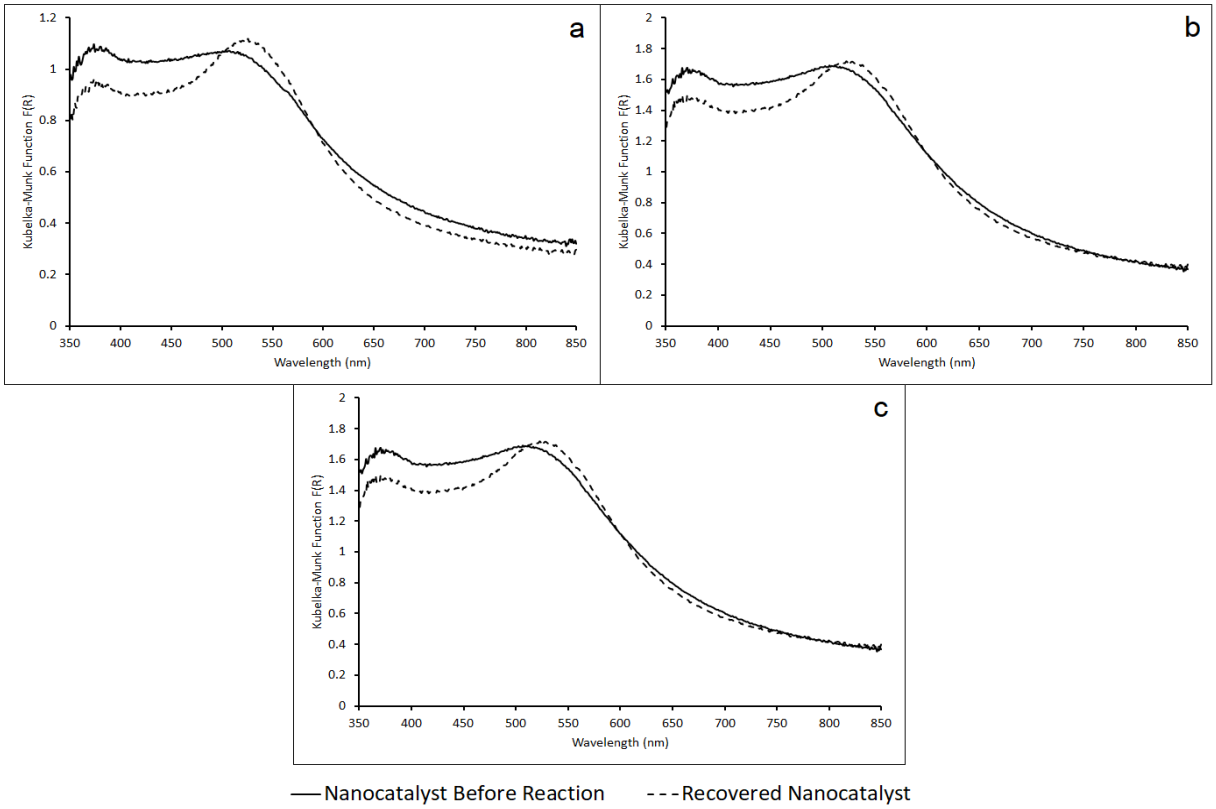

Figure 7.2. UV-Vis DR spectra of $Au_{20}/HAP\text{-}H_2$ nanocatalysts before and after 5 hour reaction (a) $Au_{20}/HAP\text{-}H_2$ 0.5% (b) $Au_{20}/HAP\text{-}H_2$ 1.0% (c) $Au_{20}/HAP\text{-}H_2$ 2.5%.

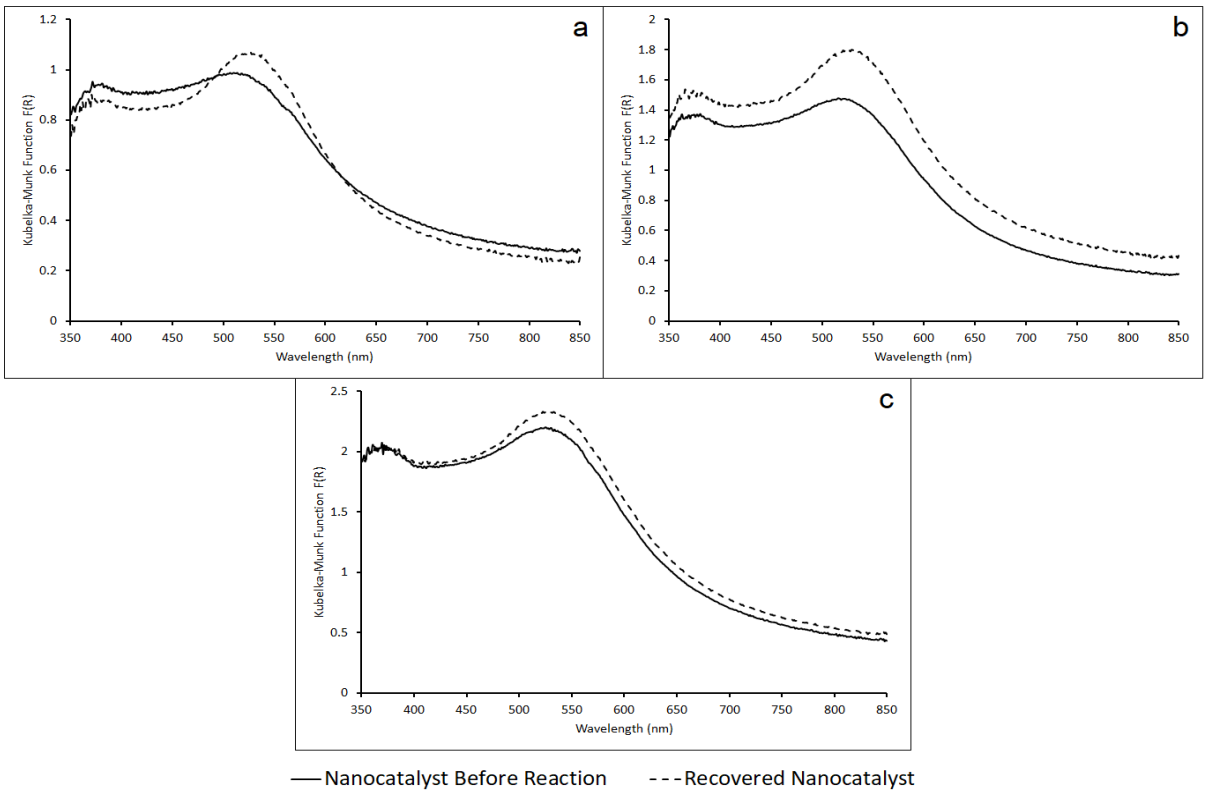

Figure 7.3. UV-Vis DR spectra of $Au_{22}/HAP\text{-}H_2$ nanocatalysts before and after 5 hour reaction (a) $Au_{22}/HAP\text{-}H_2$ 0.5% (b) $Au_{22}/HAP\text{-}H_2$ 1.0% (c) $Au_{22}/HAP\text{-}H_2$ 2.5%.

7.3.2 Reaction Mechanism

As detailed in Section 5.4.4, from the product distribution observed over the Au/HAP based nanocatalysts, nitrosobenzene and trace amounts of substituted azo-compounds were detected. This suggest that the hydrogenation of nitrobenzene occurs through the direct and to a minor extent the condensation pathways detailed in Haber's reaction scheme (Figure 5.1). Given the amount of nitrosobenzene obtained in the product mixture for the it is surprising that the condensation of the nitroso intermediates occurs with phenylhydroxylamine to form such a small amount (<1%) of azobenzene. The fact that phenylhydroxylamine was not detected, most likely means that the hydrogenation of nitrosobenzene is somewhat slower, compared to the relatively fast hydrogenation of the condensation pathway intermediates. From the product distributions observed in these reactions, the hydrogenation of nitrobenzene to nitrosobenzene seems to be the fastest step in this reaction, given the high initial concentrations of nitrosobenzene in the product mixture until the reaction reached around 60% nitrobenzene conversion. The azobenzene is not hydrogenated until nitrobenzene conversion has reached almost 100%, suggesting it has a weak interaction with the surface and other intermediates preferentially interact with the catalyst surface.

7.4 Conclusion

In conclusion increasing the Au% weight loadings increases the conversion rate of nitrobenzene to aniline but it also reduces the TOF and subsequently resulting in a relatively low Au atom economy being observed. This is due to the sintering that occurred in the nanocatalysts with higher than 0.2% weight loadings which increased the average size of the Au nanoclusters on the support surface. This also helped to show a definite size effect implying higher catalytic activity by smaller Au nanoclusters given that larger sizes were less active for the hydrogenation of nitrobenzene to aniline over HAP based nanocatalysts. The initial (1 hour

tests) high TOFs over the 0.5% Au/HAP-H_2 nanocatalysts suggest that there is an ideal size range for Au nanoclusters on HAP supports for the purpose of catalysing this reaction but that such a size range also might be quite narrow. This finding also highlights the importance of the improved size control and why methods such as impregnation and deposition precipitation are less than ideal for preparation of nanocatalysts containing very active small clusters with sizes within such a narrow size regime.

Conclusions and Future Work

Heterogeneous catalysis will benefit from the advances made in the field of nanocatalysis. With precise and careful design, safer catalysts can be produced that give minimal waste under ambient reaction conditions, avoid unnecessary reactant use and synthesis of unwanted by-products, with improved selectivity and activity through the knowledge of composition and size of the nanoparticle acting as an active site. Improved atom economy, energy efficiency, and optimal feedstock utilization can also be offered by nanocatalysis over conventional catalysis with a reduction in the overall use of precious metals where the same activity can be generated with a nanocatalyst that contains only a fraction of a percentage of the total metal content of a bulk conventional catalyst.

In this work, atomically precise nanoclusters were deposited on a range of metal-oxide as well as on a nonoxide support and activated under various conditions for the detailed catalytic testing in the hydrogenation of substituted nitro-aromatics under mild reaction conditions. The small size range, where *the nanoclusters used varied by only one or two atoms*, allowed, to gain an insight into how catalytic activity and selectivity can change as a function of the Au nanocluster size in these catalytic reactions *for the first time*. The size effect was noticeable over the titania (Degussa P25) and hydroxyapatite nanocatalysts in the catalytic hydrogenation of substituted nitro-aromatics. The gap in activity between the highest and lowest performing nanocatalysts with only a difference of one or two atoms, was less than trivial: the turnover frequencies for the best performing catalysts were 2 – 3 times higher compared to that of the worst catalysts. This gives rise to the question could a high percentage of the activity observed in previous studies that used polydisperse size distributions be related to only a few distinct atomically precise Au nanoclusters present in a mixture? While the Au_{19} nanocluster based Degussa P25 nanocatalyst gave the highest activity of the nanocluster series, the

hydroxyapatite-based nanocatalyst reversed this trend with the Au_{22} nanocluster giving the highest activity. The anatase nanocatalysts gave relatively low activities in catalytic reactions compared with the same nanoclusters supported on the titania Degussa P25 and hydroxyapatite nanocatalysts. The functional groups on the nitro-aromatic rings were also shown to increase or decrease reaction rates as a result of their respective electron withdrawing and donating ability indicated by Hammett constant values. In the future, more detailed studies could be performed to find the ideal Au nanocluster size, and support combination to maximise catalytic activity in the hydrogenation of substituted nitro-aromatics, given their already high selectivity towards desired substituted anilines.

The role of the support in preventing sintering after activation treatments was shown to be of great importance in this work. Sintering is detrimental in heterogeneous catalysts often resulting in decreased activity or in the worst case, deactivation. It was important in this study to prevent sintering so as to elucidate the true catalytic activity of the Au nanoclusters deposited on the surface. The supports that have been shown in previous studies to exhibit strong metal-support interactions showed a lower degree of nanocluster sintering compared with supports that had average metal-support interactions. Due to the limitations of characterisation techniques available and used in this work, qualitative analysis was performed while quantitative analysis of the level of sintering over the nanocatalysts was only indicative. Higher Au% weight loadings were shown to induce sintering due to the increased coverage density of Au nanoclusters on the surface. This negatively affected the catalytic activity, over the higher Au% weight loaded nanocatalysts with decreasing TOFs as the Au% weight loading increased. This observation highlights the need for developing supports that provide a high degree of sintering resistance **w**ithout significantly altering the desired catalytic activity of supported Au nanoclusters.

Finally, it was also observed that the nature of the support has an influence on the selectivity towards intermediates from either direct or condensation pathways for the hydrogenation of substituted nitro-aromatics. This was theorised to be caused by the catalysing of certain hydrogenation steps of the various intermediates formed in the catalytic hydrogenation of nitro-aromatics at different rates. Such interplay of the relative reaction rates resulted in the preferential formation of substituted azoxy- and azo-aromatics over the CeO_2 support. The functional groups on the nitro-aromatic rings not only increased or decreased reaction rates as a result of their respective electron withdrawing and donating ability, but also affected the selectivity for the formation of substituted azoxy- and azo-aromatics.

Future work could extend to the study of how nanoengineered materials, modification of the supports or adding a metal atom of a different nature creating a mixed-metal cluster active site affects selectivity and catalytic activity in catalysing of different reaction pathways of hydrogenation. The use of nanoengineered systems in catalysis is a rapidly growing field in nanocatalysis, with the use of 1D materials such as nanotubes, nanorods, nanowires and nanospheres, expanding as more synthetic methods become available for their production. The availability of methods for the wet chemical synthesis, along with other synthetic procedures is also adding to a growing library of available metal-clusters of varying sizes and unique compositions (such as tri-metallic clusters) that can be utilised in heterogeneous catalysis.

Bibliography

1. Hagen, J., Economic Importance of Catalysts. In *Industrial Catalysis*, Wiley-VCH Verlag GmbH & Co. KGaA: 2006; pp 425-428.
2. McNaught, A. D.; Wilkinson, A.; Pure, I. U. o.; Chemistry, A., *Compendium of Chemical Terminology: IUPAC Recommendations*. Blackwell Science: 1997.
3. Leeuwen, P. W. N. M. v., *Homogeneous catalysis: understanding the art*. Kluwer Academic: Dordrecht;London;Boston;, 2004.
4. Liang, S.; Hao, C.; Shi, Y., The Power of Single-Atom Catalysis. *ChemCatChem* **2015,** *7* (17), 2559-2567.
5. Thomas, J. M., The societal significance of catalysis and the growing practical importance of single-site heterogeneous catalysts. *Proceedings of the Royal Society A: Mathematical, Physical and Engineering Science* **2012,** *468* (2143), 1884-1903.
6. Cornils, B.; Herrmann, W. A., Concepts in homogeneous catalysis: the industrial view. *Journal of Catalysis* **2003,** *216* (1), 23-31.
7. Claus, P., Heterogeneously catalysed hydrogenation using gold catalysts. *Applied Catalysis A: General* **2005,** *291* (1-2), 222-229.
8. Cárdenas-Lizana, F.; Keane, M. A., The development of gold catalysts for use in hydrogenation reactions. *Journal of Materials Science* **2013,** *48* (2), 543-564.
9. König, P. M.; Roth, R.; Dietrich, S., Lock and key model system. *EPL (Europhysics Letters)* **2008,** *84* (6), 68006.
10. Kuhn, J. N.; Huang, W.; Tsung, C.-K.; Zhang, Y.; Somorjai, G. A., Structure Sensitivity of Carbon−Nitrogen Ring Opening: Impact of Platinum Particle Size from below 1 to 5 nm upon Pyrrole Hydrogenation Product Selectivity over Monodisperse Platinum Nanoparticles Loaded onto Mesoporous Silica. *Journal of the American Chemical Society* **2008,** *130* (43), 14026-14027.
11. Rioux, R. M.; Hsu, B. B.; Grass, M. E.; Song, H.; Somorjai, G. A., Influence of Particle Size on Reaction Selectivity in Cyclohexene Hydrogenation and Dehydrogenation over Silica-Supported Monodisperse Pt Particles. *Catalysis Letters* **2008,** *126* (1), 10.
12. Shimizu, K.-I.; Miyamoto, Y.; Kawasaki, T.; Tanji, T.; Tai, Y.; Satsuma, A., Chemoselective hydrogenation of nitroaromatics by supported gold catalysts: mechanistic reasons of size- and support-dependent activity and selectivity. *Journal of Physical Chemistry C* **2009,** *113* (41), 17803-17810.
13. Bratlie, K. M.; Lee, H.; Komvopoulos, K.; Yang, P.; Somorjai, G. A., Platinum nanoparticle shape effects on benzene hydrogenation selectivity. *Nano Letters* **2007,** *7* (10), 3097-3101.
14. Zaera, F., Outstanding mechanistic questions in heterogeneous catalysis. *JOURNAL OF PHYSICAL CHEMISTRY B* **2002,** *106* (16), 4043-4052.
15. Mäki-Arvela, P.; Hájek, J.; Salmi, T.; Murzin, D. Y., Chemoselective hydrogenation of carbonyl compounds over heterogeneous catalysts. *Applied Catalysis A, General* **2005,** *292* (1-2), 1-49.
16. Ntainjua N, E.; Edwards, J. K.; Carley, A. F.; Lopez-Sanchez, J. A.; Moulijn, J. A.; Herzing, A. A.; Kiely, C. J.; Hutchings, G. J., The role of the support in achieving high selectivity in the direct formation of hydrogen peroxide. *Green Chemistry* **2008,** *10* (11), 1162-1169.
17. Tolman, C. A., The 16 and 18 electron rule in organometallic chemistry and homogeneous catalysis. *Chemical Society Reviews* **1972,** *1* (3), 337-353.
18. Poli, R., The Elucidation of Mechanisms in Homogeneous Catalysis. *Comments on Inorganic Chemistry* **2009,** *30* (5-6), 177-228.
19. Hagen, J., Homogeneous Catalysis with Transition Metal Catalysts. In *Industrial Catalysis*, Wiley-VCH Verlag GmbH & Co. KGaA: 2015; pp 17-46.

20. Hashmi, A. S. K.; Lothschütz, C.; Ackermann, M.; Doepp, R.; Anantharaman, S.; Marchetti, B.; Bertagnolli, H.; Rominger, F., Gold Catalysis: In Situ EXAFS Study of Homogeneous Oxidative Esterification. *Chemistry – A European Journal* **2010,** *16* (27), 8012-8019.
21. Augustine, R. L., Whither Goest Thou, Catalysis. *Catalysis Letters* **2016,** *146* (12), 2393-2416.
22. Doornkamp, C.; Ponec, V., The universal character of the Mars and Van Krevelen mechanism. *Journal of Molecular Catalysis A: Chemical* **2000,** *162* (1), 19-32.
23. Vannice, M. A., Kinetics of catalytic reactions. 2005.
24. Libuda, J.; Freund, H. J., Molecular beam experiments on model catalysts. *Surface Science Reports* **2005,** *57* (7), 157-298.
25. Boskovic, G.; Baerns, M., Catalyst Deactivation. In *Basic Principles in Applied Catalysis*, Baerns, M., Ed. Springer Berlin Heidelberg: Berlin, Heidelberg, 2004; pp 477-503.
26. Weckhuysen, B. M., Chemical Imaging of Spatial Heterogeneities in Catalytic Solids at Different Length and Time Scales. *Angewandte Chemie International Edition* **2009,** *48* (27), 4910-4943.
27. Tinnemans, S. J.; Mesu, J. G.; Kervinen, K.; Visser, T.; Nijhuis, T. A.; Beale, A. M.; Keller, D. E.; van der Eerden, A. M. J.; Weckhuysen, B. M., Combining operando techniques in one spectroscopic-reaction cell: New opportunities for elucidating the active site and related reaction mechanism in catalysis. *Catalysis Today* **2006,** *113* (1), 3-15.
28. Somorjai, G. A., Flexible surface. Correlation between reactivity and restructuring ability. *Langmuir* **1991,** *7* (12), 3176-3182.
29. Weckhuysen, B. M., Preface: Recent advances in the in-situ characterization of heterogeneous catalysts. *Chemical Society Reviews* **2010,** *39* (12), 4557-4559.
30. Bravo-Suárez, J. J.; Srinivasan, P. D., Design characteristics of in situ and operando ultraviolet-visible and vibrational spectroscopic reaction cells for heterogeneous catalysis. *Catalysis Reviews* **2017**, 1-151.
31. van Schrojenstein Lantman, E. M.; Deckert-Gaudig, T.; Mank, A. J. G.; Deckert, V.; Weckhuysen, B. M., Catalytic processes monitored at the nanoscale with tip-enhanced Raman spectroscopy. *Nature Nanotechnology* **2012,** *7*, 583.
32. Blanc, F., Investigation of Catalytic Surfaces with Surface-Enhanced Solid-State NMR Spectroscopy. In *Nanotechnology in Catalysis*, Wiley-VCH Verlag GmbH & Co. KGaA: 2017; pp 1003-1028.
33. Ivanova, I. I.; Kolyagin, Y. G., Impact of in situ MAS NMR techniques to the understanding of the mechanisms of zeolite catalyzed reactions. *Chemical Society Reviews* **2010,** *39* (12), 5018-5050.
34. van Bokhoven, J. A.; Lamberti, C., State-of-the-Art X-Ray Spectroscopy in Catalysis. In *Nanotechnology in Catalysis*, Wiley-VCH Verlag GmbH & Co. KGaA: 2017; pp 1029-1054.
35. Singh, J.; Lamberti, C.; Van Bokhoven, J. A., Advanced X-ray absorption and emission spectroscopy: In situ catalytic studies. *Chemical Society Reviews* **2010,** *39* (12), 4754-4766.
36. Meunier, F. C., The design and testing of kinetically-appropriate operando spectroscopic cells for investigating heterogeneous catalytic reactions. *Chemical Society Reviews* **2010,** *39* (12), 4602-4614.
37. Bartholomew, C. H.; Farrauto, R. J., *Fundamentals of industrial catalytic processes*. 2nd ed.; Wiley: Hoboken, N.J, 2006.
38. Ross, J. R. H., Chapter 6 - The Kinetics and Mechanisms of Catalytic Reactions. In *Heterogeneous Catalysis*, Elsevier: Amsterdam, 2012; pp 123-142.
39. Rennie, R., *A dictionary of chemistry*. Seventh ed.; Oxford University Press: Oxford, 2016.
40. Weinberg, W. H., Eley−Rideal Surface Chemistry: Direct Reactivity of Gas Phase Atomic Hydrogen with Adsorbed Species. *Accounts of Chemical Research* **1996,** *29* (10), 479-487.
41. Mars, P.; van Krevelen, D. W., Oxidations carried out by means of vanadium oxide catalysts. *Chemical Engineering Science* **1954,** *3*, 41-59.
42. Bowker, M., The Role of Precursor States in Adsorption, Surface Reactions and Catalysis. *Topics in Catalysis* **2016,** *59* (8), 663-670.

43. Schmal, M., Adsorption–Desorption. In *Heterogeneous Catalysis and its Industrial Applications*, Springer International Publishing: Cham, 2016; pp 27-62.
44. Hawtin, P.; Lewis, J. B.; Moul, N.; Phillips, R. H., The Heats of Combustion of Graphite, Diamond and Some Non-Graphitic Carbons. *Philosophical Transactions of the Royal Society of London. Series A, Mathematical and Physical Sciences* **1966,** *261* (1116), 67-95.
45. Unnikrishnan, P.; Srinivas, D., Chapter 3 - Heterogeneous Catalysis. In *Industrial Catalytic Processes for Fine and Specialty Chemicals*, Ranade, V. V., Ed. Elsevier: Amsterdam, 2016; pp 41-111.
46. Bond, G. C., *Heterogeneous catalysis : principles and applications*. Clarendon Press: Oxford, 1974.
47. Ma, Z.; Dai, S., Development of novel supported gold catalysts: A materials perspective. *Nano Research* **2010,** *4* (1), 3-32.
48. Chen, X.; Mao, S. S., Titanium dioxide nanomaterials: synthesis, properties, modifications, and applications. *Chem Rev* **2007,** *107* (7), 2891-959.
49. Ishida, T.; Koga, H.; Okumura, M.; Haruta, M., Advances in gold catalysis and understanding the catalytic mechanism. *Chemical Record* **2016,** *16* (5), 2278-2293.
50. Yang, B.; Gong, X. Q.; Wang, H. F.; Cao, X. M.; Rooney, J. J.; Hu, P., Evidence to challenge the universality of the Horiuti-Polanyi mechanism for hydrogenation in heterogeneous catalysis: Origin and trend of the preference of a non-Horiuti-Polanyi mechanism. *Journal of The American Chemical Society* **2013,** *135* (40), 15244-15250.
51. Behafarid, F.; Roldan Cuenya, B., Towards the Understanding of Sintering Phenomena at the Nanoscale: Geometric and Environmental Effects. *Topics in Catalysis* **2013,** *56* (15), 1542-1559.
52. Campbell, C. T., The Energetics of Supported Metal Nanoparticles: Relationships to Sintering Rates and Catalytic Activity. *Accounts of Chemical Research* **2013,** *46* (8), 1712-1719.
53. Ganduglia-Pirovano, M. V.; Hofmann, A.; Sauer, J., Oxygen vacancies in transition metal and rare earth oxides: Current state of understanding and remaining challenges. *Surface Science Reports* **2007,** *62* (6), 219-270.
54. Volkman, S. K.; Yin, S.; Bakhishev, T.; Puntambekar, K.; Subramanian, V.; Toney, M. F., Mechanistic Studies on Sintering of Silver Nanoparticles. *Chemistry of Materials* **2011,** *23* (20), 4634-4640.
55. Nakaso, K.; Shimada, M.; Okuyama, K.; Deppert, K., Evaluation of the change in the morphology of gold nanoparticles during sintering. *Journal of Aerosol Science* **2002,** *33* (7), 1061-1074.
56. Hong, S.; Rahman, T. S., Rationale for the Higher Reactivity of Interfacial Sites in Methanol Decomposition on Au13/TiO2(110). *Journal of the American Chemical Society* **2013,** *135* (20), 7629-7635.
57. Farmer, J. A.; Campbell, C. T., Ceria Maintains Smaller Metal Catalyst Particles by Strong Metal-Support Bonding. *Science* **2010,** *329* (5994), 933-936.
58. Henry, C. R., Morphology of supported nanoparticles. *Progress in Surface Science* **2005,** *80* (3), 92-116.
59. Müller, P.; Kern, R., Equilibrium nano-shape change induced by epitaxial stress: effect of surface stress. *Applied Surface Science* **2000,** *164* (1), 68-71.
60. Pedersen, M. Ø.; Helveg, S.; Ruban, A.; Stensgaard, I.; Lægsgaard, E.; Nørskov, J. K.; Besenbacher, F., How a gold substrate can increase the reactivity of a Pt overlayer. *Surface Science* **1999,** *426* (3), 395-409.
61. Günter, M. M.; Ressler, T.; Bems, B.; Büscher, C.; Genger, T.; Hinrichsen, O.; Muhler, M.; Schlögl, R., Implication of the microstructure of binary Cu/ZnO catalysts for their catalytic activity in methanol synthesis. *Catalysis Letters* **2001,** *71* (1), 37-44.
62. Greeley, J.; Nørskov, J. K.; Mavrikakis, M., Electronic structure and catalysis on metal surfaces. *Annual Review of Physical Chemistry* **2002,** *53* (1), 319-348.
63. Yim, C. M.; Pang, C. L.; Hermoso, D. R.; Dover, C. M.; Muryn, C. A.; Maccherozzi, F.; Dhesi, S. S.; Pérez, R.; Thornton, G., Influence of support morphology on the bonding of molecules to nanoparticles. *Proceedings of the National Academy of Sciences* **2015,** *112* (26), 7903-7908.

64. Mavrikakis, M.; Stoltze, P.; Nørskov, J. K., Making gold less noble. *Catalysis Letters* **2000,** *64* (2), 101-106.
65. Schauermann, S.; Nilius, N.; Shaikhutdinov, S.; Freund, H.-J., Nanoparticles for Heterogeneous Catalysis: New Mechanistic Insights. *Accounts of Chemical Research* **2013,** *46* (8), 1673-1681.
66. Campbell, C. T., Catalyst-support interactions: Electronic perturbations. *Nature Chemistry* **2012,** *4* (8), 597-598.
67. Wörz, A. S.; Heiz, U.; Cinquini, F.; Pacchioni, G., Charging of Au atoms on TiO2 thin films from CO vibrational spectroscopy and DFT calculations. *Journal of Physical Chemistry B* **2005,** *109* (39), 18418-18426.
68. Márquez, A. M.; Graciani, J.; Sanz, J. F., Charge state of metal atoms on oxide supports: A systematic study based on simulated infrared spectroscopy and density functional theory. *Theoretical Chemistry Accounts* **2010,** *126* (3), 265-273.
69. Yang, X. F.; Kattel, S.; Senanayake, S. D.; Boscoboinik, J. A.; Nie, X. W.; Graciani, J.; Rodriguez, J. A.; Liu, P.; Stacchiola, D. J.; Chen, J. G. G., Low Pressure CO2 Hydrogenation to Methanol over Gold Nanoparticles Activated on a CeOx/TiO2 Interface. *JOURNAL OF THE AMERICAN CHEMICAL SOCIETY* **2015,** *137* (32), 10104-10107.
70. Roldán, A.; Ricart, J. M.; Illas, F.; Pacchioni, G., O2 activation by Au5 clusters stabilized on clean and electron-rich MgO stepped surfaces. *Journal of Physical Chemistry C* **2010,** *114* (40), 16973-16978.
71. Landman, U.; Yoon, B.; Zhang, C.; Heiz, U.; Arenz, M., Factors in gold nanocatalysis: oxidation of CO in the non-scalable size regime. *Topics in Catalysis* **2007,** *44* (1), 145-158.
72. Wang, X. X.; Chen, B. B.; Chen, G. Z.; Sun, X., Oxygen vacancies dependent Au nanoparticle deposition and CO oxidation. *RSC ADVANCES* **2016,** *6* (91), 87978-87987.
73. Lykhach, Y.; Kozlov, S. M.; Skala, T.; Tovt, A.; Stetsovych, V.; Tsud, N.; Dvorak, F.; Johanek, V.; Neitzel, A.; Myslivecek, J.; Fabris, S.; Matolin, V.; Neyman, K. M.; Libuda, J., Counting electrons on supported nanoparticles. *NATURE MATERIALS* **2016,** *15* (3), 284-284.
74. Sun, B.; Barnard, A. S., The impact of size and shape distributions on the electron charge transfer properties of silver nanoparticles. *Nanoscale* **2017,** *9* (34), 12698-12708.
75. Shao, X.; Prada, S.; Giordano, L.; Pacchioni, G.; Nilius, N.; Freund, H.-J., Tailoring the shape of metal Ad-particles by doping the oxide support. *Angewandte Chemie - International Edition* **2011,** *50* (48), 11525-11527.
76. Tauster, S. J.; Fung, S. C.; Garten, R. L., Strong metal-support interactions. Group 8 noble metals supported on TiO2. *Journal of the American Chemical Society* **1978,** *100* (1), 170-175.
77. Chandler, B. D., Strong metal-support interactions: An extra layer of complexity. *Nature Chemistry* **2017,** *9* (2), 108-109.
78. Gonzalez-DelaCruz, V. M.; Holgado, J. P.; Pereñíguez, R.; Caballero, A., Morphology changes induced by strong metal–support interaction on a Ni–ceria catalytic system. *Journal of Catalysis* **2008,** *257* (2), 307-314.
79. Raimondi, F.; Scherer, G. G.; Kötz, R.; Wokaun, A., Nanoparticles in energy technology: Examples from electrochemistry and catalysis. *Angewandte Chemie - International Edition* **2005,** *44* (15), 2190-2209.
80. Hayek, K.; Kramer, R.; Paál, Z., Metal-support boundary sites in catalysis. *Applied Catalysis A: General* **1997,** *162* (1), 1-15.
81. Khoa, N. T.; Kim, S. W.; Yoo, D.-H.; Kim, E. J.; Hahn, S. H., Size-dependent work function and catalytic performance of gold nanoparticles decorated graphene oxide sheets. *Applied Catalysis A: General* **2014,** *469*, 159-164.
82. Fu, Q.; Wagner, T., Interaction of nanostructured metal overlayers with oxide surfaces. *Surface Science Reports* **2007,** *62* (11), 431-498.
83. Liu, X.; Liu, M.-H.; Luo, Y.-C.; Mou, C.-Y.; Lin, S. D.; Cheng, H.; Chen, J.-M.; Lee, J.-F.; Lin, T.-S., Strong metal-support interactions between gold nanoparticles and ZnO nanorods in CO oxidation. *Journal of the American Chemical Society* **2012,** *134* (24), 10251-10258.

84. Tang, H.; Liu, F.; Wei, J.; Qiao, B.; Zhao, K.; Su, Y.; Jin, C.; Li, L.; Liu, J.; Wang, J.; Zhang, T., Ultrastable Hydroxyapatite/Titanium-Dioxide-Supported Gold Nanocatalyst with Strong Metal–Support Interaction for Carbon Monoxide Oxidation. *Angewandte Chemie International Edition* **2016,** *55* (36), 10606-10611.
85. Tang, H. L.; Wei, J. K.; Liu, F.; Qiao, B. T.; Pan, X. L.; Li, L.; Liu, J. Y.; Wang, J. H.; Zhang, T., Strong Metal-Support Interactions between Gold Nanoparticles and Nonoxides. *JOURNAL OF THE AMERICAN CHEMICAL SOCIETY* **2016,** *138* (1), 56-59.
86. Wang, L.; Zhang, J.; Zhu, Y. H.; Xu, S. D.; Wang, C. T.; Bian, C. Q.; Meng, X. J.; Xiao, F. S., Strong Metal-Support Interactions Achieved by Hydroxide-to-Oxide Support Transformation for Preparation of Sinter-Resistant Gold Nanoparticle Catalysts. *ACS CATALYSIS* **2017,** *7* (11), 7461-7465.
87. Tauster, S. J.; Fung, S. C., Strong metal-support interactions: Occurrence among the binary oxides of groups IIA–VB. *Journal of Catalysis* **1978,** *55* (1), 29-35.
88. Thomas, S. J. M., The Advantages of Exploring the Interface Between Heterogeneous and Homogeneous Catalysis. *ChemCatChem* **2010,** *2* (2), 127-132.
89. Zaera, F., Nanostructured materials for applications in heterogeneous catalysis. *Chemical Society Reviews* **2013,** *42* (7), 2746-2762.
90. Bell, A. T., The Impact of Nanoscience on Heterogeneous Catalysis. *Science* **2003,** *299* (5613), 1688-1691.
91. Ishida, T.; Haruta, M., Gold catalysts: Towards sustainable chemistry. *Angewandte Chemie - International Edition* **2007,** *46* (38), 7154-7156.
92. Philippot, K.; Serp, P., Concepts in Nanocatalysis. 2012.
93. Polshettiwar, V.; Varma, R. S., Green chemistry by nano-catalysis. *Green Chemistry* **2010,** *12* (5), 743-754.
94. Faraday, M., The Bakerian lecture : Experimental relations of gold (and other metals) to light. *Philosophical Transactions of the Royal Society of London* **1857,** *147* (1857), 145-181.
95. Turkevich, J.; Stevenson, P. C.; Hillier, J., A study of the nucleation and growth processes in the synthesis of colloidal gold. *Discussions of the Faraday Society* **1951,** *11*, 55-75.
96. Frens, G., Particle size and sol stability in metal colloids. *Kolloid-Zeitschrift & Zeitschrift für Polymere* **1972,** *250* (7), 736-741.
97. Haruta, M.; Kobayashi, T.; Sano, H.; Yamada, N., Novel gold catalysts for the oxidation of carbon monoxide at a temperature far below 0 °C. *Chemistry Letters* **1987,** *16* (2), 405-408.
98. Hutchings, G. J., Vapor phase hydrochlorination of acetylene: Correlation of catalytic activity of supported metal chloride catalysts. *Journal of Catalysis* **1985,** *96* (1), 292-295.
99. Okumura, M.; Fujitani, T.; Huang, J.; Ishida, T., A career in catalysis: Masatake Haruta. *ACS Catalysis* **2015,** *5* (8), 4699-4707.
100. Brust, M.; Walker, M.; Bethell, D.; Schiffrin, D. J.; Whyman, R., Synthesis of thiol-derivatised gold nanoparticles in a two-phase liquid-liquid system. *Journal of the Chemical Society, Chemical Communications* **1994,** (7), 801-802.
101. Haruta, M., Catalysis gold rush. *Nature* **2005,** *437* (7062), 1098-1099.
102. Hutchings, G. J., Catalysis by gold. *Catalysis Today* **2005,** *100* (1-2), 55-61.
103. Hashmi, A. S. K.; Hutchings, G. J., Gold catalysis. *Angewandte Chemie - International Edition* **2006,** *45* (47), 7896-7936.
104. Daniel, M.-C.; Astruc, D., Gold nanoparticles: Assembly, supramolecular chemistry, quantum-size-related properties, and applications toward biology, catalysis, and nanotechnology. *Chemical Reviews* **2004,** *104* (1), 293-346.
105. Juliusa, M.; Robertsa, S.; Fletchera, J. C. Q., A review of the use of gold catalysts in selective hydrogenation reactions. *Gold Bulletin* **2010,** *43* (4), 298-306.
106. Jin, R. C.; Zeng, C. J.; Zhou, M.; Chen, Y. X., Atomically Precise Colloidal Metal Nanoclusters and Nanoparticles: Fundamentals and Opportunities. *CHEMICAL REVIEWS* **2016,** *116* (18), 10346-10413.

107. Fang, J.; Zhang, B.; Yao, Q.; Yang, Y.; Xie, J.; Yan, N., Recent advances in the synthesis and catalytic applications of ligand-protected, atomically precise metal nanoclusters. *Coordination Chemistry Reviews* **2016,** *322*, 1-29.
108. Perala, S. R. K.; Kumar, S., On the mechanism of metal nanoparticle synthesis in the Brust-Schiffrin method. *Langmuir* **2013,** *29* (31), 9863-9873.
109. Negishi, Y.; Nakazaki, T.; Malola, S.; Takano, S.; Niihori, Y.; Kurashige, W.; Yamazoe, S.; Tsukuda, T.; Häkkinen, H., A critical size for emergence of nonbulk electronic and geometric structures in dodecanethiolate-protected Au clusters. *Journal of the American Chemical Society* **2015,** *137* (3), 1206-1212.
110. Wan, X. K.; Tang, Q.; Yuan, S. F.; Jiang, D. E.; Wang, Q. M., Au19 nanocluster featuring a v-shaped alkynyl-gold motif. 2015; Vol. 137, pp 652-655.
111. Shao, N.; Huang, W.; Gao, Y.; Wang, L.-M.; Li, X.; Wang, L.-S.; Zeng, X. C., Probing the structural evolution of medium-sized gold clusters: Aun− (n = 27−35). *Journal of the American Chemical Society* **2010,** *132* (18), 6596-6605.
112. Pande, S.; Huang, W.; Shao, N.; Wang, L. M.; Khetrapal, N.; Mei, W. N.; Jian, T.; Wang, L. S.; Zeng, X. C., Structural evolution of core-shell gold nanoclusters: Aun- (n = 42-50). 2016; Vol. 10, pp 10013-10022.
113. Khetrapal, N. S.; Bulusu, S. S.; Zeng, X. C., Structural evolution of gold clusters Aun- (n = 21-25) revisited. *J Phys Chem A* **2017,** *121* (12), 2466-2474.
114. Shao, N.; Huang, W.; Mei, W.-N.; Wang, L. S.; Wu, Q.; Zeng, X. C., Structural evolution of medium-sized gold clusters Aun–(n= 36, 37, 38): Appearance of bulk-like face centered cubic fragment. *The Journal of Physical Chemistry C* **2014,** *118* (13), 6887-6892.
115. Chen, J.; Zhang, Q. F.; Williard, P. G.; Wang, L. S., Synthesis and structure determination of a new Au20 nanocluster protected by tripodal tetraphosphine ligands. *Inorganic Chemistry* **2014,** *53* (8), 3932-3934.
116. Zhang, Q. F.; Williard, P. G.; Wang, L. S., Polymorphism of phosphine-protected gold nanoclusters: Synthesis and characterization of a new 22-gold-atom cluster. *Small* **2016,** *12* (18), 2518-25.
117. Malola, S.; Lehtovaara, L.; Enkovaara, J.; Hakkinen, H., Birth of the localized surface plasmon resonance in monolayer-protected gold nanoclusters. *Acs Nano* **2013,** *7* (11), 10263-10270.
118. Jin, R.; Zhu, Y.; Qian, H., Quantum-sized gold nanoclusters: Bridging the gap between organometallics and nanocrystals. *Chemistry - A European Journal* **2011,** *17* (24), 6584-6593.
119. Qian, H.; Zhu, M.; Wu, Z.; Jin, R., Quantum sized gold nanoclusters with atomic precision. *Accounts of Chemical Research* **2012,** *45* (9), 1470-1479.
120. Murray, R. W., Nanoelectrochemistry: Metal nanoparticles, nanoelectrodes, and nanopores. *Chemical Reviews* **2008,** *108* (7), 2688-2720.
121. Fujitani, T.; Fujitani, T.; Nakamura, I.; Akita, T.; Okumura, M., Hydrogen Dissociation by Gold Clusters. *Angewandte Chemie (International ed.)* **2009,** *48* (50), 9515-9518.
122. Kartusch, C.; van Bokhoven, J. A., Hydrogenation over gold catalysts: The interaction of gold with hydrogen. *Gold Bulletin* **2009,** *42* (4), 343-348.
123. Blumberg, L. M., Theory of Gas Chromatography. 2012.
124. Rahman, M.; Abd El-Aty, A.; Choi, J.-H.; Shin, H.-C.; Chul Shin, S.; Shim, J. H., *Basic Overview on Gas Chromatography Columns*. 2015; p 823-834.
125. McNair, H. M.; Miller, J. M., Detectors. John Wiley & Sons, Inc: Hoboken, NJ, USA, pp 104-128.
126. Ladd, M. F. C.; Palmer, R. A., *Structure determination by X-ray crystallography*. 4th ed.; Kluwer Academic/Plenum Publishers: New York, 2003.
127. Seeck, O. H.; Murphy, B. M., *X-ray diffraction: modern experimental techniques*. 1 ed.; CRC Press: Boca Raton, Florida, 2014.
128. Rennie, R., Ultraviolet–Visible Spectroscopy. In A Dictionary of Chemistry. 7 ed.; Oxford University Press: 2016.

129. Perkampus, H.-H., *UV-VIS spectroscopy and its applications*. Springer-Verlag: New York;Berlin;, 1992.
130. Weckhuysen, B. M., *In-situ Spectroscopy of Catalysts*. American Scientific Publishers: 2004.
131. Mirabella, F. M., *Modern Techniques in Applied Molecular Spectroscopy*. Wiley: 1998.
132. Glemser, O.; Sauer, H., Section 19 - Copper, Silver, Gold - Brauer, George. In *Handbook of Preparative Inorganic Chemistry (Second Edition)*, Academic Press: 1965; pp 1003-1066.
133. Hooper, T. N.; Butts, C. P.; Green, M.; Haddow, M. F.; McGrady, J. E.; Russell, C. A., Synthesis, Structure and Reactivity of Stable Homoleptic Gold(I) Alkene Cations. *Chemistry – A European Journal* **2009,** *15* (45), 12196-12200.
134. Wan, X.-K.; Tang, Q.; Yuan, S.-F.; Jiang, D.-e.; Wang, Q.-M., Au19 Nanocluster Featuring a V-Shaped Alkynyl–Gold Motif. *Journal of the American Chemical Society* **2015,** *137* (2), 652-655.
135. Chen, J.; Zhang, Q.-F.; Williard, P. G.; Wang, L.-S., Synthesis and structure determination of a new Au20 nanocluster protected by tripodal tetraphosphine ligands. *Inorganic Chemistry* **2014,** *53* (8), 3932-3934.
136. Zhang, Q.-F.; Williard, P. G.; Wang, L.-S., Polymorphism of Phosphine-Protected Gold Nanoclusters: Synthesis and Characterization of a New 22-Gold-Atom Cluster. *Small* **2016,** *12* (18), 2518.
137. Wan, X. K.; Yuan, S. F.; Lin, Z. W.; Wang, Q. M., A Chiral Gold Nanocluster Au20 Protected by Tetradentate Phosphine Ligands. *Angewandte Chemie International Edition* **2014,** *53* (11), 2923-2926.
138. Coleman, G. H.; McCloskey, C. M.; Stuart, F. A., Nitrosobenzene. *Organic Syntheses* **1945,** *25*, 80-83.
139. Liu, Y.; Tsunoyama, H.; Akita, T.; Xie, S.; Tsukuda, T., Aerobic oxidation of cyclohexane catalyzed by size-controlled au clusters on hydroxyapatite: Size effect in the sub-2 nm regime. *ACS Catalysis* **2011,** *1* (1), 2-6.
140. Hall, B. D.; Zanchet, D.; Ugarte, D., Estimating nanoparticle size from diffraction measurements. *Journal of Applied Crystallography* **2000,** *33* (6), 1335-1341.
141. Golunski, S. E., Why use platinum in catalytic converters? *Platinum Metals Review* **2007,** *51* (3), 162.
142. Satterfield, C. N., *Heterogeneous Catalysis in Industrial Practice*. Krieger: 1991.
143. Chen, X.; Mao, S. S., Titanium dioxide nanomaterials: Synthesis, properties, modifications and applications. *Chemical Reviews* **2007,** *107* (7), 2891-2959.
144. Subramanian, V.; Wolf, E. E.; Kamat, P. V., Catalysis with TiO2/Gold Nanocomposites. Effect of Metal Particle Size on the Fermi Level Equilibration. *Journal of the American Chemical Society* **2004,** *126* (15), 4943-4950.
145. Karakoti, A. S.; Monteiro-Riviere, N. A.; Aggarwal, R.; Davis, J. P.; Narayan, R. J.; Self, W. T.; McGinnis, J.; Seal, S., Nanoceria as antioxidant: Synthesis and biomedical applications. *JOM* **2008,** *60* (3), 33-37.
146. Baron, M.; Bondarehuk, O.; Stacchiola, D.; Shaikhutdinov, S.; Freund, H. J., Interaction of gold with cerium oxide supports: CeO2(111) thin films vs CeOx nanoparticles. *Journal of Physical Chemistry C* **2009,** *113* (15), 6042-6049.
147. Fihri, A.; Len, C.; Varma, R. S.; Solhy, A., Hydroxyapatite: A review of syntheses, structure and applications in heterogeneous catalysis. *Coordination Chemistry Reviews* **2017,** *347*, 48-76.
148. Kaneda, K.; Mizugaki, T., Design of High-Performance Heterogeneous Catalysts using Apatite Compounds for Liquid-Phase Organic Syntheses. *ACS CATALYSIS* **2017,** *7* (2), 920-935.
149. Liu, Y.; Tsunoyama, H.; Akita, T.; Tsukuda, T., Efficient and selective epoxidation of styrene with TBHP catalyzed by Au25 clusters on hydroxyapatite. *Chemical Communications* **2010,** *46* (4), 550-552.
150. Zhou, M.; Zeng, C.; Chen, Y.; Zhao, S.; Sfeir, M. Y.; Zhu, M.; Jin, R., Evolution from the plasmon to exciton state in ligand-protected atomically precise gold nanoparticles. *Nature Communications* **2016,** *7*, 13240.

151. Donoeva, B. G.; Ovoshchnikov, D. S.; Golovko, V. B., Establishing a Au nanoparticle size effect in the oxidation of cyclohexene using gradually changing Au catalysts. *ACS Catalysis* **2013,** *3* (12), 2986-2991.
152. Haesuwannakij, S.; Poonsawat, T.; Noikham, M.; Somsook, E.; Yakiyama, Y.; Dhital, R. N.; Sakurai, H., Size-Controlled Preparation of Gold Nanoclusters on Hydroxyapatite Through Trans-Deposition Method. *JOURNAL OF NANOSCIENCE AND NANOTECHNOLOGY* **2017,** *17* (7), 4649-4657.
153. Aldea, N.; Marginean, P.; Rednic, V.; Pintea, S.; Barz, B.; Gluhoi, A.; Nieuwenhuys, B. E.; Xie, Y.; Aldea, F.; Neumann, M., Crystalline and electronic structure of gold nanoclusters determined by EXAFS, XRD and XPS methods. *Journal of Optoelectronics and Advanced Materials* **2007,** *9* (5), 1554-1560.
154. Datye, A. K.; Xu, Q.; Kharas, K. C.; McCarty, J. M., Particle size distributions in heterogeneous catalysts: What do they tell us about the sintering mechanism? *Catalysis Today* **2006,** *111* (1), 59-67.
155. Anderson, D. P.; Alvino, J. F.; Gentleman, A.; Qahtani, H. A.; Thomsen, L.; Polson, M. I. J.; Metha, G. F.; Golovko, V. B.; Andersson, G. G., Chemically-synthesised, atomically-precise gold clusters deposited and activated on titania. *Physical Chemistry Chemical Physics* **2013,** *15* (11), 3917-3929.
156. Kamat, P. V., Photophysical, photochemical and photocatalytic aspects of metal nanoparticles. *JOURNAL OF PHYSICAL CHEMISTRY B* **2002,** *106* (32), 7729-7744.
157. Adnan, R. H.; Andersson, G. G.; Polson, M. I. J.; Metha, G. F.; Golovko, V. B., Factors influencing the catalytic oxidation of benzyl alcohol using supported phosphine-capped gold nanoparticles. *Catalysis Science and Technology* **2015,** *5* (2), 1323-1333.
158. Fang, J.; Li, J.; Zhang, B.; Yuan, X.; Asakura, H.; Tanaka, T.; Teramura, K.; Xie, J.; Yan, N., The support effect on the size and catalytic activity of thiolated Au25 nanoclusters as precatalysts. *Nanoscale* **2015,** *7* (14), 6325-6333.
159. Signoretto, M.; Menegazzo, F.; Trevisan, V.; Pinna, F.; Manzoli, M.; Boccuzzi, F., Investigation on the Stability of Supported Gold Nanoparticles. *Catalysts* **2013,** *3* (3), 656.
160. Ono, N., *The nitro group in organic synthesis*. Wiley-VCH: New York, 2001.
161. McKetta, J. J., *Encyclopedia of Chemical Processing and Design: Volume 3 - Aluminum to Asphalt: Design*. Taylor & Francis: 1977.
162. Dupont, US 3 832 364, 1972.
163. McKetta, J. J., *Chemical Processing Handbook*. Taylor & Francis: 1993.
164. Sonawane, S.; Setty, Y. P.; Sapavatu, S. N., *Chemical and Bioprocess Engineering: Trends and Developments*. Apple Academic Press: 2015.
165. Cope, O. J.; Brown, R. K., The Reduction of Nitrobenzene by Sodium Sulphide in Aqueous Ethanol. *Canadian Journal of Chemistry* **1961,** *39* (8), 1695-1710.
166. Schaschke, C., *By-product. In A Dictionary of Chemical Engineering*. First ed.; Oxford University Press: Oxford, 2014.
167. Schaschke, C., *Intermediate. In A Dictionary of Chemical Engineering*. First ed.; Oxford University Press: Oxford, 2014.
168. Haber, F., Gradual electrolytic reduction of nitrobenzene with limited cathode potential. *Z. Elektrochem.* **1898,** *22*.
169. Dupont, US 4 185 036 A, 1977.
170. BASF SE, US 6 350 911 B1, 1999.
171. García-Mota, M.; Gómez-Díaz, J.; Novell-Leruth, G.; Vargas-Fuentes, C.; Bellarosa, L.; Bridier, B.; Pérez-Ramírez, J.; López, N., A density functional theory study of the 'mythic' Lindlar hydrogenation catalyst. *Theoretical Chemistry Accounts* **2011,** *128* (4), 663-673.
172. Baumeister, P.; Blaser, H.-U.; Studer, M., Strong reduction of hydroxylamine accumulation in the catalytic hydrogenation of nitroarenes by vanadium promoters. *Catalysis Letters* **1997,** *49* (3), 219-222.
173. Stoessel, F., Experimental study of thermal hazards during the hydrogenation of aromatic nitro compounds. *Journal of Loss Prevention in the Process Industries* **1993,** *6* (2), 79-85.

174. Corma, A.; Serna, P., Chemoselective Hydrogenation of Nitro Compounds with Supported Gold Catalysts. *Science* **2006,** *313* (5785), 332-334.
175. Chen, Y.; Qiu, J.; Wang, X.; Xiu, J., Preparation and application of highly dispersed gold nanoparticles supported on silica for catalytic hydrogenation of aromatic nitro compounds. *Journal of Catalysis* **2006,** *242* (1), 227-230.
176. Wang, X.; Li, M.; Keane, M. A., Harnessing the selective catalytic action of supported gold in hydrogenation applications. *RSC Catalysis Series* **2014,** *2014-* (18), 424-461.
177. Thushara Kandaramath Hari Zahira, Y., Recent development of supported monometallic gold as heterogeneous catalyst for selective liquid phase hydrogenation reactions. *中国化学工程学报：英文版* **2015,** *23* (2), 327-336.
178. Cardenas-Lizana, F.; Gomez-Quero, S.; Idriss, H.; Keane, M. A., Gold particle size effects in the gas-phase hydrogenation of m-dinitrobenzene over Au/TiO2. *Journal of Catalysis* **2009,** *268* (2), 223-234.
179. Ohyama, J.; Esaki, A.; Koketsu, T.; Yamamoto, Y.; Arai, S.; Satsuma, A., Atomic-scale insight into the structural effect of a supported Au catalyst based on a size-distribution analysis using Cs-STEM and morphological image-processing. *Journal of Catalysis* **2016,** *335*, 24-35.
180. Serna, P.; Corma, A., Transforming Nano Metal Nonselective Particulates into Chemoselective Catalysts for Hydrogenation of Substituted Nitrobenzenes. *ACS Catalysis* **2015,** *5* (12), 7114-7121.
181. Anandkumar, M.; Vinothkumar, G.; Babu, K. S., Synergistic effect of gold supported on redox active cerium oxide nanoparticles for the catalytic hydrogenation of 4-nitrophenol. *NEW JOURNAL OF CHEMISTRY* **2017,** *41* (14), 6720-6729.
182. Hartfelder, U.; Kartusch, C.; Makosch, M.; Rovezzi, M.; Sá, J.; van Bokhoven, J. A., Particle size and support effects in hydrogenation over supported gold catalysts. *Catalysis Science and Technology* **2013,** *3* (2), 454-461.
183. Li, G.; Zeng, C.; Jin, R., Thermally robust nanoclusters for chemoselective hydrogenation of nitrobenzaldehyde derivatives in water. *Journal of the American Chemical Society* **2014,** *136* (9), 3673.
184. Serna, P.; Concepción, P.; Corma, A., Design of highly active and chemoselective bimetallic gold–platinum hydrogenation catalysts through kinetic and isotopic studies. *Journal of Catalysis* **2009,** *265* (1), 19-25.
185. Biener, J.; Wittstock, A.; Baumann, T.; Weissmüller, J.; Bäumer, M.; Hamza, A., Surface Chemistry in Nanoscale Materials. *Materials* **2009,** *2* (4), 2404.
186. Li, H.; Li, H.; Zhao, Q., Selective hydrogenation of p-chloronitrobenzene over Ni–P–B amorphous catalyst and synergistic promoting effects of B and P. *Journal of Molecular Catalysis. A, Chemical* **2008,** *285* (1), 29-35.
187. Wang, F.; Liu, J.; Xu, X., Layered material [gamma]-ZrP supported platinum catalyst for liquid-phase reaction: a highly active and selective catalyst for hydrogenation of the nitro group in para-chloronitrobenzene. *Chemical Communications* **2008,** (17), 2040-2042.
188. He, D.; Shi, H.; Wu, Y.; Xu, B.-Q., Synthesis of chloroanilines: selective hydrogenation of the nitro in chloronitrobenzenes over zirconia-supported gold catalyst. *Green Chemistry* **2007,** *9* (8), 849-851.
189. Torres, C. C.; Alderete, J. B.; Pecchi, G.; Campos, C. H.; Reyes, P.; Pawelec, B.; Vaschetto, E. G.; Eimer, G. A., Heterogeneous hydrogenation of nitroaromatic compounds on gold catalysts: Influence of titanium substitution in MCM-41 mesoporous supports. *Applied Catalysis A: General* **2016,** *517*, 110-119.
190. Turáková, M.; Salmi, T.; Eränen, K.; Wärnå, J.; Murzin, D. Y.; Králik, M., Liquid phase hydrogenation of nitrobenzene. *Applied Catalysis A, General* **2015,** *499*, 66-76.
191. Rojas, H.; Fierro, J. L. G.; Reyes, P., The solvent effect in the hydrogenation of citral over Ir and Ir-Fe/TiO2 catalysts. *Journal of the Chilean Chemical Society* **2007,** *52* (2), 1155-1159.
192. Torres, C. C.; Alderete, J. B.; Pecchi, G.; Campos, C. H.; Reyes, P.; Pawelec, B.; Vaschetto, E. G.; Eimer, G. A., Heterogeneous hydrogenation of nitroaromatic compounds on gold catalysts: Influence

of titanium substitution in MCM-41 mesoporous supports. *Applied Catalysis A, General* **2016,** *517*, 110-119.
193. Dyson, P. J.; Jessop, P. G., Solvent effects in catalysis: rational improvements of catalysts via manipulation of solvent interactions. *Catalysis Science and Technology* **2016,** *6* (1), 332-3316.
194. Boronat, M.; Concepción, P.; Corma, A.; González, S.; Illas, F.; Serna, P., A molecular mechanism for the chemoselective hydrogenation of substituted nitroaromatics with nanoparticles of gold on TiO2 catalysts: A cooperative effect between gold and the support. *Journal of the American Chemical Society* **2007,** *129* (51), 16230-16237.
195. Zanella, R.; Giorgio, S.; Henry, C. R.; Louis, C., Alternative Methods for the Preparation of Gold Nanoparticles Supported on TiO2. *The Journal of Physical Chemistry B* **2002,** *106* (31), 7634-7642.
196. Wang, L.; Zhang, J.; Wang, H.; Shao, Y.; Liu, X.; Wang, Y.-Q.; Lewis, J. P.; Xiao, F.-S., Activity and Selectivity in Nitroarene Hydrogenation over Au Nanoparticles on the Edge/Corner of Anatase. *ACS Catalysis* **2016,** *6* (7), 4110-4116.
197. Häkkinen, H., Electronic Structure: Shell Structure and the Superatom Concept. *Frontiers of Nanoscience* **2015,** *9*, 189-222.
198. Reber, A. C.; Khanna, S. N., Superatoms: Electronic and Geometric Effects on Reactivity. *Accounts of Chemical Research* **2017,** *50* (2), 255-263.
199. Kim, Y. D.; Fischer, M.; Ganteför, G., Origin of unusual catalytic activities of Au-based catalysts. *Chemical Physics Letters* **2003,** *377* (1), 170-176.
200. Molina, L.; Hammer, B., The activity of the tetrahedral Au20 cluster: charging and impurity effects. *Journal of Catalysis* **2005,** *233* (2), 399-404.
201. Hansch, C.; Leo, A.; Unger, S. H.; Kim, K. H.; Nikaitani, D.; Lien, E. J., Aromatic substituent constants for structure-activity correlations. *Journal of Medicinal Chemistry* **1973,** *16* (11), 1207-1216.
202. Coq, B.; Figueras, F., Structure–activity relationships in catalysis by metals: some aspects of particle size, bimetallic and supports effects. *Coordination Chemistry Reviews* **1998,** *178-180*, 1753-1783.
203. Cárdenas-Lizana, F.; de Pedro, Z. M.; Gómez-Quero, S.; Keane, M. A., Gas phase hydrogenation of nitroarenes: A comparison of the catalytic action of titania supported gold and silver. *Journal of Molecular Catalysis A: Chemical* **2010,** *326* (1), 48-54.
204. Makosch, M.; Sá, J.; Kartusch, C.; Richner, G.; van Bokhoven, J. A.; Hungerbühler, K., Hydrogenation of Nitrobenzene Over Au/MeOx Catalysts-A Matter of the Support. *ChemCatChem* **2012,** *4* (1), 59-63.
205. Christie, R. M.; Royal Society of, C.; Books24x, I., *Colour chemistry*. Royal Society of Chemistry: Cambridge, 2001.
206. Merino, E., Synthesis of azobenzenes: The coloured pieces of molecular materials. *Chemical Society Reviews* **2011,** *40* (7), 3835-3853.
207. Nguyen, T. H. L.; Gigant, N.; Joseph, D., Advances in Direct Metal-Catalyzed Functionalization of Azobenzenes. *ACS CATALYSIS* **2018,** *8* (2), 1546-1579.
208. Wang, M.; Funabiki, K.; Matsui, M., Synthesis and properties of bis(hetaryl)azo dyes. *Dyes and Pigments* **2003,** *57* (1), 77-86.
209. Mills, C., XCIII.-Some new azo-compounds. *Journal of the Chemical Society, Transactions* **1895,** *67* (0), 925-933.
210. Buncel, E., Catalysis in strongly acidic media and the Wallach rearrangement. *Accounts of Chemical Research* **1975,** *8* (4), 132-139.
211. Hunger, K., Mischke, P. , Rieper, W. and Zhang, S., Azo Dyes, 1. General. In *Ullmann's Encyclopedia of Industrial Chemistry*, 2017.
212. Grirrane, A.; Garcia, H.; Corma, A., Preparation of symmetric and asymmetric aromatic azo compounds from aromatic amines or nitro compounds using supported gold catalysts. *Nature Protocols* **2010,** *11* (3), 429-438.
213. Combita, D.; Concepción, P.; Corma, A., Gold catalysts for the synthesis of aromatic azocompounds from nitroaromatics in one step. *Journal of Catalysis* **2014,** *311*, 339-349.

214. Baron, M.; Bondarchuk, O.; Stacchiola, D.; Shaikhutdinov, S.; Freund, H. J., Interaction of Gold with Cerium Oxide Supports: CeO2(111) Thin Films vs CeOx Nanoparticles. *The Journal of Physical Chemistry C* **2009,** *113* (15), 6042-6049.
215. Liu, X.; Ye, S.; Li, H.-Q.; Liu, Y.-M.; Cao, Y.; Fan, K.-N., Mild, selective and switchable transfer reduction of nitroarenes catalyzed by supported gold nanoparticles. *Catalysis Science and Technology* **2013,** *3* (12), 3200-3206.
216. Kartusch, C.; Makosch, M.; Sá, J.; Hungerbuehler, K.; van Bokhoven, J. A., The Dynamic Structure of Gold Supported on Ceria in the Liquid Phase Hydrogenation of Nitrobenzene. *ChemCatChem* **2012,** *4* (2), 236-242.
217. Rodriguez, J. A.; Liu, P.; Hrbek, J.; Evans, J.; Perez, M., Water gas shift reaction on Cu and Au nanoparticles supported on CeO2(111) and ZnO(000(1)over-bar): Intrinsic activity and importance of support interactions. *ANGEWANDTE CHEMIE-INTERNATIONAL EDITION* **2007,** *46* (8), 1329-1332.
218. Luches, P.; Valeri, S., Structure, Morphology and Reducibility of Epitaxial Cerium Oxide Ultrathin Films and Nanostructures. *Materials* **2015,** *8* (9), 5818-5833.